Department of Mechanical Engineering
Aalborg University, Denmark.

Efficient finite element formulation for analysis and optimization of laminated composite shell structures

Master's Thesis

by

Henrik Fredslund Hansen & Christian Gram Hvejsel

Department of Mechanical Engineering, Aalborg University
Pontoppidanstræde 101, DK-9220 Aalborg East, Denmark

Typeset in LaTeX and printed in Aalborg, June 2007.

Preface

This Master's thesis is the result of the work carried out during the period from February to June 2007 at the 10th semester of the engineering curriculum 'Design of Mechanical Systems' offered at the Department of Mechanical Engineering, Aalborg University, Denmark. The thesis has been submitted in partial fulfilment of the requirements for the degree of Master of Science. The project has been supervised by professor, Ph.D. Erik Lund.

Aalborg, June 2007

Henrik Fredslund Hansen

Christian Gram Hvejsel

Abstract

Design of modern multi-layered composite shell structures such as wind turbine blades is a highly complex task due to the conflicting requirements of high strength and stiffness at low weight and cost. In the development of such products, design optimization methods have become an increasingly important tool in aiding the designer at obtaining rational designs. Such optimization procedures rely on computationally efficient and robust analysis tools.

The objective of the present project is to develop and implement efficient isoparametric degenerated shell finite element formulations for analysis and optimization of laminated composite shell structures.

On basis of preliminaries pertaining to the finite element analysis of laminated composite shell structures, the governing equations for linear static stress analysis and linearized buckling analysis are developed.

Formulation of degenerated isoparametric shell elements is shown and furthermore the thickness dependency of the strain-displacement relation is expressed explicitly. In combination with a linear approximation through the thickness of the inverse Jacobian matrix, explicit thickness integration is enabled. Consequently, the evaluation of element matrices may be performed efficiently for multi-layered shell elements with more than four layers. For higher number of layers, the formulation is an order of magnitude more efficient compared to layer-wise numerical integration schemes.

The explicit thickness integration scheme's similarity with the integrations performed to obtain ABD-matrices in Classical Laminated Plate Theory reveals a link to lamination parameters. Thus, the stiffness matrix may be expressed in terms of an extended set of lamination parameters which turns out to be convenient in stiffness optimization.

Structural design optimization is introduced and the maximum stiffness and the maximum stability design problem is formulated. For these problems design sensitivity analysis is shown for generalized design variables. From here, the focus is turned towards design optimization of composite laminates. Problems of non-convexity of a fibre angle parametrization is addressed by two simple examples. To provide convexity in stiffness optimization an alternative laminate parametrization is presented in terms of lamination parameters and the use with an existing laminate optimization procedure is outlined.

A number of numerical examples are shown to validate the implementations of a 9- and a 16-node version of the element formulation. Convergence and accuracy of the 'new' formulation is very similar to that of the existing isoparametric degenerated shell elements. In the thick shell range, the approximations made to enable explicit thickness integration cause some inaccuracy. For radius of curvature-to-thickness ratios above 25, the deviation of displacements compared to the existing isoparametric formulation is less than 4%. Eventually, two optimization examples confirm the performance gain in multi-layered settings.

Resumé

Design af kompositte skalstrukturer med mange lag, såsom vindmøllevinger er en yderst krævende opgave grundet de modstridende krav om høj styrke og stivhed ved lav vægt og pris. Udviklingen af sådanne komponenter baseres i stigende grad på designoptimering som et værktøj til at opnå rationelt forbedrede designs. Disse optimeringsværktøjer er afhængige af beregningseffektive og robuste analyseværktøjer.

Formålet med dette projekt er at udvikle og implementere effektive isoparametriske degenererede finite element skalelement-formuleringer til analyse og optimering af laminerede kompositte skalstrukturer.

På basis af indledende studier relateret til finite element analyse af laminerede komposit skalstrukturer opstilles de styrende ligninger for lineær elastisk statisk spændingsanalyse samt lineariseret bulingsanalyse.

Degenererede isoparametriske skalelementer formuleres og yderligere udtrykkes tøjnings-forskydningsmatricens tykkelsesafhængighed eksplicit. Kombineres dette med antagelsen om lineær variation af den inverse Jacobi matrice gennem tykkelsen muliggøres eksplicit tykkelsesintegration. Som følge heraf kan elementmatricerne evalueres beregningsmæssigt effektivt for skaller med mere end fire lag. For skaller med endnu flere lag resulterer formuleringen i betydelige besparelser med hensyn til beregningstid sammenlignet med den eksisterende lagvise integration.

Den eksplicitte tykkelsesintegrations lighedspunkter med integrationerne udført for at bestemme ABD-matricerne i klassisk laminat pladeteori afslører en relation til laminatparametre. På baggrund heraf kan stivhedsmatricen udtrykkes i et udvidet sæt af laminatparametre hvilket viser sig anvendeligt i optimeringsøjemed.

Grundlæggende begreber indenfor strukturel designoptimering introduceres og maksimum stivhed og maksimum bulingslast optimeringsproblemerne formuleres. For de ovennævnte formuleringer udledes sensitiviteter med hensyn til generaliserede designvariable. Dette specialiseres til optimering af kompositlaminater. Problemer med ikke-konveksitet ved anvendelse af en fibervinkel parametrisering illustreres ved to eksempler. For at opnå konveksitet i stivhedsoptimering foreslås en alternativ parametrisering i form af laminatparametre, hvorefter brugen af disse i en eksisterende optimeringsprocedure skitseres.

Numeriske eksempler anvendes til at verificere implementeringen af 9- og 16-knuders skalelementerne. Konvergens og nøjagtighed for de 'nye' formuleringer viser sig at være meget tæt på de eksisterende isoparametriske degenererede skalelementers ditto. For tykke skaller får approksimationerne, som er indført for at udføre tykkelsesintegrationen eksplicit, indvirkning på nøjagtigheden af resultaterne. For krumningsradius-tykkelsesforhold over 25 er afvigelserne fra den eksisterende isoparametriske formulering mindre end 4%. Slutteligt påvises elementformuleringens effektivitet for elementer med mange lag ved to optimeringseksempler.

Nomenclature

$\lfloor \cdots \rfloor$	Row vector
$\{ \cdots \}$	Column vector
$[\cdots]$	Matrix
$\boldsymbol{a}$	Vector of design variables
a	Node index
$\boldsymbol{B}$	Strain-displacement matrix
$\boldsymbol{b}$	Body force vector
C	Compliance
$\boldsymbol{C}$	Constitutive matrix (in global coordinate system)
$\boldsymbol{d}$	Global displacement vector
E	Young's modulus
$\boldsymbol{E}$	Matrix of thickness integrated constitutive properties
$\boldsymbol{F}$	Shape function derivatives with respect to natural coordinates
f	Objective function
$\boldsymbol{G}$	Shape function matrix derivatives with respect to global coordinates
$\boldsymbol{g}$	Covariant tangent base vector
$\boldsymbol{H}$	Auxiliary summation matrix
h	Shell thickness
$\boldsymbol{i}, \boldsymbol{j}, \boldsymbol{k}$	Orthonormal global base vectors
$\boldsymbol{J}$	Jacobian matrix
$\boldsymbol{K}$	Stiffness matrix
$\boldsymbol{M}$	Matrix containing thickness integrated stresses

$\boldsymbol{m}$	Material coordinate system base vector
$\boldsymbol{N}$	Shape function (interpolation) matrix
$\boldsymbol{p}$	Externally applied concentrated nodal loads
$\boldsymbol{Q}$	Constitutive matrix (in principal material coordinate system)
$\overline{\boldsymbol{Q}}$	Constitutive matrix (in material coordinate system)
R	Radius of curvature
$\boldsymbol{r}$	Work equivalent nodal loads
r_i	Natural coordinates (r, s, t) referring to ECS
$\boldsymbol{S}$	Stress matrix
$\boldsymbol{T}$	Transformation matrix
U	Elastic strain energy
$\boldsymbol{U}$	Matrix of lamina invariants
$\boldsymbol{u}, u_i$	Global displacement (u, v, w) in vector and tensor form, respectively
V	Volume
$\boldsymbol{v}_i$	Director coordinate system base vector
W	External work
w_i	Vector of weight factors used in Gauss quadrature
$\boldsymbol{x}$	Global coordinates of reference surface
z	Physical thickness coordinate
α, β	Director rotation in shell element
Δ	Square root of Jacobian matrix determinant
δ	Kinematically admissible variation.
$\boldsymbol{\varepsilon}$	Green-Lagrange strain
γ	Geometric property of reference surface; $\frac{2\Delta_V}{h\Delta_A}$
$\boldsymbol{\Gamma}_{uvw}$	Matrix containing inverse Jacobian matrices
λ	Eigenvalue, buckling load factor
ν	Poisson's ratio
$\boldsymbol{\Phi}$	Surface traction

$\boldsymbol{\phi}$	Eigenvector, buckling mode
$\boldsymbol{\sigma}$	Cauchy stress
θ	Fibre angle
ξ	Lamination parameters

Contents

1

Introduction

Recent years have seen an increasing use of laminated composite shell components for high performance structures such as aircraft wings and fuselages, wind turbine blades, ship hulls, etc. Common for these structures is a need for high stiffness and strength to weight ratios. In general, complex structural geometries in combination with the use of composite materials results in structures whose response is too complex to analyse by means of classical analytical tools. For analysis of this type of structures the method of finite elements has become the preferred tool.

Figure 1.1: Contemporary high performance composite shell structures. Courtesy of Emirates Team New Zealand and Vestas Wind Systems A/S.

Analysis, however, does not give the answer to how a structure is designed rationally in terms of favourable combinations of material and geometry. In order to synthesize a rational design amongst the virtually endless number of possibilities that the designer is faced with, systematic procedures that lead to an optimum solution, by some measure, are needed. The answer to the quest of synthesizing and designing has been structural design optimization which is a forward pointing iterative process towards a solution to the design problem at hand. The iterative nature of optimization processes involves numerous analyses and design improvements which make the optimization problem exhaustive to solve. For the reason of the cost of solving optimization problems

the technology has developed closely along with technological advances in computing capabilities.

At the Department of Mechanical Engineering, Aalborg University, the group for Computer-Aided Design has conducted research within the field through the last 15 years and developed numerous tools for design and optimization of mechanical systems. For this purpose a design system is present in MUST (MUltidisciplinary Synthesis Tool). The system is under continuous development headed by Professor Erik Lund.

It is beyond the scope of this text to give a complete overview of the capabilities of MUST. The main interest of this project is the shell element module and thus a short description of existing facilities is given. The original framework for shell elements in MUST was developed and implemented by Jensen et al. (2002) and Stegmann (2005) did a number of revisions and extensions to the implementations. The elements implemented are mainly low-order elements (stabilized and non-stabilized) and a few higher-order elements. The non-stabilized elements are denoted as the SHELLn family whereas the stabilized elements are called MITCn referring to the stabilization scheme applied (Mixed Interpolation of Tensorial Components).

The shell elements in MUST have multi-layer capabilities enabled by a layer-wise integration scheme in the shell thickness direction. For multi-layered shell elements with many layers this formulation is computationally expensive due to sampling points in each layer. In practical applications with a large number of layers, efficiency becomes an issue and in optimization it is crucial. Thus it is of interest to study how efficiency of the existing SHELLn family of elements may be improved for situations involving a large number of layers.

1.1 Theoretical background

This section gives an introduction to the fields that will be studied along with a review of present work and state-of-the-art within each field. It is not the intention to give a complete review but to address issues of importance for the present work. First, a brief review of degenerated shell elements and their generalization to multi-layered applications is given. Special attention is given to how integration through the thickness is performed efficiently by explicit integration. Based on the findings on explicit thickness integration, new possibilities for laminate optimization of generally curved shell elements arise and thus the existing possibilities are reviewed.

1.1.1 Degenerated shell elements

Degenerated shell elements have been the work-horse among elements for finite element analysis of shells. The reason for this is the relatively simple formulation similar to that of the isoparametric solid element formalism. In fact, the degenerated shell element formulation is obtained by imposing certain physically based constraints on the behaviour of shell-like solid elements. This was first shown in a paper published by Ahmad et al. (1970). Despite it's attractive features the formulation is computationally expensive which one of the fathers of degenerated shell elements already presented a

remedy for in Zienkiewicz et al. (1971) which we will return to later.

Multi-layered shells

In order to accommodate for analysis of laminated composite shells, the degenerated shell element was generalized to incorporate multi-layered elements by Panda and Natarajan (1981). To integrate through the thickness, a transformation of the natural thickness coordinate to a layer-wise natural thickness coordinate was introduced. This implies that the numerical integration through the thickness is performed by sampling the integrand at e.g. two positions in the thickness direction in each layer. For shells with a large number of layers this formulation is computationally inefficient and with the increased use of such structures combined with a need for efficiency in e.g. optimization applications, interest in enhancing the computational efficiency emerged. Again, the interest turned towards the use of explicit thickness integration which is described in the next section.

Explicit thickness integration

The discussion above indicates that the degenerated shell element is inefficient for multi-layered shells with many layers. To increase the performance of the degenerated shell elements, explicit (exact) integration through the thickness is applied upon approximations of the thickness variation of the inverse Jacobian. Use of explicit integration through the thickness also reveals a link to the well-known ABD-approach as applied to plates in Classical Lamination Theory, see e.g. Jones (1999).

The first steps of explicit thickness integration of degenerated shell elements were taken by Zienkiewicz et al. (1971) who pointed out that the assumptions made in degenerated shell elements are in fact the assumptions of classical first order shell theory enabling explicit integration through the thickness. However, it seems that explicit thickness integration did not receive much attention until Milford and Schnobrich (1986) put some effort into applying explicit thickness integration to degenerated 'thin' shells with focus on geometrically non-linear problems. The work by Yunus et al. (1989) showed that explicit thickness integration could be used advantageously in the evaluation of element matrices of doubly curved, multi-layered composite shells with a large number of layers. In the same period also Vlachoutsis (1990) studied explicitly thickness integrated shell elements and especially he investigated how the geometric configuration influences the accuracy of the approximations introduced to enable explicit thickness integration. Prema Kumar and Palaninathan (1997) investigated the influence on accuracy and efficiency of different assumptions about the inverse Jacobian matrix. For this purpose three integration schemes were proposed and compared to the layer-wise integration scheme developed by Panda and Natarajan (1981). The models contain the assumption of constant and linear variation of the inverse Jacobian matrix and furthermore a modified model with linear variation with further assumptions that increase the performance even more. The efficiency gain of explicit thickness integration reported by Yunus et al. (1989) was confirmed for all three models. In 1999 Prema Kumar and Palaninathan (1999) extended the formulation to include geometrically non-linear problems and examples revealed substantial savings in computational time without significant loss in accuracy.

1.1.2 Laminate optimization

The task of designing a laminate encompasses a unique choice of material, orientation and thickness for each layer of the laminate. It is definitely not a trivial task, partly due to the complex coupling phenomena encountered, but also the nature of the problem in terms of discrete design variables combined with non-convex design spaces renders the problem difficult. Rational design of laminated composite plate and shell structures has been subject to extensive research during the last three decades or so, and it is not the intention to give a complete review of the research within the field but rather an overview of the challenges encountered and some of the answers to these. For in-depth reviews see e.g. Abrate (1994) or Venkataraman and Haftka (1999).

If the laminae material for all layers is given beforehand, the most natural parametrization is one that directly takes physical quantities such as layer orientation and thickness of each layer as the design variables. Such a parametrization has a straightforward physical interpretation and may be realized within the limitations due to manufacturing considerations. The downside, however, is that the design space is non-convex and consequently the popular gradient-based algorithms only guarantee local optimum solutions. Alternatively, a re-formulation of the problem is introduced with the so-called lamination parameters. The material properties of an orthotropic (or an anisotropic) material may be described in terms of the lamina invariants that are invariant under coordinate transformations. This has the result that the trigonometric functions causing non-convexity are avoided. By use of lamina invariants, the constitutive relations for a laminate consisting of layers of the same orthotropic material may be described in terms of similar laminate invariants that make use of the so-called lamination parameters. Such a description was first given by Tsai and Pagano (1968) and later extended from Kirchhoff kinematics to FSDT by Grenestedt (1994). Up to 12 lamination parameters were used as design variables in the design of discs and plates as shown by e.g. Miki (1982) and Miki and Sugiyama (1993). These publications, however, only apply to the design of plates for either in-plane or bending loads for which the feasible regions of the lamination parameters are known analytically. For the more general setting of simultaneous in-plane and bending loads the feasible regions have not been determined. Instead of seeking closed-form expressions that yield angles and thicknesses for given lamination parameters, Foldager et al. (1998) employed an identification procedure to solve the inverse problem of identifying a physical lay-up from a set of lamination parameters. This makes it possible to exploit the desirable convex properties of lamination parameters in stiffness design. The method is of completely general nature and should be extendible to any number of lamination parameters.

1.2 Objective of project

Based on the findings above, the objective of the present project is to *develop and implement* an efficient degenerated shell element formulation for analysis and optimization of multi-layered composite structures. The platform of implementation is the MUltidisciplinary Synthesis Tool.

The element is to be formulated for linear static stress and linearized buckling analysis. It must handle laminated composite shell structures with a large number of layers efficiently, and work as a biquadratic 9-node element and a bicubic 16-node element. Performance and accuracy comparisons between existing and the 'new' element formulations are required in order to reveal advantages and limitations of the new elements.

Furthermore, an extension of the applicability of lamination parameters is sought, such that these can be used for generally curved degenerated shell elements.

1.2.1 Outline of thesis

The thesis is divided into a number of chapters organized as follows:

Chapter 2 introduces basic concepts needed in the remaining part of the thesis.
Chapter 3 develops the discrete governing equations of linear elastic finite element analysis and those for linearized buckling followed by a brief outline of numerical integration.
Chapter 4 contains the formulation of the degenerated shell elements and describes explicit thickness integration schemes in detail.
Chapter 5 presents structural design optimization as a tool to obtain optimum stiffness or optimum stability designs. More specifically, laminate optimization is treated for the previously mentioned design objectives.
Chapter 6 gives numerical examples that verify the implementation and asses the accuracy and performance of the new shell elements.

2

Basic concepts

THE PURPOSE OF THIS CHAPTER is to present some preliminary basic concepts that form the basis for the remainder of the report. First, the kinematic assumptions of First order Shear Deformation Theory are addressed, leading to the idea of relating shell geometry to a reference surface. Subsequently, the covariant tangent base vectors related to the reference surface are introduced as a means of obtaining a unique description of the Material Coordinate System applied in shell analysis. Eventually, the constitutive properties of a composite material is addressed along with a description of the transformations needed to analyze a shell structure.

2.1 Shells

In the following we shall use the term *shell* about a solid with one characteristic dimension significantly smaller than the two other dimensions characterising the extension of the geometry. In general, the bottom and top boundaries of the shell will be curved, and thus the plate may be seen as a special case of a shell, i.e. plates are regarded simply as shells with no curvature. With regard to structural efficiency, the main advantage of shell structures are their ability to carry relatively large loads compared to their weight if designed correctly, i.e. preferably the shell should carry loads as membrane stresses. The analysis of shell structures could be performed by full 3D theory of elasticity but since this would be time-consuming and cumbersome, kinematic assumptions are applied to simplify the analysis.

Different kinematic assumptions have been applied in the derivation of shell theories, leading to a large variety of theories. These are split into the following three groups: Classical Shell Theory (CST), First order Shear Deformation Theory (FSDT) and higher order shell theories. In the following the focus will be on FSDT since the degenerated shell element is based on this theory.

The kinematic assumptions of FSDT are, that

1. normals remain straight, but not necessarily normal to the reference surface (in order to include transverse shear strains)
2. normals are *inextensible*, i.e. $\varepsilon_3 = 0$

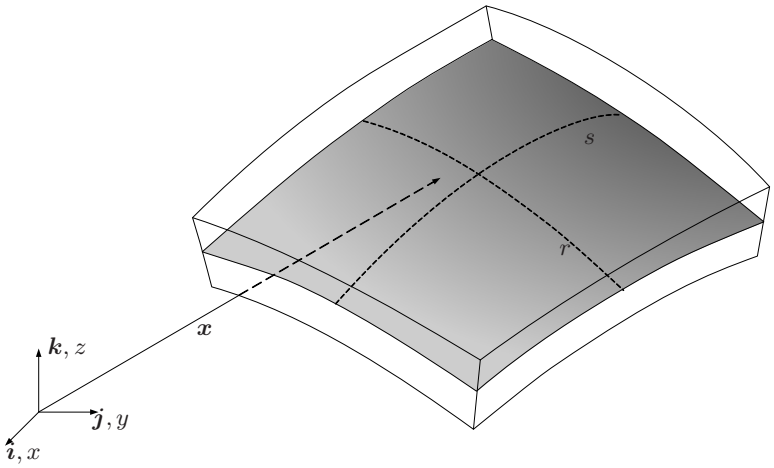

Figure 2.1: Illustration of a shell with position vector $\boldsymbol{x}(r, s, t)$ including reference surface with curvilinear coordinates r and s.

Due to the kinematic assumptions stated above, the displacement field throughout the shell is now described completely in terms of reference surface displacements and rotations of shell normals. In order to describe the displacement field a unique geometry description is required. The geometry of the shell is also related to the *reference surface* along with a thickness at each point in the reference surface seen in Figure 2.1. Thus the task of describing geometry and displacements of a shell structure is reduced to a two-dimensional problem, namely that of describing geometry and displacements of the reference surface. Consequently, we relate geometric properties throughout the shell to properties of the reference surface.

2.2 Differential geometry

This section defines terminology used in the description of geometric properties of surfaces. The presentation is not claimed to be rigorous or exhaustive but serves to introduce the concepts needed in the formulation of shell elements.

For the purpose of obtaining a mathematical description of the shell shown in Figure 2.1, we introduce a parametrization of the reference surface in the parameters r and s as shown in Figure 2.1. Thus, each point contained in the reference surface may be described uniquely from these parameters. For shells folding into themselves overlaps will make the parametrization non-unique. In the following we presume that this does not happen. Furthermore a parameter t is introduced to describe the position of points located perpendicular to the reference surface. From the three parameters introduced above, r, s and t, (termed 'natural coordinates' in FE terminology) we are able to describe the position vector of the shell, $\boldsymbol{x}$, provided that the direction of the thickness is given.

$$\boldsymbol{x}(r, s, t) = \boldsymbol{x}_0(r, s) + t\tfrac{h}{2}\boldsymbol{v}_3(r, s) \tag{2.1}$$

Here, h is the physical shell thickness and $\boldsymbol{x}_0$ is the reference surface for which the parameter t equals zero. This implies that the top and bottom surfaces of the shell are

obtained for $t = \pm 1$.

The unit normal vector, $\boldsymbol{v}_3$, is established from the reference surface *covariant tangent base vectors*, $\boldsymbol{g}_\alpha$, that are defined as

$$\boldsymbol{g}_\alpha \equiv \frac{\partial \boldsymbol{x}_0}{\partial r^\alpha} \tag{2.2}$$

Where r^α denotes differentiation with respect to r or s. It is seen that $\boldsymbol{g}_1$ and $\boldsymbol{g}_2$ span the tangent plane at each point of the reference surface and thus the unit normal vector, $\boldsymbol{v}_3$, is calculated from the normalized cross product of the two base vectors

$$\boldsymbol{v}_3 = \boldsymbol{g}_3 = \frac{\boldsymbol{g}_1 \times \boldsymbol{g}_2}{|\boldsymbol{g}_1 \times \boldsymbol{g}_2|} \tag{2.3}$$

Similarly to the definition used in equation (2.2), all three covariant tangent base vectors at any point within the shell are defined by

$$\boldsymbol{g}_i \equiv \frac{\partial \boldsymbol{x}}{\partial r^i} \tag{2.4}$$

r^i denotes differentiation with respect to r, s or t. Upon expansion the expressions of the three tangent base vectors are

$$\boldsymbol{g}_1 = \left\lfloor \frac{\partial x}{\partial r} \quad \frac{\partial y}{\partial r} \quad \frac{\partial z}{\partial r} \right\rfloor \quad \boldsymbol{g}_2 = \left\lfloor \frac{\partial x}{\partial s} \quad \frac{\partial y}{\partial s} \quad \frac{\partial z}{\partial s} \right\rfloor \quad \boldsymbol{g}_3 = \left\lfloor \frac{\partial x}{\partial t} \quad \frac{\partial y}{\partial t} \quad \frac{\partial z}{\partial t} \right\rfloor \tag{2.5}$$

As we will see in Section 3.5 these are equal to the entries of the Jacobian matrix.

In general, the tangent base vectors are non-orthonormal.

2.3 Coordinate systems

In this section various local coordinate systems are defined. These are utilized in setting up element matrices which is done by numerical integration. Thus, at a number of sampling points, geometric and constitutive properties of the shell are evaluated which necessitates a number of unambiguously defined orthomormal coordinate systems.

2.3.1 Element coordinate system

The first coordinate system, that arises in a natural way, is the curvilinear Element Coordinate System (ECS) equal to the covariant tangent base vectors $\boldsymbol{g}_i$ defined in equation (2.4), see Figure 2.2. Constitutive properties are most conveniently described in a Cartesian coordinate system whereby the need for a such arises. For this purpose the Material Coordinate System (MCS) is generated uniquely based on the ECS.

Remark that the ECS is dependent on node numbering and element orientation. Since the MCS is based on the ECS, discontinuities between material coordinate systems in adjacent elements may occur and thus an incorrect interpretation of orthotropic material orientation, θ. The remedy is to create a user defined ECS as described in Jensen et al. (2002).

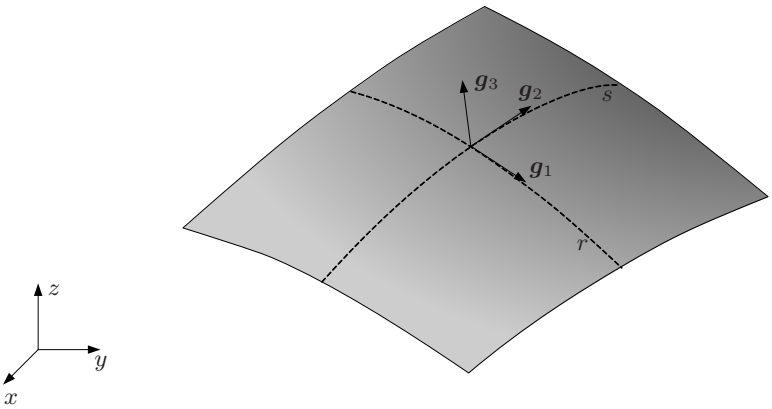

Figure 2.2: Illustration of global Cartesian xyz-coordinate system and element coordinate system defined by covariant tangent base vectors $\boldsymbol{g}_i$.

2.3.2 Material coordinate system

The material coordinate system is used as the natural system in which to describe constitutive properties. As such, it is a Cartesian coordinate system closely related to the element coordinate system. The Cartesian material coordinate system, $\boldsymbol{m}_i$, has two axes tangent to the surface and it's third axis normal to the surface. Thus it's third axis is identical to the thickness unit normal vector, i.e. $\boldsymbol{m}_3 = \boldsymbol{g}_3 = \boldsymbol{v}_3$.
The remaining two axes need to be set up in a unique way. The implementation in MUST is based on the definition given by Hughes (2000) where it is ensured that the angle between $\boldsymbol{g}_1$ and $\boldsymbol{m}_1$ is equal to the angle between $\boldsymbol{g}_2$ and $\boldsymbol{m}_2$. To do so, two auxiliary vectors $\boldsymbol{b}$ and $\boldsymbol{c}$ are defined.

$$\boldsymbol{b} = \frac{\frac{1}{2}(\boldsymbol{g}_1 + \boldsymbol{g}_2)}{\left|\frac{1}{2}(\boldsymbol{g}_1 + \boldsymbol{g}_2)\right|} \qquad \boldsymbol{c} = \frac{\boldsymbol{m}_3 \times \boldsymbol{b}}{|\boldsymbol{m}_3 \times \boldsymbol{b}|} \tag{2.6}$$

$\boldsymbol{b}$ may be interpreted as the unit vector that bisects the angle between the two tangent base vectors, whereas $\boldsymbol{c}$ is normal to $\boldsymbol{b}$ and $\boldsymbol{m}_3$ and thus contained in the tangent plane, see Figure 2.3.

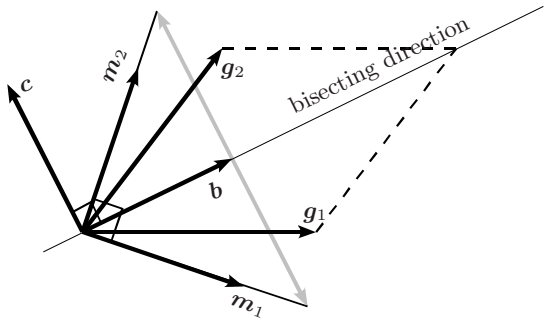

Figure 2.3: Construction of in-plane part of material coordinate system, $\boldsymbol{m}_1$ and $\boldsymbol{m}_2$, through auxiliary vectors and tangent base vectors.

From the auxiliary vectors we define the remaining material coordinate system (unit length) base vectors as

$$\boldsymbol{m}_1 = \frac{\sqrt{2}}{2}(\boldsymbol{b} - \boldsymbol{c}) \qquad \boldsymbol{m}_2 = \frac{\sqrt{2}}{2}(\boldsymbol{b} + \boldsymbol{c}) \tag{2.7}$$

If the previous discussion was restricted to isotropic materials, the description of coordinate systems could be ended here. However, this is not the case since the shell elements are to be used for analysis of laminated composite shell structures. Thus we need an additional coordinate system to complete the description of the local coordinate systems. Namely, the principal material directions.

2.3.3 Principal material directions

The principal material directions are used in connection with orthotropic materials since the constitutive properties of such materials are conveniently described in this basis (this will be treated in more detail in Section 2.4). The principal material directions are depicted in Figure 2.4 where the in-plane axes are denoted by 1 and 2. Direction 1 is aligned with the fibres and direction 2 is perpendicular to this direction. The third axis is not shown at the figure since this is coincident with the $\boldsymbol{m}_3$ axis of the MCS. In general, the principal material directions will not be coincident with the MCS but rather they are rotated in the tangent plane by an angle θ around the common normal, $\boldsymbol{m}_3$. Thus a plane transformation is applied to transform constitutive properties between the two coordinate systems, this is treated in Section 2.4.1

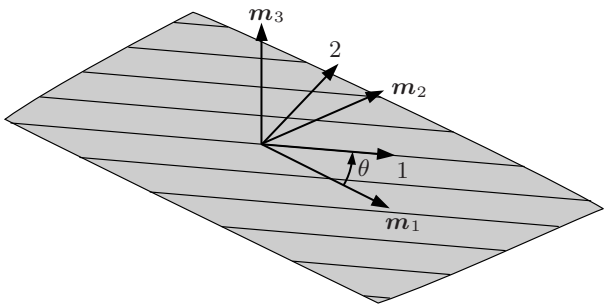

Figure 2.4: A single ply with aligned fibres to illustrate the principal material coordinate system (123-coordinate system) and the material coordinate system, $\boldsymbol{m}_i$.

The introduction of the various coordinate systems defined above naturally calls for transformations to relate constitutive properties in the different coordinate systems to each other. Thus the next section gives a description of the constitutive matrix in different coordinate systems.

2.4 Constitutive relations

This section is devoted to a description of constitutive relations with focus on orthotropic materials. A composite structure, in this case a laminate, is made up of

orthotropic layers in some stacking sequence. To be able to determine the mechanical response of a composite we first need to understand the behaviour of a single orthotropic ply. We start out by stating the assumptions applied when analysing structures made up of orthotropic materials.

For an orthotropic ply it is assumed that the fibres are uniformly distributed whereby the constitutive relations may be simplified. Thus it is assumed that the properties of each ply may be regarded as homogeneous at the macroscopic level despite the inherently inhomogeneous nature of a composite.

When performing analysis by displacement based finite elements a way to relate stresses to the determined displacement and thus strains is needed. By applying the assumption of linear elastic material behaviour the constitutive law, known as Hooke's generalized law provides the sought relation.

$$\boldsymbol{\sigma} = \boldsymbol{C}\boldsymbol{\varepsilon} \tag{2.8}$$

Here the stresses $\boldsymbol{\sigma}$ are related to strains $\boldsymbol{\varepsilon}$ in a linear manner through the constitutive matrix $\boldsymbol{C}$.

With the above assumptions the constitutive matrix can be shown to contain 81 entries. Exploiting symmetry conditions and making strain energy considerations it can be shown that only 21 constants are needed in the description of anisotropic materials.

$$\begin{Bmatrix} \sigma_x \\ \sigma_y \\ \sigma_z \\ \tau_{xy} \\ \tau_{yz} \\ \tau_{xz} \end{Bmatrix} = \begin{bmatrix} C_{11} & C_{12} & C_{13} & C_{14} & C_{15} & C_{16} \\ C_{12} & C_{22} & C_{23} & C_{24} & C_{25} & C_{26} \\ C_{13} & C_{23} & C_{33} & C_{34} & C_{35} & C_{36} \\ C_{14} & C_{24} & C_{34} & C_{44} & C_{45} & C_{46} \\ C_{15} & C_{25} & C_{35} & C_{45} & C_{55} & C_{56} \\ C_{16} & C_{26} & C_{36} & C_{46} & C_{56} & C_{66} \end{bmatrix} \begin{Bmatrix} \varepsilon_x \\ \varepsilon_y \\ \varepsilon_z \\ \gamma_{xy} \\ \gamma_{yz} \\ \gamma_{xz} \end{Bmatrix} \tag{2.9}$$

The constitutive relations of orthotropic materials are simplified when described in the principal material coordinate system.

$$\begin{Bmatrix} \sigma_1 \\ \sigma_2 \\ \sigma_3 \\ \tau_{12} \\ \tau_{23} \\ \tau_{13} \end{Bmatrix} = \begin{bmatrix} Q_{11} & Q_{12} & Q_{13} & 0 & 0 & 0 \\ Q_{21} & Q_{22} & Q_{23} & 0 & 0 & 0 \\ Q_{31} & Q_{32} & Q_{33} & 0 & 0 & 0 \\ 0 & 0 & 0 & Q_{44} & 0 & 0 \\ 0 & 0 & 0 & 0 & Q_{55} & 0 \\ 0 & 0 & 0 & 0 & 0 & Q_{66} \end{bmatrix} \begin{Bmatrix} \varepsilon_1 \\ \varepsilon_2 \\ \varepsilon_3 \\ \gamma_{12} \\ \gamma_{23} \\ \gamma_{13} \end{Bmatrix} \tag{2.10}$$

The constants Q may be described in terms of engineering constants as done by e.g. Gürdal et al. (1999)

$$\begin{aligned} Q_{11} &= \frac{E_1\left(1-\nu_{23}\nu_{32}\right)}{\psi}, \quad Q_{12} = \frac{E_1\left(\nu_{21}+\nu_{23}\nu_{31}\right)}{\psi}, \quad Q_{13} = \frac{E_1\left(\nu_{31}+\nu_{21}\nu_{32}\right)}{\psi} \\ Q_{21} &= \frac{E_2\left(\nu_{12}+\nu_{13}\nu_{32}\right)}{\psi}, \quad Q_{22} = \frac{E_2\left(1-\nu_{13}\nu_{31}\right)}{\psi}, \quad Q_{23} = \frac{E_2\left(\nu_{12}\nu_{31}+\nu_{32}\right)}{\psi} \\ Q_{31} &= \frac{E_3\left(\nu_{13}+\nu_{12}\nu_{32}\right)}{\psi}, \quad Q_{32} = \frac{E_3\left(\nu_{13}\nu_{21}+\nu_{23}\right)}{\psi}, \quad Q_{33} = \frac{E_3\left(1-\nu_{12}\nu_{21}\right)}{\psi} \end{aligned} \tag{2.11}$$

$$Q_{44} = G_{12} \quad , \quad Q_{55} = G_{23} \quad , \quad Q_{66} = G_{13} \tag{2.12}$$

Where $\psi = 1 - \nu_{12}\nu_{21} - \nu_{13}\nu_{31} - \nu_{12}\nu_{23}\nu_{31} - \nu_{13}\nu_{21}\nu_{32} - \nu_{23}\nu_{32}$

Because of reciprocal relations, three of the engineering constants of equation (2.11) are dependent. Hereby the constitutive relation between the applied stresses and the resulting strains can be described by nine independent constants.

2.4.1 Transformation of constitutive properties

In Section 2.3 we defined two Cartesian coordinate systems in addition to the global, namely the principal material directions and the Material Coordinate System. These coordinate systems were introduced to simplify the constitutive description. The price to pay for this simplification is the need for transformations of constitutive properties. The transformations between the different coordinate systems are provided through transformation matrices as depicted in Figure 2.5. In the following each of the transformations are given some attention.

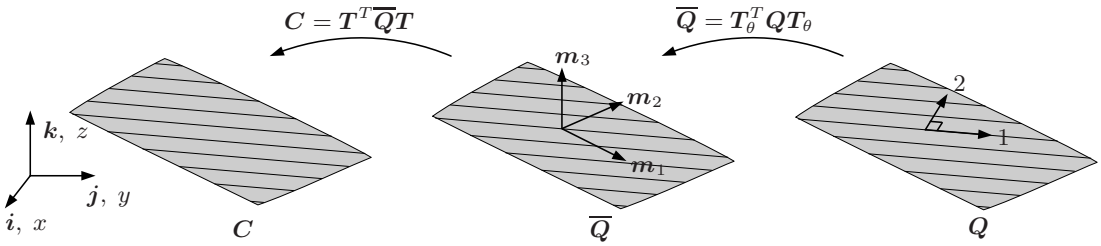

Figure 2.5: Transformation of constitutive properties between global, material and principal material coordinate system.

The transformation of constitutive properties from the material coordinate system to the global Cartesian coordinate system is achieved by the transformation shown in equation (2.13), see e.g. Cook et al. (2002).

$$\boldsymbol{T} = \begin{bmatrix} a_1^2 & b_1^2 & c_1^2 & a_1b_1 & b_1c_1 & c_1a_1 \\ a_2^2 & b_2^2 & c_2^2 & a_2b_2 & b_2c_2 & c_2a_2 \\ a_3^2 & b_3^2 & c_3^2 & a_3b_3 & b_3c_3 & c_3a_3 \\ 2a_1a_2 & 2b_1b_2 & 2c_1c_2 & a_1b_2 + a_2b_1 & b_1c_2 + b_2c_1 & c_1a_2 + c_2a_1 \\ 2a_2a_3 & 2b_2b_3 & 2c_2c_3 & a_2b_3 + a_3b_2 & b_2c_3 + b_3c_2 & c_2a_3 + c_3a_2 \\ 2a_1a_3 & 2b_1b_3 & 2c_1c_3 & a_1b_3 + a_3b_1 & b_1c_3 + b_3c_1 & c_1a_3 + c_3a_1 \end{bmatrix} \tag{2.13}$$

Here the entries of the transformation matrix are given by direction cosines based on the shortest angle regardless of sign, between the global coordinate system and the material coordinate system in the following way

$$\begin{aligned} a_1 &= \cos(\boldsymbol{i}, \boldsymbol{m}_1) & b_1 &= \cos(\boldsymbol{j}, \boldsymbol{m}_1) & c_1 &= \cos(\boldsymbol{k}, \boldsymbol{m}_1) \\ a_2 &= \cos(\boldsymbol{i}, \boldsymbol{m}_2) & b_2 &= \cos(\boldsymbol{j}, \boldsymbol{m}_2) & c_2 &= \cos(\boldsymbol{k}, \boldsymbol{m}_2) \\ a_3 &= \cos(\boldsymbol{i}, \boldsymbol{m}_3) & b_3 &= \cos(\boldsymbol{j}, \boldsymbol{m}_3) & c_3 &= \cos(\boldsymbol{k}, \boldsymbol{m}_3) \end{aligned} \tag{2.14}$$

If the analysis is to be applied to an orthotropic material the constitutive properties are most naturally given in principal material directions that are not necessarily oriented in the same direction as the material coordinate system. The principal material directions are rotated with respect to the material coordinate system by an angle θ around the normal, $\boldsymbol{m}_3$, which constitutes a plane rotation. The transformation matrix of a plane transformation is given by

$$\boldsymbol{T}_\theta = \begin{bmatrix} c^2 & s^2 & 0 & cs & 0 & 0 \\ s^2 & c^2 & 0 & -cs & 0 & 0 \\ 0 & 0 & 1 & 0 & 0 & 0 \\ -2cs & 2cs & 0 & c^2 - s^2 & 0 & 0 \\ 0 & 0 & 0 & 0 & c & -s \\ 0 & 0 & 0 & 0 & s & c \end{bmatrix} \tag{2.15}$$

Where the direction cosines for a plane rotation by use of trigonometric identities reduce to

$$c = \cos(\theta) \qquad s = \sin(\theta) \tag{2.16}$$

3

Finite elements in structural mechanics

The aim of this chapter is to derive the governing finite element equations of structural mechanics for linear static stress analysis. From the principle of virtual work, the governing equations are derived, which upon discretization results in the linear finite element equilibrium equations. Furthermore, a short introduction to linearized buckling analysis is given. It is assumed that the reader is familiar with the theory of elasticity and finite element theory and thus some of the basic concepts are stated and used without further proof.

3.1 Preliminaries

For the purpose of deriving the FE-equations used in linear elastic stress analysis we first recapitulate some of the basic definitions of linear elasticity. For an extensive treatment of this theory the reader is referred to e.g. Sokolnikoff (1946).

The general boundary value problem in solid mechanics is illustrated in Figure 3.1. Given some well-defined body whose geometry and material properties are known, determine the deformed configuration, stresses and strains upon external actions in terms of prescribed displacements and loads.

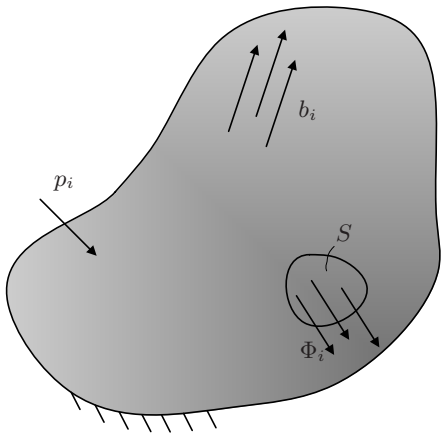

Figure 3.1: Boundary value problem in solid mechanics.

To solve the above we start by introducing the strain measure. When a body located in three-dimensional space is acted upon by forces an initial straight line segment within

the undeformed configuration will in general be subjected to translation, rotation and elongation or compression. The result of these deformations is the deformed configuration and a measure of deformation is given by the strain measure. An analysis of deformation, described in the coordinate system of the undeformed configuration, results in a second order tensor known as the Green-Lagrange strain tensor.

$$\varepsilon_{ij} = \tfrac{1}{2}\left(u_{i,j} + u_{j,i} + u_{k,i}u_{k,j}\right) \tag{3.1}$$

In linear elasticity deformations are assumed to be small and thus the deformation of the elastic body may be related to the undeformed configuration. Assuming the derivatives of the displacements, u, to be small compared to unity the last term of (3.1) may be omitted and we arrive at the linearized Green-Lagrange strain tensor.

$$\varepsilon_{ij} = \tfrac{1}{2}\left(u_{i,j} + u_{j,i}\right) \tag{3.2}$$

The strains are associated to stresses by a constitutive relation, in this case Hooke's generalized law applies since the material is assumed to be linear elastic. This relation was shown in Section 2.4 in matrix notation and is repeated here in index notation.

$$\sigma_{ij} = C_{ijkl}\varepsilon_{kl} \tag{3.3}$$

Here the constitutive matrix relates the Green-Lagrange strain to the Cauchy stress. In general, this does not apply since the stresses and strains should be work conjugate, i.e. the strain energy must be the same independent of the chosen stress/strain measure. Thus if Green-Lagrange strain, is used the stress measure should be the second Piola-Kirchoff stress tensor and similarly if the true strain measure is applied, stresses are described by the Cauchy stress definition. In the case of small strains, the error introduced by utilizing the Cauchy stress tensor in combination with Green-Lagrange strain is negligible.

The stresses within the body must be in equilibrium according to Newtons second law. Thus by observing an infinitesimal block at equilibrium, subjected to an arbitrary three-dimensional stress state and body forces b_i, it is found that equation (3.4) must be fulfilled. The block is assumed to be in static equilibrium and thus the acceleration term is omitted.

$$\sigma_{ji,j} + b_i = 0 \tag{3.4}$$

Equations (3.2), (3.3) and (3.4) constitutes the problem to be solved. Thus we need to determine three unknown displacements u_i, six stresses σ_{ij} and six strains ε_{ij} that fulfil the boundary conditions of the problem, i.e. prescribed displacements and tractions at the boundary of the continuum. The surface tractions are related to the internal stresses by

$$\Phi_i = \sigma_{ji}n_j \tag{3.5}$$

where n_j is the surface unit normal.

Remark that the six strains are given in terms of three displacements, which requires a set of compatibility equations also to be obeyed. The governing equations presented above in combination with the boundary conditions are referred to as the *strong form* of the BVP since the equations must be met at each point within the body.

3.2 Energy considerations and variational methods

To derive the FE equilibrium equations the principle of virtual work is applied. The principle of virtual work may be derived from the equilibrium equation (3.4) as done in e.g Przemieniecki (1968) or Zienkiewicz (1977). It is often referred to as the *weak form*, since the equilibrium equations are only satisfied in an integral sense.

Assuming the continuum to be at an equilibrium state (for simplicity assumed to be quasi-static) a virtual kinematically admissible displacement δu_i is imposed and it is stated that the equilibrium equations must be fulfilled in integral sense.

$$\int_V \sigma_{ij,j}\delta u_i \, dV + \int_V b_i \delta u_i \, dV = 0 \tag{3.6}$$

Utilising the rules of product differentiation on the first term

$$\int_V \left((\sigma_{ij}\delta u_i)_{,j} - \sigma_{ij}\delta u_{i,j} \right) \, dV + \int_V b_i \delta u_i \, dV = 0 \tag{3.7}$$

By use of Gauss' divergence theorem which relates a surface integral to a volume integral and the fact that $\delta u_{i,j} = \delta \varepsilon_{ij}$, the *principle of virtual work* arises

$$\int_V \sigma_{ij}\delta\varepsilon_{ij} \, dV = \int_V b_i \delta u_i \, dV + \int_S \Phi_i \delta u_i \, dS \tag{3.8}$$

The principle of virtual work states that at equilibrium the work done by external forces during a virtual displacement must equal the work done by internal forces. This principle constitutes the most general statement of equilibrium and assumes no specific constitutive law. In the next section we introduce a finite element discretization to equation (3.8) and thereby obtain the equilibrium equations in FE form.

3.3 Discretization

For arbitrary boundary value problems equation (3.8) is not solvable analytically. To circumvent this the continuum is discretized into a number of finite elements, see Figure 3.2. The idea of discretizing the structure into finite elements is that instead of seeking continuous functions for the displacement field throughout the domain we seek a solution at discrete nodal points and interpolate geometry and displacements element-wise between nodal points. To obtain the solution at the nodal point a sparse system of linear equations must be solved which is done efficiently by a digital computer.

3.3.1 Interpolation and shape functions

To interpolate from nodal degrees of freedom within an element the concept of shape functions is introduced. For an extensive description of shape functions the reader is referred to e.g. Zienkiewicz (1977) or Cook et al. (2002). Shape functions used in interpolating geometry and displacement of the 9- and 16-node isoparametric elements are given in Appendix A.

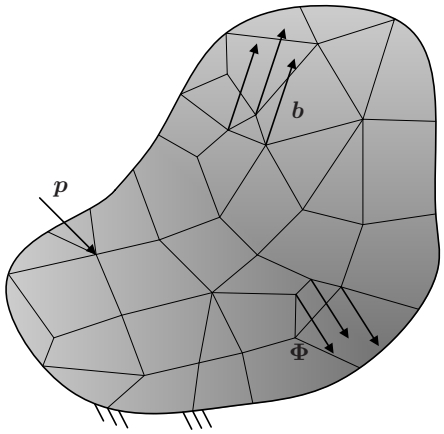

Figure 3.2: Discretized boundary value problem in solid mechanics.

The main idea is that each node within the element has a corresponding shape function that evaluates to 1 (and all other to 0) at it's node. For coordinates not belonging to a node, each shape function will have a positive value and the sum of all shape functions equals 1. Thus the shape functions may be seen as weight factors on the contribution from each node.

If we by $\boldsymbol{x}$ denote the approximated geometry within a finite element, the geometry is interpolated from the shape function matrix $\boldsymbol{N}_a$ and the nodal coordinates $\boldsymbol{x}_a$ by

$$\boldsymbol{x} = \begin{Bmatrix} x \\ y \\ z \end{Bmatrix} = \boldsymbol{N}_a \boldsymbol{x}_a \tag{3.9}$$

Where a is a node index, indicating summation.

For isoparametric elements, geometry and displacements within the element are interpolated by the same shape functions. Thereby internal displacements are interpolated from discrete nodal displacements by

$$\boldsymbol{u} = \begin{Bmatrix} u \\ v \\ w \end{Bmatrix} = \boldsymbol{N}_a \boldsymbol{d}_a \tag{3.10}$$

The node index, a, is omitted in the following. Strains within each element may be determined as derivatives of equation (3.10)

$$\boldsymbol{\varepsilon} = \boldsymbol{\partial N d} \equiv \boldsymbol{B d} \tag{3.11}$$

Where $\boldsymbol{B}$ is the strain-displacement matrix obtained as the derivatives of the shape functions, with respect to *global coordinates*. Here denoted by the partial differential operator, $\boldsymbol{\partial}$.

The interpolations introduced above are used to discretize the governing equations.

3.3.2 Discrete governing equations

To derive the discrete governing equations *for an element*, the principle of virtual work from (3.8) is written in matrix notation.

$$\int_V \delta\boldsymbol{\varepsilon}^T\boldsymbol{\sigma}\, dV = \int_V \delta\boldsymbol{u}^T\boldsymbol{b}\, dV + \int_S \delta\boldsymbol{u}^T\boldsymbol{\Phi}\, dS + \delta\boldsymbol{d}^T\boldsymbol{p} \tag{3.12}$$

where the last appended term contains applied concentrated nodal loads.

Kinematically admissible variations of the interpolated displacements and strains within each element, equation (3.10) and (3.11) are inserted in equation (3.12) and re-arrangement yields.

$$\delta\boldsymbol{d}^T\left(\int_V \boldsymbol{B}^T\boldsymbol{\sigma}\, dV - \int_V \boldsymbol{N}^T\boldsymbol{b}\, dV - \int_S \boldsymbol{N}^T\boldsymbol{\Phi}\, dS - \boldsymbol{p}\right) = \boldsymbol{0} \tag{3.13}$$

Since this must hold for arbitrary virtual displacements, $\delta\boldsymbol{d}^T$, the term within the bracket must equal zero. Substitute Hooke's law, equation (2.8) along with the strain-displacement relation, equation (3.11), i.e. $\boldsymbol{\sigma} = \boldsymbol{C}\boldsymbol{\varepsilon} = \boldsymbol{C}\boldsymbol{B}\boldsymbol{d}^e$ and re-arrange to obtain.

$$\int_V \boldsymbol{B}^T\boldsymbol{C}\boldsymbol{B}\, dV\boldsymbol{d}^e = \int_V \boldsymbol{N}^T\boldsymbol{b}\, dV + \int_S \boldsymbol{N}^T\boldsymbol{\Phi}\, dS + \boldsymbol{p} \Rightarrow \tag{3.14}$$

$$\boldsymbol{K}^e\boldsymbol{d}^e = \boldsymbol{r}^e \tag{3.15}$$

where the element stiffness matrix $\boldsymbol{K}^e$ and the equivalent nodal load vector $\boldsymbol{r}^e$ are given by

$$\boldsymbol{K}^e = \int_V \boldsymbol{B}^T\boldsymbol{C}\boldsymbol{B}\, dV \tag{3.16}$$

$$\boldsymbol{r}^e = \int_V \boldsymbol{N}^T\boldsymbol{b}\, dV + \int_S \boldsymbol{N}^T\boldsymbol{\Phi}\, dS + \boldsymbol{p} \tag{3.17}$$

As described in e.g. Hughes (2000) the element stiffness matrix $\boldsymbol{K}^e$ and the equivalent nodal load vector $\boldsymbol{r}^e$ can be assembled to form the global stiffness matrix and the global vector of equivalent nodal loads

$$\boldsymbol{K} = \sum_{e=1}^{N^e} \boldsymbol{K}^e \qquad \boldsymbol{r} = \sum_{e=1}^{N^e} \boldsymbol{r}^e \tag{3.18}$$

Whereby the global system of linear equations to be solved is

$$\boldsymbol{K}\boldsymbol{d} = \boldsymbol{r} \tag{3.19}$$

Here $\boldsymbol{d}$ is a column vector containing all nodal degrees of freedom (with length equal to nodal degrees of freedom n_{DOF}), $\boldsymbol{r}$ is a column vector of length n_{DOF} containing consistent nodal loads and $\boldsymbol{K}$ is the symmetric global stiffness matrix of dimension $n_{DOF} \times n_{DOF}$.

3.3.3 Stress recovery

Having solved for nodal displacements in equation (3.19), strains within each element are determined from equation (3.11). Thus stresses are obtained via Hooke's law in matrix form

$$\boldsymbol{\sigma} = \boldsymbol{CBd} \tag{3.20}$$

In displacement based finite element solutions the accuracy of stresses and strains is an order lower than that of the displacements since stresses are derived from displacements via strains. It has been shown that at some points within the element stresses are super convergent, i.e. of comparable accuracy to that of displacements. Stresses are calculated at these point and inter-/extrapolated to the remaining domain of the element. For isoparametric elements these super-convergent points are the Gauss points of one quadrature order lower than that required for full integration.

3.4 Linearized buckling

So far, the presentation has been limited to linear static stress analysis and we implicitly assumed that the structure comes to rest at a stable position of equilibrium. It is a well-known phenomenon that slender members loaded in compression may fail in buckling by sudden conversion of membrane strain energy to bending strain energy. In this section we address the issue of linearized bifurcation buckling analysis which may be used in case of small deformations and no imperfections. The critical load determined from a linear buckling analysis will always be an upper limit on the load-carrying capacity of the structure since inevitable imperfections in real structures tend to reduce the actual capacity. It turns out that the linearized buckling problem constitutes a linear eigenvalue problem.

Under the assumptions made in linear elastic analysis where *equilibrium is set up for the undeformed configuration* of the structure, certain possibly important effects are not accounted for. In linear analysis it is assumed that the stiffness is independent of the state of deformation and stresses. A more thorough description, which is beyond the scope of this presentation, accounts for a gradual change of stiffness with deformation by describing the *equilibrium of the deformed configuration*. Such a description is given within the framework of a fully geometrically non-linear theory, see e.g. Zienkiewicz (1977). In this section we take a first step into the geometrically non-linear regime by studying the linearized buckling problem. The basic idea in linearized buckling analysis is that the net stiffness of a structure is composed of the stiffness from geometry and material and some contribution (or reduction) stemming from the current state of loading and deformation. The first stiffness is the one introduced above as the stiffness matrix $\boldsymbol{K}$ whereas the additional contribution to the net stiffness is accounted for by the so-called initial stress stiffness matrix, $\boldsymbol{K}_\sigma$ or the geometrical stiffness matrix. So, the net stiffness of the structure is

$$\boldsymbol{K}_{net} = \boldsymbol{K} + \lambda \boldsymbol{K}_\sigma \tag{3.21}$$

where the stress stiffness matrix is

$$\boldsymbol{K}_\sigma = \int_V \boldsymbol{G}^T \boldsymbol{S} \boldsymbol{G} \, dV \tag{3.22}$$

Here, $\boldsymbol{G}$ is a matrix with shape function derivatives with respect to global coordinates and $\boldsymbol{S}$ is the initial stress matrix containing the stresses as obtained from a static stress analysis of some reference load, $\boldsymbol{r}_0$

$$\boldsymbol{S} = \begin{bmatrix} \sigma_x \boldsymbol{I}_3 & \tau_{xy}\boldsymbol{I}_3 & \tau_{xz}\boldsymbol{I}_3 \\ & \sigma_y \boldsymbol{I}_3 & \tau_{yz}\boldsymbol{I}_3 \\ sym. & & \sigma_z \boldsymbol{I}_3 \end{bmatrix} \tag{3.23}$$

We shall not derive the general expression of the stress stiffness matrix. Instead, a physical interpretation of the seemingly abstract mathematics is given.

From equation (3.21) and (3.22) it is seen that the contribution to the net stiffness from $\boldsymbol{K}_\sigma$ depends on the amplification of the reference load, $\boldsymbol{r} = \lambda \boldsymbol{r}_0$. Compressive stresses tend to reduce the net stiffness and at some critical load level, λ_{cr}, the net stiffness becomes singular with respect to the eigenvector of deformations, $\boldsymbol{\phi}$. This corresponds to an eigenvalue problem where we are interested in the critical amplification factor λ_{cr} that causes the structure to buckle without any change in applied nodal loads, i.e. a non-trivial solution to

$$(\boldsymbol{K} + \lambda_j \boldsymbol{K}_\sigma)\, \boldsymbol{\phi}_j = \boldsymbol{0}; \qquad j = 1, 2, ..., n_{DOF} \tag{3.24}$$

where $\boldsymbol{\phi}$ is the j'th eigenvector which defines the buckling mode shape but not the magnitude of displacements in the buckled configuration.

3.5 Numerical integration of element matrices

In this section we introduce the concept of natural coordinates and Gauss quadrature as used in evaluating element matrices. In the following we focus on evaluation of the element stiffness matrix since it illustrates the principles used to evaluate element matrices. For a more extensive treatment the reader is referred to Zienkiewicz (1977) or Cook et al. (2002).

For the FE method to be useful in an industrial context it should be applicable to all types of geometries and loading conditions. This does not comply with the fact that convergence can not be ensured for distorted meshes. In fact, distorted meshes are virtually unavoidable if elements are formulated in Cartesian coordinates. The workaround to this problem is to introduce natural coordinates since this ensures convergence Zienkiewicz (1977).

The natural coordinates are introduced as a mapping of the physical xyz-coordinates. Figure 3.3 A) shows an arbitrary distorted element in the physical (x, y) Cartesian coordinate system with a curved natural coordinate system, and B) shows the same element in the natural (r, s)-coordinate system. It is important that the mapping is unique, which poses some restrictions on allowable element distortion. Introduction of natural coordinates also means that element boundaries are described very simple. All element boundaries have one of their natural coordinates fixed equal to ± 1 resulting in simple limits of integration for element matrices that hereby run from -1 to 1. This is the first step towards utilizing Gauss quadrature in the evaluation of element matrices.

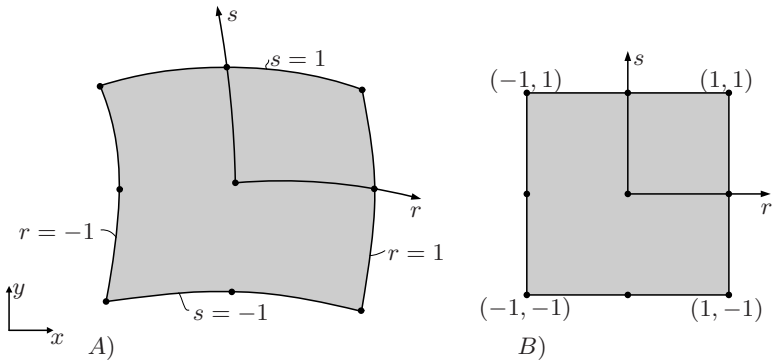

Figure 3.3: Illustration of element in A) Cartesian coordinate system and B) the same element in natural coordinates.

To change integration variables from global Cartesian coordinates to natural coordinates, the Jacobian determinant $|\boldsymbol{J}|$ is introduced. The Jacobian determinant relates the volume in the global coordinate system to the corresponding volume in the natural coordinate system, i.e. $dxdydz = |J|drdsdt$.

$$\boldsymbol{K}^e = \int_V \boldsymbol{B}^T\boldsymbol{C}\boldsymbol{B}\, dV = \int_{-1}^{1}\int_{-1}^{1}\int_{-1}^{1} \boldsymbol{B}^T\boldsymbol{C}\boldsymbol{B}\,|\boldsymbol{J}|\; drdsdt \tag{3.25}$$

As introduced in equation (3.11) the strain-displacement matrix, $\boldsymbol{B}$, contains derivatives of the shape functions with respect to global coordinates. To proceed, the derivatives with respect to natural coordinates are obtained by use of the chain rule of differentiation which reveals a way to obtain derivatives with respect to global coordinates.

$$\begin{Bmatrix} \frac{\partial \boldsymbol{N}}{\partial r} \\ \frac{\partial \boldsymbol{N}}{\partial s} \\ \frac{\partial \boldsymbol{N}}{\partial t} \end{Bmatrix} = \underbrace{\begin{bmatrix} \frac{\partial x}{\partial r} & \frac{\partial y}{\partial r} & \frac{\partial z}{\partial r} \\ \frac{\partial x}{\partial s} & \frac{\partial y}{\partial s} & \frac{\partial z}{\partial s} \\ \frac{\partial x}{\partial t} & \frac{\partial y}{\partial t} & \frac{\partial z}{\partial t} \end{bmatrix}}_{\equiv \boldsymbol{J}} \begin{Bmatrix} \frac{\partial \boldsymbol{N}}{\partial x} \\ \frac{\partial \boldsymbol{N}}{\partial y} \\ \frac{\partial \boldsymbol{N}}{\partial z} \end{Bmatrix} = \begin{bmatrix} \boldsymbol{g}_1 \\ \boldsymbol{g}_2 \\ \boldsymbol{g}_3 \end{bmatrix} \begin{Bmatrix} \frac{\partial \boldsymbol{N}}{\partial x} \\ \frac{\partial \boldsymbol{N}}{\partial y} \\ \frac{\partial \boldsymbol{N}}{\partial z} \end{Bmatrix} \tag{3.26}$$

Here it is seen that the entries of the Jacobian matrix $\boldsymbol{J}$ may be formed from the covariant tangent base vectors, $\boldsymbol{g}_i$, defined in Section 2.2.

By rearranging equation (3.26) it is seen that the derivatives of the shape function matrix with respect to global coordinates may be replaced by the inverse Jacobian matrix multiplied by derivatives with respect to natural coordinates.

$$\begin{Bmatrix} \frac{\partial \boldsymbol{N}}{\partial x} \\ \frac{\partial \boldsymbol{N}}{\partial y} \\ \frac{\partial \boldsymbol{N}}{\partial z} \end{Bmatrix} = \boldsymbol{J}^{-1} \begin{Bmatrix} \frac{\partial \boldsymbol{N}}{\partial r} \\ \frac{\partial \boldsymbol{N}}{\partial s} \\ \frac{\partial \boldsymbol{N}}{\partial t} \end{Bmatrix} \tag{3.27}$$

Derivatives with respect to natural coordinates are readily available when the shape functions are formulated in natural coordinates as shown in Appendix A.

Now, the integral in equation (3.25) can be evaluated by Gauss quadrature with which an integral with integration limits from -1 to 1 can be replaced by a sum of integrand

samplings multiplied by appropriate weight factors. Thus equation (3.25) is evaluated as

$$\boldsymbol{K}^e \approx \sum_{i=1}^{m}\sum_{j=1}^{n}\sum_{k=1}^{o} w_i w_j w_k \boldsymbol{B}^T \boldsymbol{C} \boldsymbol{B} \, |\boldsymbol{J}| \tag{3.28}$$

3.6 Summary

In this chapter the governing equations of linear static stress analysis by finite elements have been presented. In addition, the linearized buckling problem is established followed by an introduction to numerical evaluation of element matrices. In the next chapter the formulation of degenerated shell elements is presented as a specialization of the developments above.

4

Shell elements

Finite element analysis of shell structures is an active field of research and continuing progress and development is evident. This chapter describes the formulation of continuum based shell elements also called degenerated solid elements first introduced by Ahmad et al. (1970). The geometry and displacement interpolation of degenerated isoparametric shell elements is given along with a description of the definition of the so-called director coordinate system. Subsequently, three integration schemes are presented and it is shown how they are applied to obtain element matrices. Eventually, the reduced constitutive relations for degenerated shell elements are developed and lamination parameters are introduced as an alternative parametrization of the element stiffness matrix. All of the above is valid for laminated shell elements with layer-wise constant thickness layers.

4.1 Continuum-based shell elements

The idea of the degeneration concept is to eliminate nodes from a solid element by imposing on it kinematic constraints and assumptions, that represent shell-like behaviour.

In principle a shell structure is a special type of solid structure and one may be tempted to model the structure by solid elements as shown in Figure 4.1, *A*). However, quadratic displacement variation through the thickness seems unnecessary considering the fact that normals virtually remain straight and undeformed even for thick shell structures. Thus it is natural to model shell structures by solids whose top and bottom edges are curved whereas edges in the thickness direction are straight lines as shown in Figure 4.1, *B*). Both approaches pose difficulties in that stiffness in the thickness direction for thin shells is considerably lower than in-plane stiffness which leads to ill-conditioning. The remedy is to introduce another assumption, namely that of normals being inextensible and consequently the displacement through the thickness of the shell may be described in terms of displacements and rotations of nodes, see Figure 4.1 *C*), on the *reference surface*. The assumptions introduced in the degeneration process resemble the kinematic assumptions employed in FSDT plate theories as introduced in Section 2.1.

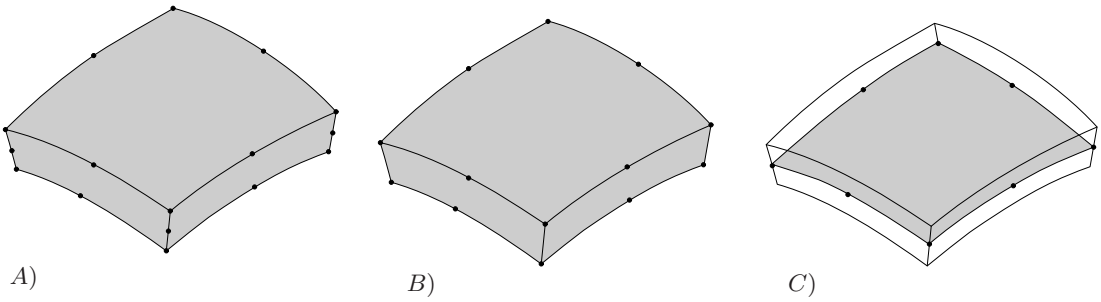

Figure 4.1: Degeneration process of A) 20-node solid element to B) 16-node solid element to C) 8-node shell element.

As we will show soon, the degeneration process leads to five degrees of freedom at each node of the reference surface. Three translations of the node and two rotations of the node director. In the attempt to model curved geometries with linear elements or when modelling junctions, the node directors at a common node of adjacent elements may differ. This has the consequence that node rotations α and β are defined different in the common node of the adjacent elements. The result is a discontinuity in the displacement field which is undesirable. The fix implemented in MUST is to average adjacent node directors to obtain a single node director definition at each node. Of course this is an approximation that is acceptable if the difference in adjacent node director orientations is small. In case of modelling curved geometries, the common averaged node director comes closer to each of the original node directors with mesh refinement. For junctions, no improvement is gained in this way. The problem may be solved by introducing a 6'th nodal degree of freedom. This 6'th degree of freedom, however, is associated with a non-physical drilling stiffness. The issue may be solved in various ways. In most commercial programs an artificial non-physically based stiffness is associated to the drilling stiffness whereas other more theoretically based approaches make use of e.g. the Hu-Washizu principle in the formulation of elements. So far, none of these measures have been taken in MUST.

The remaining of this chapter is devoted to details of the isoparametric degenerated shell element formulation and explicit integration through the thickness.

4.1.1 Geometry

In the element shown in Figure 4.2, a curvilinear coordinate system (r, s, t) is defined. Having defined the element in Figure 4.2 in terms of global nodal coordinates the need arises to describe the global coordinates of *internal* points given by natural curvilinear coordinates.

The relation between the coordinates of a point given in a curvilinear basis (r, s, t) and it's corresponding coordinates in global Cartesian coordinates $\boldsymbol{x} = \lfloor x, y, z \rfloor^T$ is

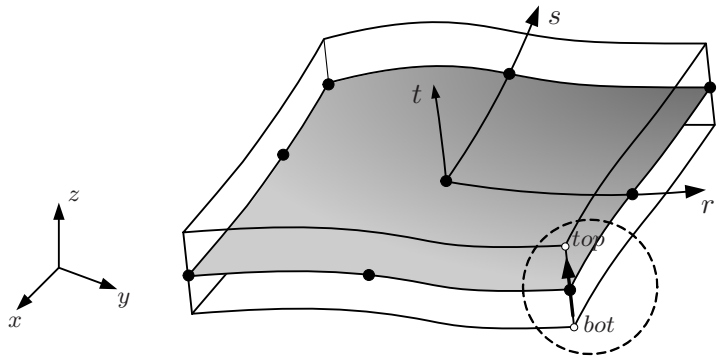

Figure 4.2: Degenerated shell element with curvilinear coordinate system and definition of top and bottom node location.

interpolated from global nodal coordinates $\boldsymbol{x}_a$ with the shape functions of Appendix A.

$$\begin{aligned}\boldsymbol{x}\,(r,s,t) &= \sum_a N_a(r,s)\left(\tfrac{1+t}{2}\boldsymbol{x}_a^{top} + \tfrac{1-t}{2}\boldsymbol{x}_a^{bot}\right)\\ &= \sum_a N_a\left(\tfrac{1}{2}\left(\boldsymbol{x}_a^{top} + \boldsymbol{x}_a^{bot}\right) + \tfrac{t}{2}\left(\boldsymbol{x}_a^{top} - \boldsymbol{x}_a^{bot}\right)\right)\end{aligned} \tag{4.1}$$

For the sake of brevity the indication of (r,s)-dependency has been omitted in the resulting expression and will be so in the remaining of the text. The first inner term corresponds to the *coordinates of the reference surface nodes*

$$\boldsymbol{x}_a = \tfrac{1}{2}\left(\boldsymbol{x}_a^{top} + \boldsymbol{x}_a^{bot}\right) \tag{4.2}$$

The second inner term in equation (4.1) represents a vector from the bottom to the top node. In each node this vector is normalized by the nodal shell thickness h_a to define the so-called *node director* $\boldsymbol{v}_3^a$

$$\boldsymbol{v}_3^a = \tfrac{1}{h_a}\left(\boldsymbol{x}_a^{top} - \boldsymbol{x}_a^{bot}\right) \tag{4.3}$$

Consequently, the geometry has been degenerated and is now described in terms of reference surface nodal coordinates, node directors and nodal shell thicknesses.

$$\boldsymbol{x} = \begin{Bmatrix} x \\ y \\ z \end{Bmatrix} = \sum_a N_a\left(\boldsymbol{x}_a + \tfrac{t}{2}h_a\boldsymbol{v}_3^a\right) \tag{4.4}$$

In practice node directors are not calculated by degeneration of top and bottom nodes of solid elements. Rather node directors are determined on basis of the reference surface geometry as shown below in equation (4.5).

4.1.2 Director coordinate system

In each node a local *Cartesian* coordinate system called the *director coordinate system* is set up. The purpose of this coordinate system is to define axes of rotational degrees

of freedom of the node director. Its third axis is the node director introduced above. This section describes how the node director and the two other axes are established.

In each node of the element the node director (indicating the thickness direction of the element) is defined as the unit normal of the reference surface tangent plane at the node as defined in equation (2.3).

$$\boldsymbol{v}_3^a = \frac{\boldsymbol{g}_1^a \times \boldsymbol{g}_2^a}{|\boldsymbol{g}_1^a \times \boldsymbol{g}_2^a|} \tag{4.5}$$

where the covariant tangent base vectors are interpolated by $\boldsymbol{g}_1^a = \sum_a N_{a,r} x_i^a$ and $\boldsymbol{g}_2^a = \sum_a N_{a,s} x_i^a$.

To complete the local Cartesian coordinate system two other unit base vectors must be determined uniquely. Several schemes for this task exist since the choice of the two remaining base vectors is arbitrary as long as they form an orthonormal base with $\boldsymbol{v}_3^a$. The following scheme is used by default in MUST, see Jensen et al. (2002). If $\boldsymbol{v}_3^a = \pm\boldsymbol{j}$ then the two other mutually orthogonal base vectors are given by $\boldsymbol{v}_2^a = \boldsymbol{i}$ and $\boldsymbol{v}_1^a = \boldsymbol{k}$. Otherwise the base vectors are determined as $\boldsymbol{v}_1^a = \frac{\boldsymbol{j}\times\boldsymbol{v}_3^a}{|\boldsymbol{j}\times\boldsymbol{v}_3^a|}$ and $\boldsymbol{v}_2^a = \boldsymbol{v}_3^a \times \boldsymbol{v}_1^a$.

$\boldsymbol{v}_1^a$ and $\boldsymbol{v}_2^a$ are used to define two rotational degrees of freedom of the director vector $\boldsymbol{v}_3^a$ as it is shown below.

4.1.3 Displacement field

By definition displacement is the difference between the position of a point in deformed and undeformed configuration, respectively. If we by pre-subscript "$*$" denote the deformed configuration with respect to an undeformed configuration (no pre-subscript) and introduce the degenerated description of the shell geometry from (4.4) we may write

$$\begin{aligned}
\boldsymbol{u} &= {}_*\boldsymbol{x} - \boldsymbol{x} && (4.6)\\
&= \sum_a N_a \left({}_*\boldsymbol{x}_a - \boldsymbol{x}_a\right) + \sum_a N_a \tfrac{t}{2} h_a \left({}_*\boldsymbol{v}_3^a - \boldsymbol{v}_3^a\right) && (4.7)\\
&= \sum_a N_a \boldsymbol{u}_a + \sum_a N_a \tfrac{t}{2} h_a \left({}_*\boldsymbol{v}_3^a - \boldsymbol{v}_3^a\right) && (4.8)
\end{aligned}$$

In the expression above the $\boldsymbol{u}^a$ ='s are translational nodal degrees of freedom and the last term represents the relative displacement of the node directors. Thus the displacement of an arbitrary point within the shell is represented as an interpolation of nodal displacements and relative displacements of node directors. Now we correlate the relative displacement of the director vector to two rotational nodal degrees of freedom. The two degrees of freedom are the rotations of the director vector $\boldsymbol{v}_3^a$ around $\boldsymbol{v}_1^a$ and $\boldsymbol{v}_2^a$ respectively, see Figure 4.3.

If rotations are assumed to be small, $\sin(\alpha) \approx \alpha$, a rotation of $\boldsymbol{v}_3^a$ around $\boldsymbol{v}_1^a$ by α results in a relative global displacement

$${}_\alpha\boldsymbol{u}_a = -\alpha \boldsymbol{v}_2^a \tag{4.9}$$

A small rotation β around $\boldsymbol{v}_2^a$ results in a relative global displacement

$$_{\beta}\boldsymbol{u}_a = \beta \boldsymbol{v}_1^a \tag{4.10}$$

i.e. a relative global displacement due to α and β of

$$_{*}\boldsymbol{v}_3^a - \boldsymbol{v}_3^a = \beta \boldsymbol{v}_1^a - \alpha \boldsymbol{v}_2^a \tag{4.11}$$

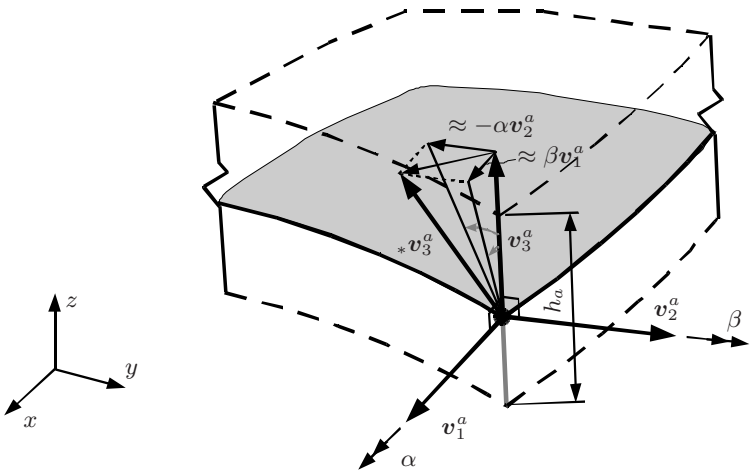

Figure 4.3: Resulting global displacements due to nodal rotations of $\boldsymbol{v}_3$.

This result is inserted in equation (4.8)

$$\boldsymbol{u} = \sum_a N_a \boldsymbol{u}_a + \sum_a N_a \tfrac{t}{2} h_a \left(\beta \boldsymbol{v}_1^a - \alpha \boldsymbol{v}_2^a\right) \tag{4.12}$$

Thus the displacement of each point in the shell is related to five degrees of freedom at each node. As shown previously in equation (3.10) this is written as

$$\boldsymbol{u} = \begin{Bmatrix} u \\ v \\ w \end{Bmatrix} = \boldsymbol{N}\boldsymbol{d} \tag{4.13}$$

where the shape function matrix is

$$\boldsymbol{N} = \left[\cdots \left| \begin{matrix} N_a & 0 & 0 & -N_a \frac{h_a}{2} t v_{21}^a & N_a \frac{h_a}{2} t v_{11}^a \\ 0 & N_a & 0 & -N_a \frac{h_a}{2} t v_{22}^a & N_a \frac{h_a}{2} t v_{12}^a \\ 0 & 0 & N_a & -N_a \frac{h_a}{2} t v_{23}^a & N_a \frac{h_a}{2} t v_{13}^a \end{matrix} \right| \cdots \right] \tag{4.14}$$

and the nodal degrees of freedom are collected in a vector

$$\boldsymbol{d} = \left\lfloor \cdots \left\lfloor u^a \quad v^a \quad w^a \quad \alpha^a \quad \beta^a \right\rfloor \cdots \right\rfloor^T \tag{4.15}$$

Having described the displacement throughout the shell in terms of nodal displacements the next step is to relate nodal displacements to displacement derivatives needed for strain evaluation.

4.1.4 Strain-displacement relations

Strains are given in terms of displacement derivatives

$$\begin{aligned}\{\varepsilon\} &= \lfloor \varepsilon_x \quad \varepsilon_y \quad \varepsilon_z \quad \gamma_{xy} \quad \gamma_{yz} \quad \gamma_{zx} \rfloor^T = \lfloor \varepsilon_x \quad \varepsilon_y \quad \varepsilon_z \quad 2\varepsilon_{xy} \quad 2\varepsilon_{yz} \quad 2\varepsilon_{zx} \rfloor^T \\ &= \lfloor u_{,x} \quad v_{,y} \quad w_{,z} \quad u_{,y}+v_{,x} \quad v_{,z}+w_{,y} \quad u_{,z}+w_{,x} \rfloor^T \end{aligned} \tag{4.16}$$

Now we need to express derivatives of the displacements with respect to global coordinate axes.

By the chain rule of differentiation the displacement derivatives with respect to global Cartesian coordinates are given by displacement derivatives with respect to natural coordinates multiplied by the derivatives of natural coordinates with respect to global coordinates, i.e. $\frac{\partial \boldsymbol{u}}{\partial \boldsymbol{x}} = \frac{\partial \boldsymbol{u}}{\partial \boldsymbol{r}} \frac{\partial \boldsymbol{r}}{\partial \boldsymbol{x}}$. The first term on the right-hand side is given below in (4.19) and the second term is obtained as the inverse Jacobian matrix.

$$\begin{Bmatrix} u_{,x} \\ u_{,y} \\ u_{,z} \\ v_{,x} \\ v_{,y} \\ v_{,z} \\ w_{,x} \\ w_{,y} \\ w_{,z} \end{Bmatrix} = \begin{bmatrix} \boldsymbol{J}^{-1} & \boldsymbol{0} & \boldsymbol{0} \\ \boldsymbol{0} & \boldsymbol{J}^{-1} & \boldsymbol{0} \\ \boldsymbol{0} & \boldsymbol{0} & \boldsymbol{J}^{-1} \end{bmatrix} \begin{Bmatrix} u_{,r} \\ u_{,s} \\ u_{,t} \\ v_{,r} \\ v_{,s} \\ v_{,t} \\ w_{,r} \\ w_{,s} \\ w_{,t} \end{Bmatrix} = \boldsymbol{\Gamma}_{uvw} \begin{Bmatrix} u_{,r} \\ u_{,s} \\ u_{,t} \\ v_{,r} \\ v_{,s} \\ v_{,t} \\ w_{,r} \\ w_{,s} \\ w_{,t} \end{Bmatrix} \tag{4.17}$$

where $\boldsymbol{J}$ is the Jacobian matrix whose entries are evaluated from the geometry interpolation in (4.4).

$$\begin{aligned} \boldsymbol{J} &= \begin{bmatrix} \frac{\partial x}{\partial r} & \frac{\partial y}{\partial r} & \frac{\partial z}{\partial r} \\ \frac{\partial x}{\partial s} & \frac{\partial y}{\partial s} & \frac{\partial z}{\partial s} \\ \frac{\partial x}{\partial t} & \frac{\partial y}{\partial t} & \frac{\partial z}{\partial t} \end{bmatrix} \\ &= \sum_a \begin{bmatrix} N_{a,r}\left(x^a + \frac{t}{2} h_a v_{31}^a\right) & N_{a,r}\left(y^a + \frac{t}{2} h_a v_{32}^a\right) & N_{a,r}\left(z^a + \frac{t}{2} h_a v_{33}^a\right) \\ N_{a,s}\left(x^a + \frac{t}{2} h_a v_{31}^a\right) & N_{a,s}\left(y^a + \frac{t}{2} h_a v_{32}^a\right) & N_{a,s}\left(z^a + \frac{t}{2} h_a v_{33}^a\right) \\ N_a \frac{1}{2} h_a v_{31}^a & N_a \frac{1}{2} h_a v_{32}^a & N_a \frac{1}{2} h_a v_{33}^a \end{bmatrix} \end{aligned} \tag{4.18}$$

In (4.17) the derivatives of displacements with respect to natural coordinates are obtained by differentiation of (4.13) with only the shape function matrix depending on the natural coordinates (r, s).

$$\begin{Bmatrix} u_{,r} \\ u_{,s} \\ u_{,t} \\ v_{,r} \\ v_{,s} \\ v_{,t} \\ w_{,r} \\ w_{,s} \\ w_{,t} \end{Bmatrix} = \left[\begin{array}{c|ccccc|c} & N_{a,r} & 0 & 0 & -N_{a,r}\frac{h_a}{2}tv_{21}^a & N_{a,r}\frac{h_a}{2}tv_{11}^a & \\ & N_{a,s} & 0 & 0 & -N_{a,s}\frac{h_a}{2}tv_{21}^a & N_{a,s}\frac{h_a}{2}tv_{11}^a & \\ & 0 & 0 & 0 & -N_a\frac{h_a}{2}v_{21}^a & -N_a\frac{h_a}{2}v_{11}^a & \\ & 0 & N_{a,r} & 0 & -N_{a,r}\frac{h_a}{2}tv_{22}^a & N_{a,r}\frac{h_a}{2}tv_{12}^a & \\ \cdots & 0 & N_{a,s} & 0 & -N_{a,s}\frac{h_a}{2}tv_{22}^a & N_{a,s}\frac{h_a}{2}tv_{12}^a & \cdots \\ & 0 & 0 & 0 & -N_a\frac{h_a}{2}v_{22}^a & -N_a\frac{h_a}{2}v_{12}^a & \\ & 0 & 0 & N_{a,r} & -N_{a,r}\frac{h_a}{2}tv_{23}^a & N_{a,r}\frac{h_a}{2}tv_{13}^a & \\ & 0 & 0 & N_{a,s} & -N_{a,s}\frac{h_a}{2}tv_{23}^a & N_{a,s}\frac{h_a}{2}tv_{13}^a & \\ & 0 & 0 & 0 & -N_a\frac{h_a}{2}v_{23}^a & -N_a\frac{h_a}{2}v_{13}^a & \end{array}\right] \begin{Bmatrix} \vdots \\ u^a \\ v^a \\ w^a \\ \alpha^a \\ \beta^a \\ \vdots \end{Bmatrix} = \boldsymbol{F}\boldsymbol{d} \tag{4.19}$$

Now if we substitute (4.19) back into (4.17) we obtain the derivatives of the global displacements with respect to the global coordinates. Pre-multiplying by matrix $\boldsymbol{H}$ provides summation of displacement derivatives in order to obtain strains as shown in equation (4.16), i.e.

$$\boldsymbol{\varepsilon} = \boldsymbol{H}\boldsymbol{\Gamma}_{uvw}\boldsymbol{F}\boldsymbol{d} \equiv \boldsymbol{H}\boldsymbol{G}\boldsymbol{d} \equiv \boldsymbol{B}\boldsymbol{d} \tag{4.20}$$

where the auxiliary summation matrix $\boldsymbol{H}$ is given by

$$\boldsymbol{H} = \begin{bmatrix} 1 & 0 & 0 & 0 & 0 & 0 & 0 & 0 & 0 \\ 0 & 0 & 0 & 0 & 1 & 0 & 0 & 0 & 0 \\ 0 & 0 & 0 & 0 & 0 & 0 & 0 & 0 & 1 \\ 0 & 1 & 0 & 1 & 0 & 0 & 0 & 0 & 0 \\ 0 & 0 & 0 & 0 & 0 & 1 & 0 & 1 & 0 \\ 0 & 0 & 1 & 0 & 0 & 0 & 1 & 0 & 0 \end{bmatrix} \tag{4.21}$$

From equation (4.20) the strain-displacement matrix $\boldsymbol{B}$ is obtained by appropriate matrix multiplications of matrices developed above.

In the next section we further develop the interpolation matrix derivatives in $\boldsymbol{F}$ to obtain $\boldsymbol{B}$'s explicit thickness dependency which is used in Section 4.2.2.

Thickness dependency

To enable explicit thickness integration of element matrices we need to express $\boldsymbol{B}$'s thickness dependency explicitly. To do so matrix $\boldsymbol{F}$ is decomposed into two sub-matrices that are independent of the thickness coordinate. Furthermore the thickness variation of the inverse Jacobian matrix is assumed to be linear as done in Prema Kumar and Palaninathan (1997). Vlachoutsis (1990) showed that this assumption is reasonable for thin shells, i.e. $\left|\frac{h}{R}\right| \ll 1$. In Section 6.3.2 it is studied how low this ratio should be in order to obtain acceptable results.

For reasons that will become obvious later, a change in thickness coordinate variable from natural coordinate t to a physical thickness coordinate[1], z, is introduced, i.e. substitute z for $\frac{h_a}{2}t$ in $\boldsymbol{F}$. Thus it is possible to decompose $\boldsymbol{F}$ into $\boldsymbol{F}_1$ and $\boldsymbol{F}_2$ that are

[1]This z-coordinate should not be confused with the global z-coordinate. In the remaining, no distinction is made between thickness and global z since the difference should be obvious from the context.

independent of z and consequently express the z dependency of $\boldsymbol{F}$ explicitly. In doing so we also presume that the shell thickness h_a is constant throughout the element and denoted by h. This assumption, however, is not very restrictive since individual plies physically have constant thickness.

$$\boldsymbol{F} = \boldsymbol{F}_1 + z\boldsymbol{F}_2 \tag{4.22}$$

with

$$\boldsymbol{F}_1 = \left[\begin{array}{c|ccccc|c} & N_{a,r} & 0 & 0 & 0 & 0 & \\ & N_{a,s} & 0 & 0 & 0 & 0 & \\ & 0 & 0 & 0 & -N_a\frac{h_a}{2}v^a_{21} & -N_a\frac{h_a}{2}v^a_{11} & \\ & 0 & N_{a,r} & 0 & 0 & 0 & \\ \cdots & 0 & N_{a,s} & 0 & 0 & 0 & \cdots \\ & 0 & 0 & 0 & -N_a\frac{h_a}{2}v^a_{22} & -N_a\frac{h_a}{2}v^a_{12} & \\ & 0 & 0 & N_{a,r} & 0 & 0 & \\ & 0 & 0 & N_{a,s} & 0 & 0 & \\ & 0 & 0 & 0 & -N_a\frac{h_a}{2}v^a_{23} & -N_a\frac{h_a}{2}v^a_{13} & \end{array}\right] \tag{4.23}$$

$$\boldsymbol{F}_2 = \left[\begin{array}{c|ccccc|c} & 0 & 0 & 0 & -N_{a,r}v^a_{21} & N_{a,r}v^a_{11} & \\ & 0 & 0 & 0 & -N_{a,s}v^a_{21} & N_{a,s}v^a_{11} & \\ & 0 & 0 & 0 & 0 & 0 & \\ & 0 & 0 & 0 & -N_{a,r}v^a_{22} & N_{a,r}v^a_{12} & \\ \cdots & 0 & 0 & 0 & -N_{a,s}v^a_{22} & N_{a,s}v^a_{12} & \cdots \\ & 0 & 0 & 0 & 0 & 0 & \\ & 0 & 0 & 0 & -N_{a,r}v^a_{23} & N_{a,r}v^a_{13} & \\ & 0 & 0 & 0 & -N_{a,s}v^a_{23} & N_{a,s}v^a_{13} & \\ & 0 & 0 & 0 & 0 & 0 & \end{array}\right] \tag{4.24}$$

For the inverse Jacobian matrix the approximate explicit thickness dependency is introduced as

$$\boldsymbol{J}^{-1} \approx \boldsymbol{J}_A^{-1} + t\boldsymbol{J}_V^{-1} = \boldsymbol{J}_A^{-1} + z\tfrac{2}{h}\boldsymbol{J}_V^{-1} \tag{4.25}$$

where

$$\begin{aligned} \boldsymbol{J}_A^{-1} &= \tfrac{1}{2}\left(\boldsymbol{J}^{-1}|_{t=1.0} + \boldsymbol{J}^{-1}|_{t=-1.0}\right) \\ \boldsymbol{J}_V^{-1} &= \tfrac{1}{2}\left(\boldsymbol{J}^{-1}|_{t=1.0} - \boldsymbol{J}^{-1}|_{t=-1.0}\right) \end{aligned} \tag{4.26}$$

Both expressions in equation (4.26) are evaluated each time $\boldsymbol{G}$ or $\boldsymbol{B}$ are needed as shown below.

For the sake of brevity subsequent relations are developed for the u-components of $\boldsymbol{G}$ only, i.e. the first sub-matrix of

$$\boldsymbol{G} = \begin{bmatrix} \boldsymbol{G}^u \\ \boldsymbol{G}^v \\ \boldsymbol{G}^w \end{bmatrix} \tag{4.27}$$

By substituting into $\boldsymbol{G}^u$ the approximate explicit expression for the u-components of $\boldsymbol{F}$ in (4.22) and the linear approximation for the inverse Jacobian (4.25) and re-arranging.

$$\boldsymbol{G}^u = \boldsymbol{J}^{-1}\boldsymbol{F}^u \tag{4.28}$$

$$= \left(\boldsymbol{J}_A^{-1} + z\tfrac{2}{h}\boldsymbol{J}_V^{-1}\right)\left(\boldsymbol{F}_1^u + z\boldsymbol{F}_2^u\right) \tag{4.29}$$

$$= \underbrace{\boldsymbol{J}_A^{-1}\boldsymbol{F}_1^u}_{G_1^u} + z\underbrace{\left(\boldsymbol{J}_A^{-1}\boldsymbol{F}_2^u + \tfrac{2}{h}\boldsymbol{J}_V^{-1}\boldsymbol{F}_1^u\right)}_{G_2^u} + z^2\underbrace{\tfrac{2}{h}\boldsymbol{J}_V^{-1}\boldsymbol{F}_2^u}_{G_3^u} \tag{4.30}$$

Similarly $\boldsymbol{G}^v$ and $\boldsymbol{G}^w$ are obtained, i.e.

$$\boldsymbol{G} = \boldsymbol{G}_1 + z\boldsymbol{G}_2 + z^2\boldsymbol{G}_3 \tag{4.31}$$

Recall that $\boldsymbol{B} = \boldsymbol{H}\boldsymbol{G}$ and hence the strain-displacement matrix attains the same form as $\boldsymbol{G}$.

$$\boldsymbol{B} = \boldsymbol{B}_1 + z\boldsymbol{B}_2 + z^2\boldsymbol{B}_3 \tag{4.32}$$

Now we have decomposed the strain-displacement matrix into three sub-matrices that are independent of the thickness coordinate which reveals the approximate explicit thickness dependency. The explicit dependencies of equation (4.31) and (4.32) are used in the further developments in obtaining element matrices, though, further approximations may be introduced due to the fact that $\boldsymbol{G}_3$ and $\boldsymbol{B}_3$ contain entries of negligible magnitude compared to the remaining matrices contained in $\boldsymbol{G}$ and $\boldsymbol{B}$. This is utilized in Section 4.2.2 to obtain further reductions in element formulation time without little loss of information.

4.2 Thickness integration

In this section it is shown how thickness integrations to obtain element matrices are performed for layered elements as shown in Figure 4.4. First, the usual *layer-wise thickness integration* scheme of Panda and Natarajan (1981) is presented and afterwards a more efficient *explicit thickness integration* is shown, see e.g. Yunus et al. (1989) and Prema Kumar and Palaninathan (1997, 1999).

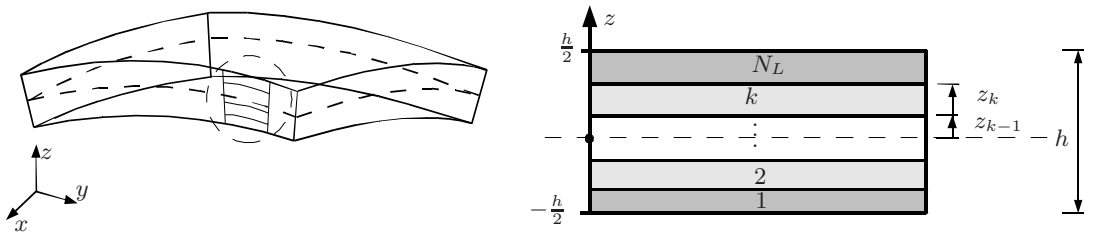

Figure 4.4: Layered shell with lay-up definition; coordinates and layer numbering.

The expression for the stiffness matrix from equation (3.25) is stated again here for reference.

$$\boldsymbol{K}^e = \int_{-1}^{1}\int_{-1}^{1}\int_{-1}^{1} \boldsymbol{B}^T\boldsymbol{C}\boldsymbol{B}\,|\boldsymbol{J}|\;drdsdt \tag{4.33}$$

4.2.1 Layer-wise thickness integration

For layered shell elements the thickness integration is performed by dividing the element into a number of sub-elements each representing a layer and subsequently *layer-wise numerical integration* is enabled by transforming the natural thickness coordinate into *natural layer coordinates*. For full numerical integration of e.g. a 9-node shell element this yields $3 \times 3 \times 2N^L$ sampling points where shape functions and derivatives are evaluated. For elements with a large number of layers this becomes computationally expensive.

Stiffness matrix

To employ layer-wise numerical integration through the thickness the natural thickness coordinate t is transformed into a layer-wise natural thickness coordinate, t_l. The layer-wise coordinate runs from -1 to 1 from the bottom to the top of each layer.

$$t = -1 + \frac{1}{h}\left(2\sum_{k=1}^{l} h_k - h_l\,(1 - t_l)\right) \tag{4.34}$$

Here h_k is the summed thickness of the preceding layers and h_l is the l'th layer thickness, see Figure 4.5.

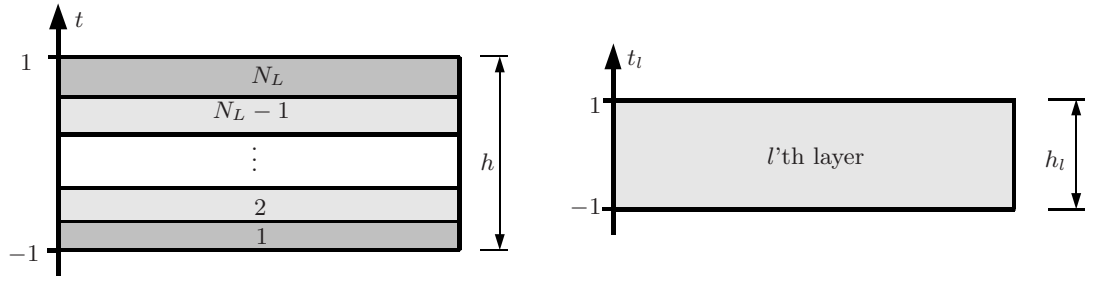

Figure 4.5: Change from natural coordinate, t, to layerwise natural coordinate, t_l.

Now to integrate the stiffness matrix of equation (4.33) the layer-wise coordinates are substituted for the natural thickness coordinate which means that

$$dt = \tfrac{h_l}{h} dt_l \tag{4.35}$$

Consequently the integration of equation (4.33) is evaluated as a sum over all layers, with each layer integrated numerically from -1 to 1 in all three coordinate directions.

$$\boldsymbol{K}^e = \sum_{k=1}^{N^L} \int_{-1}^{1}\int_{-1}^{1}\int_{-1}^{1} \boldsymbol{B}^T\boldsymbol{C}\boldsymbol{B}\,|\boldsymbol{J}|\,\tfrac{h_k}{h}\; dr ds dt_k \tag{4.36}$$

4.2.2 Explicit thickness integration

In this section the approximate explicit thickness dependencies developed in Section 4.1.4 are introduced to the element matrices. Consequently the approximate

explicit thickness integration may be performed outside the in-plane integrations which results in substantial savings on computational expense for elements with many layers. In addition to this, a link is established to the ABD-matrices as known from Classical Laminated Plate Theory. The definition of the lay-up is shown in Figure 4.4.

Stiffness matrix

In the expression for the stiffness matrix (4.33) a change of variable is performed by substituting $z = t\frac{h}{2} \Rightarrow dt = \frac{2}{h}dz$.

$$\boldsymbol{K}^e = \int_{-1}^{1}\int_{-1}^{1}\int_{-1}^{1} \boldsymbol{B}^T\boldsymbol{C}\boldsymbol{B}\,|\boldsymbol{J}|\; drdsdt = \int_{-1}^{1}\int_{-1}^{1}\int_{-\frac{h}{2}}^{\frac{h}{2}} \boldsymbol{B}^T\boldsymbol{C}\boldsymbol{B}\,|\boldsymbol{J}|\,\tfrac{2}{h}\; dzdrds \tag{4.37}$$

Before we proceed with the evaluation of the integrals above we introduce the explicit thickness dependency of the Jacobian determinant $|\boldsymbol{J}|$ as shown in Prema Kumar and Palaninathan (1999). Let the square root of the Jacobian determinant at the top and bottom of the shell be given by.

$$\Delta_{top} = \sqrt{|\boldsymbol{J}|}_{t=1.0} \tag{4.38}$$

$$\Delta_{bot} = \sqrt{|\boldsymbol{J}|}_{t=-1.0} \tag{4.39}$$

then the thickness average and slope of the determinant square roots are

$$\Delta_A = \tfrac{1}{2}\left(\Delta_{top} + \Delta_{bot}\right) \tag{4.40}$$

$$\Delta_V = \tfrac{1}{2}\left(\Delta_{top} - \Delta_{bot}\right) \tag{4.41}$$

Consequently the square root of the Jacobian determinant is given explicitly through the thickness by the following linear expression

$$\Delta = \Delta_A + \tfrac{2}{h} z \Delta_V \tag{4.42}$$

Thereby the Jacobian determinant through the thickness is expressed explicitly in terms of the Jacobian determinant square root at the bottom and the top of the shell.

$$|\boldsymbol{J}| = \Delta^2 = \Delta_A^2\left(1 + 2z\gamma + z^2\gamma^2\right) \tag{4.43}$$

where $\gamma = \frac{2}{h}\frac{\Delta_V}{\Delta_A}$. Thus the Jacobian matrix is only set up in the reference surface based on evaluations of the Jacobian matrix at the bottom and the top of the shell surface. Compared to setting up the Jacobian matrix in each layer the previous developments result in substantial efficiency gain for shells with many layers.

Now in (4.37) we introduce the integrand's explicit dependency on z by substituting (4.32) and (4.43) to obtain

$$\begin{aligned}\boldsymbol{K}^e &= \int_{-1}^{1}\int_{-1}^{1}\int_{-\frac{h}{2}}^{\frac{h}{2}} \left(\boldsymbol{B}_1{}^T + z\boldsymbol{B}_2{}^T + z^2\boldsymbol{B}_3{}^T\right)\boldsymbol{C}\left(\boldsymbol{B}_1 + z\boldsymbol{B}_2 + z^2\boldsymbol{B}_3\right) \\ &\qquad \left(1 + 2z\gamma + z^2\gamma^2\right)\tfrac{2}{h}\Delta_A^2\, dzdrds \\ &= \int_{-1}^{1}\int_{-1}^{1}\int_{-\frac{h}{2}}^{\frac{h}{2}} \left(\boldsymbol{B}_1{}^T\boldsymbol{C}\boldsymbol{B}_1 + z\boldsymbol{B}_1{}^T\boldsymbol{C}\boldsymbol{B}_2 + z^2\boldsymbol{B}_1{}^T\boldsymbol{C}\boldsymbol{B}_3\right. \\ &\qquad + z\boldsymbol{B}_2{}^T\boldsymbol{C}\boldsymbol{B}_1 + z^2\boldsymbol{B}_2{}^T\boldsymbol{C}\boldsymbol{B}_2 + z^3\boldsymbol{B}_2{}^T\boldsymbol{C}\boldsymbol{B}_3 \\ &\qquad \left. + z^2\,\boldsymbol{B}_3{}^T\boldsymbol{C}\boldsymbol{B}_1 + z^3\boldsymbol{B}_3{}^T\boldsymbol{C}\boldsymbol{B}_2 + z^4\boldsymbol{B}_3{}^T\boldsymbol{C}\boldsymbol{B}_3\right) \\ &\qquad \left(1 + 2z\gamma + z^2\gamma^2\right)\tfrac{2}{h}\Delta_A^2\, dzdrds \end{aligned} \tag{4.44}$$

The thickness integral in (4.44) is carried out separately for each term. Recall that the $\boldsymbol{B}_{1,2,3}$-matrices are thickness independent and that the constitutive properties are constant for each layer k, i.e. $\boldsymbol{C}_k$ is constant and thus we obtain

$$\begin{aligned}\boldsymbol{K}^e = \int_{-1}^{1}\int_{-1}^{1} &\left(\boldsymbol{B}_1{}^T\boldsymbol{E}_1\boldsymbol{B}_1 + \boldsymbol{B}_1{}^T\boldsymbol{E}_2\boldsymbol{B}_2 + \boldsymbol{B}_1{}^T\boldsymbol{E}_3\boldsymbol{B}_3\right. \\ &+ \boldsymbol{B}_2{}^T\boldsymbol{E}_2\boldsymbol{B}_1 + \boldsymbol{B}_2{}^T\boldsymbol{E}_3\boldsymbol{B}_2 + \boldsymbol{B}_2{}^T\boldsymbol{E}_4\boldsymbol{B}_3 \\ &\left. + \boldsymbol{B}_3{}^T\boldsymbol{E}_3\boldsymbol{B}_1 + \boldsymbol{B}_3{}^T\boldsymbol{E}_4\boldsymbol{B}_2 + \boldsymbol{B}_3{}^T\boldsymbol{E}_5\boldsymbol{B}_3\right)\tfrac{2}{h}\Delta_A^2\, drds \end{aligned} \tag{4.45}$$

where $\boldsymbol{E}$-matrices are thickness integrated constitutive properties.

$$\boldsymbol{E}_1 = \sum_{k=1}^{N_L}\boldsymbol{C}_k\int_{z_{k-1}}^{z_k}\left(1 + 2z\gamma + z^2\gamma^2\right)dz = \sum_{k=1}^{N_L}\boldsymbol{C}_k\left(var_1 + 2\gamma var_2 + \gamma^2 var_3\right)_k \tag{4.46a}$$

$$\boldsymbol{E}_2 = \sum_{k=1}^{N_L}\boldsymbol{C}_k\int_{z_{k-1}}^{z_k} z\left(1 + 2z\gamma + z^2\gamma^2\right)dz = \sum_{k=1}^{N_L}\boldsymbol{C}_k\left(var_2 + 2\gamma var_3 + \gamma^2 var_4\right)_k \tag{4.46b}$$

$$\boldsymbol{E}_3 = \sum_{k=1}^{N_L}\boldsymbol{C}_k\int_{z_{k-1}}^{z_k} z^2\left(1 + 2z\gamma + z^2\gamma^2\right)dz = \sum_{k=1}^{N_L}\boldsymbol{C}_k\left(var_3 + 2\gamma var_4 + \gamma^2 var_5\right)_k \tag{4.46c}$$

$$\boldsymbol{E}_4 = \sum_{k=1}^{N_L}\boldsymbol{C}_k\int_{z_{k-1}}^{z_k} z^3\left(1 + 2z\gamma + z^2\gamma^2\right)dz = \sum_{k=1}^{N_L}\boldsymbol{C}_k\left(var_4 + 2\gamma var_5 + \gamma^2 var_6\right)_k \tag{4.46d}$$

$$\boldsymbol{E}_5 = \sum_{k=1}^{N_L}\boldsymbol{C}_k\int_{z_{k-1}}^{z_k} z^4\left(1 + 2z\gamma + z^2\gamma^2\right)dz = \sum_{k=1}^{N_L}\boldsymbol{C}_k\left(var_5 + 2\gamma var_6 + \gamma^2 var_7\right)_k \tag{4.46e}$$

$$var_1 = \quad (z_k - z_{k-1}) \tag{4.47a}$$

$$var_2 = \tfrac{1}{2}\left(z_k^2 - z_{k-1}^2\right) \tag{4.47b}$$

$$\vdots$$

$$var_7 = \tfrac{1}{7}\left(z_k^7 - z_{k-1}^7\right) \tag{4.47c}$$

Thus we are able to integrate explicitly in the thickness direction much like it is done in obtaining the ABD-matrices of CLPT. The sums in equation (4.46) are evaluated once for each in-plane integration point in the reference surface while the in-plane integrations (r, s) in (4.45) are performed by full numerical integration. Consequently, the integration of e.g. the stiffness matrix requires $3 \times 3 \times 2$ evaluations, where the last 2 are inverse Jacobian evaluations at the bottom and the top of the shell as in equation (4.26). In case of laminates consisting of a single (orthotropic) material with different orientation in each layer, the stiffness matrix can be expressed linearly in terms of the so-called lamination parameters which is shown in Section 4.2.3.

Stress stiffness matrix

Similarly as for the stiffness matrix the stress stiffness matrix is developed by substituting the thickness dependencies and performing explicit integration through the thickness. In natural coordinates the element stress stiffness matrix from equation (3.22) reads

$$\boldsymbol{K}_\sigma^e = \int_{-1}^{1}\int_{-1}^{1}\int_{-1}^{1} \boldsymbol{G}^T \boldsymbol{S} \boldsymbol{G}\, |\boldsymbol{J}|\; drdsdt \tag{4.48}$$

It is rewritten by a change of thickness variable, substituting $z = t\frac{h}{2} \Rightarrow dt = \frac{2}{h}dz$.

$$\boldsymbol{K}_\sigma^e = \int_{-1}^{1}\int_{-1}^{1}\int_{-\frac{h}{2}}^{\frac{h}{2}} \boldsymbol{G}^T \boldsymbol{S} \boldsymbol{G}\, |\boldsymbol{J}|\, \tfrac{2}{h}\; dzdrds \tag{4.49}$$

$\boldsymbol{G}$'s and $|\boldsymbol{J}|$'s explicit dependencies on z are introduced by substituting (4.31) and $|\boldsymbol{J}| = \Delta_A^2\left(1 + 2z\gamma + z^2\gamma^2\right)$, where $\gamma = \frac{2}{h}\frac{\Delta_V}{\Delta_A}$ into (4.49) to obtain

$$\begin{aligned}
\boldsymbol{K}_\sigma^e = \int_{-1}^{1}\int_{-1}^{1}\int_{-\frac{h}{2}}^{\frac{h}{2}} & \left(\boldsymbol{G}_1{}^T + z\boldsymbol{G}_2{}^T + z^2\boldsymbol{G}_3{}^T\right) \boldsymbol{S} \left(\boldsymbol{G}_1 + z\boldsymbol{G}_2 + z^2\boldsymbol{G}_3\right) \\
& \left(1 + 2z\gamma + z^2\gamma^2\right) \tfrac{2}{h}\Delta_A^2\; dzdrds \\
= \int_{-1}^{1}\int_{-1}^{1}\int_{-\frac{h}{2}}^{\frac{h}{2}} & \left(\boldsymbol{G}_1{}^T\boldsymbol{S}\boldsymbol{G}_1 + z\boldsymbol{G}_1{}^T\boldsymbol{S}\boldsymbol{G}_2 + z^2\boldsymbol{G}_1{}^T\boldsymbol{S}\boldsymbol{G}_3\right. \\
& + z\boldsymbol{G}_2{}^T\boldsymbol{S}\boldsymbol{G}_1 + z^2\boldsymbol{G}_2{}^T\boldsymbol{S}\boldsymbol{G}_2 + z^3\boldsymbol{G}_2{}^T\boldsymbol{S}\boldsymbol{G}_3 \\
& \left. + z^2\,\boldsymbol{G}_3{}^T\boldsymbol{S}\boldsymbol{G}_1 + z^3\boldsymbol{G}_3{}^T\boldsymbol{S}\boldsymbol{G}_2 + z^4\boldsymbol{G}_3{}^T\boldsymbol{S}\boldsymbol{G}_3\right) \\
& \left(1 + 2z\gamma + z^2\gamma^2\right) \tfrac{2}{h}\Delta_A^2\; dzdrds
\end{aligned} \tag{4.50}$$

Now, the explicit thickness dependency of the stresses, $\boldsymbol{S}$ is introduced. A *layer-wise linear distribution of stresses* is assumed. Thus within the k'th layer

$$\boldsymbol{S}_k = \boldsymbol{S}_k^A + z\boldsymbol{S}_k^V \qquad ; \qquad z_{k-1} \le z \le z_k \tag{4.51}$$

where the coefficients of the linear variation are determined from a stress evaluation at the upper and lower Gauss point through the thickness, respectively.

$$\boldsymbol{S}_k^V = \frac{\boldsymbol{S}_k^{up} - \boldsymbol{S}_k^{low}}{z_k^{up} - z_k^{low}} \qquad and \qquad \boldsymbol{S}_k^A = \boldsymbol{S}_k^{up} - z_k^{up}\boldsymbol{S}_k^V \tag{4.52}$$

Now introduce the above and the integration through the thickness is performed separately whereby the resulting expression for the stress stiffness matrix becomes

$$\begin{aligned}\boldsymbol{K}_{\sigma}^{e} = \int_{-1}^{1}\int_{-1}^{1} \big(&\boldsymbol{G}_1{}^T \boldsymbol{M}_1^A \boldsymbol{G}_1 + \boldsymbol{G}_1{}^T \boldsymbol{M}_2^A \boldsymbol{G}_2 + \boldsymbol{G}_1{}^T \boldsymbol{M}_3^A \boldsymbol{G}_3 \\ &+\boldsymbol{G}_2{}^T \boldsymbol{M}_2^A \boldsymbol{G}_1 + \boldsymbol{G}_2{}^T \boldsymbol{M}_3^A \boldsymbol{G}_2 + \boldsymbol{G}_2{}^T \boldsymbol{M}_4^A \boldsymbol{G}_3 \\ &+\boldsymbol{G}_3{}^T \boldsymbol{M}_3^A \boldsymbol{G}_1 + \boldsymbol{G}_3{}^T \boldsymbol{M}_4^A \boldsymbol{G}_2 + \boldsymbol{G}_3{}^T \boldsymbol{M}_5^A \boldsymbol{G}_3 \\ &+\boldsymbol{G}_1{}^T \boldsymbol{M}_1^V \boldsymbol{G}_1 + \boldsymbol{G}_1{}^T \boldsymbol{M}_2^V \boldsymbol{G}_2 + \boldsymbol{G}_1{}^T \boldsymbol{M}_3^V \boldsymbol{G}_3 \\ &+\boldsymbol{G}_2{}^T \boldsymbol{M}_2^V \boldsymbol{G}_1 + \boldsymbol{G}_2{}^T \boldsymbol{M}_3^V \boldsymbol{G}_2 + \boldsymbol{G}_2{}^T \boldsymbol{M}_4^V \boldsymbol{G}_3 \\ &+ \boldsymbol{G}_3{}^T \boldsymbol{M}_3^V \boldsymbol{G}_1 + \boldsymbol{G}_3{}^T \boldsymbol{M}_4^V \boldsymbol{G}_2 + \boldsymbol{G}_3{}^T \boldsymbol{M}_5^V \boldsymbol{G}_3 \big) \tfrac{2}{h} \Delta_A^2 \, drds \end{aligned} \tag{4.53}$$

where

$$\boldsymbol{M}_1^A = \sum_{k=1}^{N_L} \boldsymbol{S}_k^A \left(var_1 + 2\gamma var_2 + \gamma^2 var_3 \right)_k \tag{4.54a}$$

$$\boldsymbol{M}_2^A = \sum_{k=1}^{N_L} \boldsymbol{S}_k^A \left(var_2 + 2\gamma var_3 + \gamma^2 var_4 \right)_k \tag{4.54b}$$

$$\boldsymbol{M}_3^A = \sum_{k=1}^{N_L} \boldsymbol{S}_k^A \left(var_3 + 2\gamma var_4 + \gamma^2 var_5 \right)_k \tag{4.54c}$$

$$\boldsymbol{M}_4^A = \sum_{k=1}^{N_L} \boldsymbol{S}_k^A \left(var_4 + 2\gamma var_5 + \gamma^2 var_6 \right)_k \tag{4.54d}$$

$$\boldsymbol{M}_5^A = \sum_{k=1}^{N_L} \boldsymbol{S}_k^A \left(var_5 + 2\gamma var_6 + \gamma^2 var_7 \right)_k \tag{4.54e}$$

$$\boldsymbol{M}_1^V = \sum_{k=1}^{N_L} \boldsymbol{S}_k^V \left(var_2 + 2\gamma var_3 + \gamma^2 var_4 \right)_k \tag{4.54f}$$

$$\boldsymbol{M}_2^V = \sum_{k=1}^{N_L} \boldsymbol{S}_k^V \left(var_3 + 2\gamma var_4 + \gamma^2 var_5 \right)_k \tag{4.54g}$$

$$\boldsymbol{M}_3^V = \sum_{k=1}^{N_L} \boldsymbol{S}_k^V \left(var_4 + 2\gamma var_5 + \gamma^2 var_6 \right)_k \tag{4.54h}$$

$$\boldsymbol{M}_4^V = \sum_{k=1}^{N_L} \boldsymbol{S}_k^V \left(var_5 + 2\gamma var_6 + \gamma^2 var_7 \right)_k \tag{4.54i}$$

$$\boldsymbol{M}_5^V = \sum_{k=1}^{N_L} \boldsymbol{S}_k^V \left(var_6 + 2\gamma var_7 + \gamma^2 var_8 \right)_k \tag{4.54j}$$

Thus we may integrate through the thickness explicitly in obtaining the initial-stress stiffness matrix.

Internal force vector

To evaluate the internal strain energy efficiently in e.g. equation (5.4), it is expedient to calculate the internal force vector. The internal force vector is obtained by integrating the equilibrium stresses throughout the volume as shown in equation (3.13) to (3.15).

$$\boldsymbol{r}^e = \int_V \boldsymbol{B}^T \boldsymbol{\sigma} \, dV \tag{4.55}$$

In natural coordinates this integral reads

$$\boldsymbol{r}^e = \int_{-1}^{1}\int_{-1}^{1}\int_{-1}^{1} \boldsymbol{B}^T \boldsymbol{\sigma} \, |\boldsymbol{J}| \; drdsdt \tag{4.56}$$

Rewrite by a change of thickness coordinate, substituting $z = t\frac{h}{2} \Rightarrow dt = \frac{2}{h}dz$.

$$\boldsymbol{r}^e = \int_{-1}^{1}\int_{-1}^{1}\int_{-\frac{h}{2}}^{\frac{h}{2}} \boldsymbol{B}^T \boldsymbol{\sigma} \, |\boldsymbol{J}| \, \tfrac{2}{h} \; dzdrds \tag{4.57}$$

Now we express the explicit thickness dependency of the stresses, $\boldsymbol{\sigma}$. Again, we assume a *layer-wise linear distribution of stresses*. Thus within the k'th layer we may write

$$\boldsymbol{\sigma}_k = \boldsymbol{\sigma}_k^A + z\boldsymbol{\sigma}_k^V \qquad ; \qquad z_{k-1} \le z \le z_k \tag{4.58}$$

where the coefficients of the linear variation are determined from a stress evaluation at the upper and lower Gauss point through the thickness, respectively.

$$\boldsymbol{\sigma}_k^V = \frac{\boldsymbol{\sigma}_k^{up} - \boldsymbol{\sigma}_k^{low}}{z_k^{up} - z_k^{low}} \qquad and \qquad \boldsymbol{\sigma}_k^A = \boldsymbol{\sigma}_k^{up} - z_k^{up}\boldsymbol{\sigma}_k^V \tag{4.59}$$

Now introduce the above and the remaining explicit thickness dependencies of the integrand in equation (4.57), i.e. $\boldsymbol{B} = \boldsymbol{B}_1 + z\boldsymbol{B}_2 + z^2\boldsymbol{B}_3$ and $|\boldsymbol{J}| = \Delta_A^2\left(1 + 2z\gamma + z^2\gamma^2\right)$ whereby

$$\begin{aligned}\boldsymbol{r}^e = \int_{-1}^{1}\int_{-1}^{1} \big[&\boldsymbol{B}_1^T\boldsymbol{M}_1^A + \boldsymbol{B}_2^T\boldsymbol{M}_2^A + \boldsymbol{B}_3^T\boldsymbol{M}_3^A \\ &+ \boldsymbol{B}_1^T\boldsymbol{M}_1^V + \boldsymbol{B}_2^T\boldsymbol{M}_2^V + \boldsymbol{B}_3^T\boldsymbol{M}_3^V\big] \, \tfrac{2}{h}\Delta_A^2 \; drds\end{aligned} \tag{4.60}$$

with $\boldsymbol{M}$'s containing thickness integrated stresses that are evaluated separately as

$$\boldsymbol{M}_1^A = \sum_{k=1}^{N_L} \boldsymbol{\sigma}_k^A \left(var_1 + 2\gamma var_2 + \gamma^2 var_3\right)_k \tag{4.61a}$$

$$\boldsymbol{M}_2^A = \sum_{k=1}^{N_L} \boldsymbol{\sigma}_k^A \left(var_2 + 2\gamma var_3 + \gamma^2 var_4\right)_k \tag{4.61b}$$

$$\boldsymbol{M}_3^A = \sum_{k=1}^{N_L} \boldsymbol{\sigma}_k^A \left(var_3 + 2\gamma var_4 + \gamma^2 var_5\right)_k \tag{4.61c}$$

$$\boldsymbol{M}_1^V = \sum_{k=1}^{N_L} \boldsymbol{\sigma}_k^V \left(var_2 + 2\gamma var_3 + \gamma^2 var_4\right)_k \tag{4.61d}$$

$$\boldsymbol{M}_2^V = \sum_{k=1}^{N_L} \boldsymbol{\sigma}_k^V \left(var_3 + 2\gamma var_4 + \gamma^2 var_5\right)_k \tag{4.61e}$$

$$\boldsymbol{M}_3^V = \sum_{k=1}^{N_L} \boldsymbol{\sigma}_k^V \left(var_4 + 2\gamma var_5 + \gamma^2 var_6\right)_k \tag{4.61f}$$

Here var_i's still contain differences of the k'th top and bottom layer coordinates to the i'th power as shown in (4.47).

Further approximations

In Section 4.1.4 we indicated a possibility of obtaining further reductions in element formulation time by neglecting the contribution of $\boldsymbol{G}_3$ and $\boldsymbol{B}_3$ to $\boldsymbol{G}$ and $\boldsymbol{B}$, respectively. The rationale for doing so, is that matrices $\boldsymbol{G}_3$ and $\boldsymbol{B}_3$ contain only negligible terms for most problems that are modelled as shells. If this is utilized we may neglect all terms of the element matrices containing one of these matrices. For the stiffness matrix this means that the number of integrand terms in equation (4.45) is reduced from 9 to 5. For the stress stiffness matrix the same amount of terms is cut analogously as for the stiffness matrix. These reductions result in further reductions in element formulation time since costly matrix multiplications are saved by truncating these terms. The price for these reductions is loss of the information contained in the $\boldsymbol{G}_3$ and $\boldsymbol{B}_3$ matrices. Later, this loss is shown to be negligible compared to the efficiency gain.

Summary

In the previous sections three thickness integration schemes were presented. The *layer-wise* through thickness integration scheme (SHELL9), the *explicit* thickness integration scheme (SHELL9Expl) and the *explicit* thickness integration scheme with further approximations (SHELL9ExplApp). The first scheme employs numerical integration in all three spatial variables r, s and t meaning that the number of sampling points is proportional to the number of layers i.e. $(3 \times 3 \times 2N^L)$ for full integration of a 9-node shell element) and thus inefficient for multi-layered elements with a large number of layers. The alternative formulation assumes a linear variation of the inverse Jacobian matrix which reduces the number of sampling points to a top and bottom point evaluation for each in-plane sampling point in the reference surface, i.e. $(3 \times 3 \times 2)$.

The through the thickness integration is carried out separately without shape function evaluations which renders the method efficient for elements with many layers. A comparison of the efficiency of the two approaches is given in Section 6.4.

In the next section we describe constitutive matrices and different ways of handling them, eventually leading to a convex parametrization of the stiffness matrix.

4.2.3 Constitutive relations

In the following the reduced constitutive relations are described as they are applied in the formulation of degenerated solid elements. Modifications of the constitutive relations that enforce shell assumptions are presented along with necessary coordinate transformations. In continuation of this the plane rotation transformation is reformulated in lamina invariants and used to develop a laminate parametrization in lamination parameters which is possible for *laminates consisting of layers of the same material*. Parametrizing in lamination parameters renders the stiffness matrix linear in the lamination parameters. This has advantages that are desirable in design optimization.

Reduced constitutive relations

In Section 2.1 the FSDT assumptions were introduced. Namely, that mid surface normals are inextensible which amounts to no transverse normal strains, i.e. $\varepsilon_3 = 0$. At the same time transverse normal stresses are assumed to be negligible for thin to moderately thick shells, $\sigma_3 = 0$. Obviously these assumptions are mutually conflicting due to Poisson effects, so in order to enforce both assumptions the constitutive relations are modified resulting in the so-called reduced constitutive relations. Also, the reduced constitutive relations incorporate corrections of the transverse shear stiffnesses.

The zero transverse normal stress condition is enforced by writing out the expression for the transverse normal stress σ_3 in an orthotropic material, equation (2.10).

$$\begin{aligned} \sigma_3 &= Q_{13}\varepsilon_1 + Q_{23}\varepsilon_2 + Q_{33}\varepsilon_3 = 0 \Leftrightarrow \\ \varepsilon_3 &= -\frac{Q_{13}\varepsilon_1 + Q_{23}\varepsilon_2}{Q_{33}} = 0 \end{aligned} \tag{4.62}$$

In order to meet the zero transverse normal stress condition and the zero transverse normal strain for any strain state we see from the equations above that $Q_{13} = Q_{23} = Q_{33} = 0$. Thus the orthotropic stress-strain relation, (2.10), in principal material directions for a single ply in degenerated shell element becomes

$$\begin{Bmatrix} \sigma_1 \\ \sigma_2 \\ \sigma_3 \\ \tau_{12} \\ \tau_{23} \\ \tau_{13} \end{Bmatrix} = \begin{bmatrix} Q_{11} & Q_{12} & 0 & 0 & 0 & 0 \\ Q_{21} & Q_{22} & 0 & 0 & 0 & 0 \\ 0 & 0 & 0 & 0 & 0 & 0 \\ 0 & 0 & 0 & Q_{44} & 0 & 0 \\ 0 & 0 & 0 & 0 & Q_{55} & 0 \\ 0 & 0 & 0 & 0 & 0 & Q_{66} \end{bmatrix} \begin{Bmatrix} \varepsilon_1 \\ \varepsilon_2 \\ \varepsilon_3 \\ \gamma_{12} \\ \gamma_{23} \\ \gamma_{13} \end{Bmatrix} \tag{4.63}$$

The transverse shear stiffness coefficients Q_{55} and Q_{66} are corrected in order to correlate the strain energy of the constant through the thickness shear strain to the strain

energy of the more correct parabolic shear strain distribution through the thickness. For laminates consisting of layers with shear stiffness terms of approximately equal magnitude, MUST corrects the transverse shear stiffness terms by an approximate shear correction factor of $k = 0.8$ and for sandwich structures consisting of a compliant core between thin stiff face sheets $k = 1.0$, i.e. no correction is applied due to the fact, that sandwich structures actually do exhibit (almost) constant shear strain through the core, whereas the thin face sheets do not contribute to the shear stiffness very much, see Jensen et al. (2002) for a thorough discussion of these matters.

Lamina invariants

In Section 2.4.1 it was shown how to transform constitutive properties from principal material coordinate system to the element coordinate system by a plane rotation, $\overline{\boldsymbol{Q}} = \boldsymbol{T}_\theta^T \boldsymbol{Q} \boldsymbol{T}_\theta$. By this transformation the constitutive matrix in the MCS, $\overline{\boldsymbol{Q}}$, attains the form

$$\overline{\boldsymbol{Q}} = \begin{bmatrix} \overline{Q}_{11} & \overline{Q}_{12} & 0 & \overline{Q}_{14} & 0 & 0 \\ \overline{Q}_{12} & \overline{Q}_{22} & 0 & \overline{Q}_{24} & 0 & 0 \\ 0 & 0 & 0 & 0 & 0 & 0 \\ \overline{Q}_{14} & \overline{Q}_{24} & 0 & \overline{Q}_{44} & 0 & 0 \\ 0 & 0 & 0 & 0 & \overline{Q}_{55} & \overline{Q}_{56} \\ 0 & 0 & 0 & 0 & \overline{Q}_{56} & \overline{Q}_{66} \end{bmatrix} \tag{4.64}$$

Here the entries of $\overline{\boldsymbol{Q}}$ involve trigonometric functions to a power of up to four. These trigonometric functions render e.g. the stiffness non-convex in fiber angles which is undesirable in structural design optimization. Therefore an other parametrization is sought, namely in terms of lamination parameters that make use of the so-called lamina invariants.

Lamina invariants are material properties that are invariant under coordinate transformations. The lamina invariants U_1 to U_6 are derived by employing trigonometric identities and rearrangements of the expressions for the transformed constitutive matrix $\overline{\boldsymbol{Q}}$, see e.g. Jones (1999). In terms of constitutive properties in the principal material coordinate system, the invariants are

$$U_1 = \tfrac{1}{8}\left(3Q_{11} + 3Q_{22} + 2Q_{12} + 4Q_{44}\right) \tag{4.65a}$$
$$U_2 = \tfrac{1}{2}\left(Q_{11} - Q_{22}\right) \tag{4.65b}$$
$$U_3 = \tfrac{1}{8}\left(Q_{11} + Q_{22} - 2Q_{12} - 4Q_{44}\right) \tag{4.65c}$$
$$U_4 = \tfrac{1}{8}\left(Q_{11} + Q_{22} + 6Q_{12} - 4Q_{44}\right) \tag{4.65d}$$
$$U_5 = \tfrac{1}{2}\left(Q_{55} + Q_{66}\right) \tag{4.65e}$$
$$U_6 = \tfrac{1}{2}\left(Q_{55} - Q_{66}\right) \tag{4.65f}$$

By use of the invariants the entries of $\overline{\boldsymbol{Q}}$ are given by

$$\begin{Bmatrix} \overline{Q}_{11} \\ \overline{Q}_{22} \\ \overline{Q}_{12} \\ \overline{Q}_{55} \\ \overline{Q}_{66} \\ \overline{Q}_{56} \\ \overline{Q}_{44} \\ \overline{Q}_{14} \\ \overline{Q}_{24} \end{Bmatrix} = \underbrace{\begin{bmatrix} U_1 & U_2 & 0 & U_3 & 0 \\ U_1 & -U_2 & 0 & U_3 & 0 \\ U_4 & 0 & 0 & -U_3 & 0 \\ U_5 & U_6 & 0 & 0 & 0 \\ U_5 & -U_6 & 0 & 0 & 0 \\ 0 & 0 & -U_6 & 0 & 0 \\ \frac{1}{2}(U_1 - U_4) & 0 & 0 & -U_3 & 0 \\ 0 & 0 & \frac{1}{2}U_2 & 0 & U_3 \\ 0 & 0 & \frac{1}{2}U_2 & 0 & -U_3 \end{bmatrix}}_{\equiv \boldsymbol{U}} \begin{Bmatrix} 1 \\ \cos 2\theta \\ \sin 2\theta \\ \cos 4\theta \\ \sin 4\theta \end{Bmatrix} \tag{4.66}$$

This reformulation of constitutive properties is not of much use by itself but it paves the road for an other way of explicitly integrating constitutive properties through the thickness as needed in e.g. degenerated shell elements.

Lamination parameters in shell elements

In Section 4.2.2 it was shown how the thickness integration in degenerated elements is carried out explicitly. To obtain the stiffness matrix a product of the strain-displacement matrix and the constitutive matrix is integrated. For laminates that consist of layers of the same material oriented at different angles, the thickness integrated constitutive properties can be expressed in terms of the so-called lamination parameters. In this section we develop the relation between thickness integrated constitutive properties from equation (4.46) and the lamination parameters, ξ. First, we define the various lamination parameters and then develop them into a form suitable for use with the explicitly thickness integrated constitutive properties.

Let 28 lamination parameters be defined by

$$\xi^A_{[1,2,3,4]} = \frac{1}{2}\int_{-1}^{1} \begin{bmatrix} \cos 2\theta_k & \sin 2\theta_k & \cos 4\theta_k & \sin 4\theta_k \end{bmatrix}^T dt \tag{4.67a}$$

$$\xi^B_{[1,2,3,4]} = \frac{2}{2}\int_{-1}^{1} t \begin{bmatrix} \cos 2\theta_k & \sin 2\theta_k & \cos 4\theta_k & \sin 4\theta_k \end{bmatrix}^T dt \tag{4.67b}$$

$$\xi^D_{[1,2,3,4]} = \frac{3}{2}\int_{-1}^{1} t^2 \begin{bmatrix} \cos 2\theta_k & \sin 2\theta_k & \cos 4\theta_k & \sin 4\theta_k \end{bmatrix}^T dt \tag{4.67c}$$

$$\xi^E_{[1,2,3,4]} = \frac{4}{2}\int_{-1}^{1} t^3 \begin{bmatrix} \cos 2\theta_k & \sin 2\theta_k & \cos 4\theta_k & \sin 4\theta_k \end{bmatrix}^T dt \tag{4.67d}$$

$$\xi^F_{[1,2,3,4]} = \frac{5}{2}\int_{-1}^{1} t^4 \begin{bmatrix} \cos 2\theta_k & \sin 2\theta_k & \cos 4\theta_k & \sin 4\theta_k \end{bmatrix}^T dt \tag{4.67e}$$

$$\xi^G_{[1,2,3,4]} = \frac{6}{2}\int_{-1}^{1} t^5 \begin{bmatrix} \cos 2\theta_k & \sin 2\theta_k & \cos 4\theta_k & \sin 4\theta_k \end{bmatrix}^T dt \tag{4.67f}$$

$$\xi^H_{[1,2,3,4]} = \frac{7}{2}\int_{-1}^{1} t^6 \begin{bmatrix} \cos 2\theta_k & \sin 2\theta_k & \cos 4\theta_k & \sin 4\theta_k \end{bmatrix}^T dt \tag{4.67g}$$

A change from natural thickness coordinate, t, to physical thickness coordinate, z, is made by substituting $t = \frac{2}{h}z \Rightarrow dt = \frac{2}{h}dz$.

$$\begin{aligned}
\xi^A_{[1,2,3,4]} =& \frac{1}{2}\int_{-\frac{h}{2}}^{\frac{h}{2}} \lfloor \cos 2\theta_k \quad \sin 2\theta_k \quad \cos 4\theta_k \quad \sin 4\theta_k \rfloor^T \tfrac{2}{h} dz \\
=& \frac{1}{h}\sum_{k=1}^{N^L} (var_1)_k \lfloor \cos 2\theta_k \quad \sin 2\theta_k \quad \cos 4\theta_k \quad \sin 4\theta_k \rfloor^T && (4.68a) \\
\xi^B_{[1,2,3,4]} =& \frac{2}{2}\int_{-\frac{h}{2}}^{\frac{h}{2}} \left(\tfrac{2}{h}z\right) \lfloor \cos 2\theta_k \quad \sin 2\theta_k \quad \cos 4\theta_k \quad \sin 4\theta_k \rfloor^T \tfrac{2}{h} dz \\
=& \frac{4}{h^2}\sum_{k=1}^{N^L} (var_2)_k \lfloor \cos 2\theta_k \quad \sin 2\theta_k \quad \cos 4\theta_k \quad \sin 4\theta_k \rfloor^T && (4.68b) \\
\xi^D_{[1,2,3,4]} =& \frac{3}{2}\int_{-\frac{h}{2}}^{\frac{h}{2}} \left(\tfrac{2}{h}z\right)^2 \lfloor \cos 2\theta_k \quad \sin 2\theta_k \quad \cos 4\theta_k \quad \sin 4\theta_k \rfloor^T \tfrac{2}{h} dz \\
=& \frac{12}{h^3}\sum_{k=1}^{N^L} (var_3)_k \lfloor \cos 2\theta_k \quad \sin 2\theta_k \quad \cos 4\theta_k \quad \sin 4\theta_k \rfloor^T && (4.68c) \\
\xi^E_{[1,2,3,4]} =& \frac{4}{2}\int_{-\frac{h}{2}}^{\frac{h}{2}} \left(\tfrac{2}{h}z\right)^3 \lfloor \cos 2\theta_k \quad \sin 2\theta_k \quad \cos 4\theta_k \quad \sin 4\theta_k \rfloor^T \tfrac{2}{h} dz \\
=& \frac{32}{h^4}\sum_{k=1}^{N^L} (var_4)_k \lfloor \cos 2\theta_k \quad \sin 2\theta_k \quad \cos 4\theta_k \quad \sin 4\theta_k \rfloor^T && (4.68d) \\
\xi^F_{[1,2,3,4]} =& \frac{5}{2}\int_{-\frac{h}{2}}^{\frac{h}{2}} \left(\tfrac{2}{h}z\right)^4 \lfloor \cos 2\theta_k \quad \sin 2\theta_k \quad \cos 4\theta_k \quad \sin 4\theta_k \rfloor^T \tfrac{2}{h} dz \\
=& \frac{80}{h^5}\sum_{k=1}^{N^L} (var_5)_k \lfloor \cos 2\theta_k \quad \sin 2\theta_k \quad \cos 4\theta_k \quad \sin 4\theta_k \rfloor^T && (4.68e) \\
\xi^G_{[1,2,3,4]} =& \frac{6}{2}\int_{-\frac{h}{2}}^{\frac{h}{2}} \left(\tfrac{2}{h}z\right)^5 \lfloor \cos 2\theta_k \quad \sin 2\theta_k \quad \cos 4\theta_k \quad \sin 4\theta_k \rfloor^T \tfrac{2}{h} dz \\
=& \frac{192}{h^6}\sum_{k=1}^{N^L} (var_6)_k \lfloor \cos 2\theta_k \quad \sin 2\theta_k \quad \cos 4\theta_k \quad \sin 4\theta_k \rfloor^T && (4.68f) \\
\xi^H_{[1,2,3,4]} =& \frac{7}{2}\int_{-\frac{h}{2}}^{\frac{h}{2}} \left(\tfrac{2}{h}z\right)^6 \lfloor \cos 2\theta_k \quad \sin 2\theta_k \quad \cos 4\theta_k \quad \sin 4\theta_k \rfloor^T \tfrac{2}{h} dz \\
=& \frac{448}{h^7}\sum_{k=1}^{N^L} (var_7)_k \lfloor \cos 2\theta_k \quad \sin 2\theta_k \quad \cos 4\theta_k \quad \sin 4\theta_k \rfloor^T && (4.68g)
\end{aligned}$$

Now we will employ lamination parameters in the expressions for the thickness integrated constitutive properties from equation (4.46). Below, we use the (layer independent) transformation from material coordinate system to global coordinate

system, $\boldsymbol{T}$, to introduce the constitutive properties in material coordinate system, $\overline{\boldsymbol{Q}}$. Next we use the assumption that *all layers are of the same material* and consequently the lamina invariants are taken outside the layer summation. Note that, the step from equation (4.70) to (4.71) *is not correct* since $\boldsymbol{U}\,[1, \cos 2\theta, \sin 2\theta, \cos 4\theta, \sin 4\theta]$ yields the entries of matrix $\overline{\boldsymbol{Q}}$ in a vector form as seen in (4.66), these are to be arranged as in equation (4.64). In the implementation, however, this issue is solved by simply placing the entries in a matrix of the correct size. The last step is to recognise the sums of trigonometric terms as the lamination parameters defined above.

$$\boldsymbol{E}_1 = \sum_{k=1}^{N_L} \boldsymbol{C}_k \int_{z_{k-1}}^{z_k} \left(1 + 2z\gamma + z^2\gamma^2\right) dz \tag{4.69}$$

$$= \boldsymbol{T}^T \sum_{k=1}^{N_L} \overline{\boldsymbol{Q}}_k \int_{z_{k-1}}^{z_k} \left(1 + 2z\gamma + z^2\gamma^2\right) dz \boldsymbol{T} \tag{4.70}$$

$$= \boldsymbol{T}^T \boldsymbol{U} \sum_{k=1}^{N_L} \lfloor 1 \quad \cos 2\theta_k \quad \sin 2\theta_k \quad \cos 4\theta_k \quad \sin 4\theta_k \rfloor^T \int_{z_{k-1}}^{z_k} \left(1 + 2z\gamma + z^2\gamma^2\right) dz \boldsymbol{T} \tag{4.71}$$

$$= \boldsymbol{T}^T \boldsymbol{U} \left(h \lfloor 1 \quad \xi_1^A \quad \xi_2^A \quad \xi_3^A \quad \xi_4^A \rfloor^T + 2\gamma \tfrac{h^2}{4} \lfloor 0 \quad \xi_1^B \quad \xi_2^B \quad \xi_3^B \quad \xi_4^B \rfloor^T + \right.$$
$$\left. \gamma^2 \tfrac{h^3}{12} \lfloor 1 \quad \xi_1^D \quad \xi_2^D \quad \xi_3^D \quad \xi_4^D \rfloor^T \right) \boldsymbol{T} \tag{4.72}$$

Corresponding to the above, matrices $\boldsymbol{E}_2$, $\boldsymbol{E}_3$, $\boldsymbol{E}_4$ and $\boldsymbol{E}_5$ are obtained.

$$\boldsymbol{E}_2 = \boldsymbol{T}^T \boldsymbol{U} \left(\tfrac{h^2}{4} \lfloor 0 \quad \xi_1^B \quad \xi_2^B \quad \xi_3^B \quad \xi_4^B \rfloor^T + 2\gamma \tfrac{h^3}{12} \lfloor 1 \quad \xi_1^D \quad \xi_2^D \quad \xi_3^D \quad \xi_4^D \rfloor^T + \right.$$
$$\left. \gamma^2 \tfrac{h^4}{32} \lfloor 0 \quad \xi_1^E \quad \xi_2^E \quad \xi_3^E \quad \xi_4^E \rfloor^T \right) \boldsymbol{T} \tag{4.73a}$$

$$\boldsymbol{E}_3 = \boldsymbol{T}^T \boldsymbol{U} \left(\tfrac{h^3}{12} \lfloor 1 \quad \xi_1^D \quad \xi_2^D \quad \xi_3^D \quad \xi_4^D \rfloor^T + 2\gamma \tfrac{h^4}{32} \lfloor 0 \quad \xi_1^E \quad \xi_2^E \quad \xi_3^E \quad \xi_4^E \rfloor^T + \right.$$
$$\left. \gamma^2 \tfrac{h^5}{80} \lfloor 1 \quad \xi_1^F \quad \xi_2^F \quad \xi_3^F \quad \xi_4^F \rfloor^T \right) \boldsymbol{T} \tag{4.73b}$$

$$\boldsymbol{E}_4 = \boldsymbol{T}^T \boldsymbol{U} \left(\tfrac{h^4}{32} \lfloor 0 \quad \xi_1^E \quad \xi_2^E \quad \xi_3^E \quad \xi_4^E \rfloor^T + 2\gamma \tfrac{h^5}{80} \lfloor 1 \quad \xi_1^F \quad \xi_2^F \quad \xi_3^F \quad \xi_4^F \rfloor^T + \right.$$
$$\left. \gamma^2 \tfrac{h^6}{192} \lfloor 0 \quad \xi_1^G \quad \xi_2^G \quad \xi_3^G \quad \xi_4^G \rfloor^T \right) \boldsymbol{T} \tag{4.73c}$$

$$\boldsymbol{E}_5 = \boldsymbol{T}^T \boldsymbol{U} \left(\tfrac{h^5}{80} \lfloor 1 \quad \xi_1^F \quad \xi_2^F \quad \xi_3^F \quad \xi_4^F \rfloor^T + 2\gamma \tfrac{h^6}{192} \lfloor 0 \quad \xi_1^G \quad \xi_2^G \quad \xi_3^G \quad \xi_4^G \rfloor^T + \right.$$
$$\left. \gamma^2 \tfrac{h^7}{448} \lfloor 1 \quad \xi_1^H \quad \xi_2^H \quad \xi_3^H \quad \xi_4^H \rfloor^T \right) \boldsymbol{T} \tag{4.73d}$$

Thus we have obtained expressions for the thickness integrated constitutive properties in terms of lamination parameters. Consequently, the stiffness matrix in equation (4.45) may be expressed in lamination parameters as well.

4.3 Summary

This concludes the chapter on degenerated shell elements. The steps in degenerating solid elements to shell elements are shown by introducing the kinematic assumptions of FSDT. The usual scheme for integrating layered degenerated shell elements completely numerically, was shown. Afterwards an alternative scheme is shown by introducing explicit thickness dependencies of the inverse Jacobian matrix. This enables explicit integration through the thickness to evaluate various element matrices which increases the efficiency in element formulation time for elements with many layers compared to the conventional integration scheme. A further reduction in element formulation time is obtained by further truncation of negligible terms of the strain-displacement relations. Eventually, the reduced constitutive relations for shells are presented and further developed to obtain expressions for the element stiffness matrix in terms of lamination parameters.

5

Structural design optimization

In the search for performance of engineering structures, optimization methods are employed increasingly along with access to numerical processing power. Restricting ourselves to structural design it is fair to say that any design task may be formulated as an optimization problem. As soon as the design task has been formulated as an optimization problem we may take advantage of mathematical methods developed within optimization theory.

5.1 Classes of structural optimization problems

Optimization may aid the designer at different levels of the design phase. Ranging from topology optimization applied at conceptual design stages over shape optimization that returns the optimum shape for a given topology to sizing optimization which may be used even at a detailed design level.

Yet another question in the design of a structure is the optimal choice of material and if applicable also orientation. Depending on the specific design problem at hand the available materials may be given in advance and in case of orthotropic materials being used in a laminate, the optimal lay-up in terms of layer thicknesses and orientations remains to be determined.

5.2 The optimization problem

Usually the structure to design has to fulfil one or multiple purposes. Obviously, by some measure, some solutions are better than other feasible solutions. A measure of how well or bad a given solution performs is evaluated through the *objective function*, f that is evaluated on basis of an analysis. At the same time space, money, physics, etc. may pose *constraints*, g and h, to our freedom of design. The objective and the constraints are explicit or implicit functions of the current design parametrized in terms of design variables, a_i. The *design variables* are a set of quantities that together constitute a certain configuration or design, and the task is to find the most favourable set that does not violate the constraints and at the same time minimizes the objective function. This task is solved by an optimization algorithm.

The objective function and the constraints are *scalar* functions of the vector of design variables. The constraints may be expressed as equalities and/or inequalities. The latter representing the most general case. This problem is usually expressed mathematically

in the following way.

$$\textbf{minimize } f(\boldsymbol{a}) \tag{5.1}$$

$$\textbf{subject to} \begin{cases} h_i(\boldsymbol{a}) = 0 & i = 1 \dots m \\ g_j(\boldsymbol{a}) \leq 0 & j = 1 \dots n \\ \underline{a}_k \leq a_k \leq \overline{a}_k & k = 1 \dots o \end{cases} \tag{5.2}$$

The last set of constraints are the side constraints that are upper and lower bounds on the design variables. The objective function and the constraints may be explicit or implicit. Implicit functions corresponds to being blindfolded in the search for an optimum, significantly complicating matters. This is the situation for most constraints within structural mechanics.

To solve the optimization problem an array of different techniques and algorithms exist and it is not the scope of this text to go into detail of this aspect. As indicated above the design variables may be of *continuous* or *discrete* nature. In general it is easier to solve continuous design variable problems compared to equivalent discrete design variable problems. This relates to the possibility of obtaining *sensitivities* or gradient information for continuous problems which is invaluable in the search for an optimum. This type of problem may be solved by gradient based methods that return a global optimum solution if the design space is convex.

In short structural optimization is a tool to obtain efficient structures that perform well taking into account the constraints posed. At the same time one should be aware that a risk of introducing new and unexpected failure modes exists and that the optimizer only does what it is asked to, namely to minimize the objective without violating any constraints posed, whatsoever.

In the following we present two specific types of optimization problems encountered in structural design optimization. The first one is that of designing a structure with the *maximum stiffness* for a given amount of material. The second type of optimization problem is the task of *maximizing the lowest buckling load* of a structure. Design sensitivity analysis for both types of optimization problems is treated in terms of generalized design variables first and subsequently we specialize to *orthotropic laminate optimization*. Various parametrizations for laminate optimization are discussed and in particular design sensitivity analysis with *lamination parameters* as design variables is investigated.

5.3 Maximum stiffness design

In many high performance applications such as wind turbine blades, aircraft structures and the like, stiffness is of major importance for the structural performance. Stiffness in itself is not difficult to obtain if it was not for simultaneous call for low structural weight. Thus, often we are faced with a multi-criterion problem, namely to maximize structural stiffness while minimizing weight. As shown above, we must have a single *scalar objective function* for the optimization problem to be meaningful. So, either an objective function is formed as a weighted sum of the two objectives or alternatively one

of the objectives is eliminated by choosing a satisfactory value for it and then include this target value as a constraint instead.

The usual way of handling the maximum stiffness design of lightweight structures is to agree on a maximum allowable weight and then gain as much performance as possible for the chosen acceptable amount of material usage. In maximum stiffness design we want to reduce displacements caused by externally applied loads. Therefore, the objective is typically chosen to be the compliance. The compliance C is defined as *the work, W, done by the applied forces in reaching an equilibrium deformed state.*

$$C(\boldsymbol{a}) \equiv W(\boldsymbol{a}) = \boldsymbol{r}^T \boldsymbol{d} \tag{5.3}$$

For a linear elastic structure the work done by the applied forces is related to the elastic strain energy in the following way

$$W = \boldsymbol{r}^T \boldsymbol{d} = \boldsymbol{d}^T \boldsymbol{K} \boldsymbol{d} = 2U \tag{5.4}$$

Thus the compliance is related to the elastic strain energy and consequently the minimum compliance optimization problem may be expressed in terms of the internal strain energy.

$$\textbf{minimize } U(\boldsymbol{a}) \tag{5.5}$$

$$\textbf{subject to} \quad \boldsymbol{K}\boldsymbol{d} = \boldsymbol{r} \tag{5.6}$$

5.4 Maximum stability design

Stiffness maximization tends to favour membrane states of stress since this gives the best material utilization compared to bending dominated designs. It is a well-known fact that structural members loaded in compression are prone to buckling failure and therefore it may be important to cope with buckling failure in stiffness optimization problems, equally. In practical design, although non-conservative due to unavoidable manufacturing imperfections, the lowest linear buckling load may be used as a measure of structural strength against stability failure. So in order to maximize the stability of a structure, the task is to *maximize the lowest buckling load.* Formally this is stated as

$$\textbf{maximize } min\{\lambda(\boldsymbol{a})\} \tag{5.7}$$

5.5 Design sensitivity analysis

The purpose of this section is to describe how design sensitivity analysis is applied in obtaining optimized designs based on rational decisions.

Design sensitivity analysis relies on a parametrization of the analysis model which has been treated above. With a parametrized model it is possible to obtain information on how a small change of a design variable affects the objective function and thus the overall performance of the structure. This may be carried out analytically or numerically by finite differences. In the following we derive expressions for the sensitivities of the compliance and the buckling load.

5.5.1 Sensitivity of stiffness

As stated in Section 5.3 the compliance is related to the elastic strain energy and thus the sensitivities with respect to compliance can be stated in terms of derivatives of the elastic strain energy. The elastic strain energy of an FE-discretized structure at equilibrium is given by

$$U = \tfrac{1}{2}\boldsymbol{d}^T\boldsymbol{K}\boldsymbol{d} \tag{5.8}$$

To obtain the sensitivity, the expression is differentiated with respect to a design variable, a_i, from a vector of generalized design variables, $\boldsymbol{a}$.

$$\frac{\partial U}{\partial a_i} = \frac{1}{2}\left(\frac{d\boldsymbol{d}^T}{da_i}\boldsymbol{K}\boldsymbol{d} + \boldsymbol{d}^T\frac{\partial \boldsymbol{K}}{\partial a_i}\boldsymbol{d} + \boldsymbol{d}^T\boldsymbol{K}\frac{d\boldsymbol{d}}{da_i}\right) \tag{5.9}$$

Exploiting symmetry of the stiffness matrix, $\boldsymbol{K}$, we combine the first and last term in the bracket

$$\frac{\partial U}{\partial a_i} = \frac{1}{2}\boldsymbol{d}^T\frac{\partial \boldsymbol{K}}{\partial a_i}\boldsymbol{d} + \boldsymbol{d}^T\boldsymbol{K}\frac{d\boldsymbol{d}}{da_i} \tag{5.10}$$

To do further simplifications of the expression above, the FE equilibrium equation, (5.6), is differentiated with respect to a design variable

$$\frac{\partial \boldsymbol{K}}{\partial a_i}\boldsymbol{d} + \boldsymbol{K}\frac{d\boldsymbol{d}}{da_i} = \frac{\partial \boldsymbol{r}}{\partial a_i} \tag{5.11}$$

By assuming design independent nodal loads, $\frac{\partial \boldsymbol{r}}{\partial a_i} = 0$, the following relation is obtained

$$\boldsymbol{K}\frac{d\boldsymbol{d}}{da_i} = -\frac{\partial \boldsymbol{K}}{\partial a_i}\boldsymbol{d} \tag{5.12}$$

This expression resembles the FE equilibrium equation, (5.6), now with the unknowns being the displacement sensitivities, $\frac{d\boldsymbol{d}}{da_i}$. The right hand side of this expression is called the pseudo-load vector. The stiffness matrix sensitivities, $\frac{\partial \boldsymbol{K}}{\partial a_i}$, are readily evaluated at element level either as analytical sensitivities or finite difference approximations. The displacements are known from the solution of the equilibrium equation. With the factorized stiffness matrix at hand (from the solution of the equilibrium equation) the displacement sensitivities are simply obtained by solving the above system of equations with the pseudo-load vector as the new right hand side, which is computationally efficient since the solution only requires forward backward substitutions. This way of obtaining the displacement sensitivities is used later in obtaining sensitivities of the stress stiffness matrix in equation (5.21). In case of sensitivity analysis of the elastic strain energy, the need for solving (5.12) is omitted in case of design independent loads. This is seen by substitution of equation (5.12) into (5.10) whereby the sensitivities can be expressed as

$$\frac{\partial U}{\partial a_i} = -\frac{1}{2}\boldsymbol{d}^T\frac{\partial \boldsymbol{K}}{\partial a_i}\boldsymbol{d} = -\frac{1}{2}\sum_{e=1}^{N}(\boldsymbol{d}^e)^T\frac{\partial \boldsymbol{K}^e}{\partial a_i}\boldsymbol{d}^e \tag{5.13}$$

Hereby the design sensitivity of the elastic strain energy with respect a design variable, a_i, is expressed as a sum of sensitivities at the element level. Until now the design variables have been expressed as generalized and thus apply for any choice of design variables. In Appendix B it is shown how the sensitivities of the stiffness matrix with respect to lamination parameters are obtained analytically.

5.5.2 Sensitivity of buckling load

As we want to maximize the buckling load of a structure we need to express the sensitivity of the lowest buckling load with respect to some design variable as shown in Lund (2007). If we for simplicity assume that the lowest buckling load (eigenvalue) is distinct and thus not multiple, we obtain the sensitivity by simply differentiating the expression for the linear buckling problem equation (3.24), that is repeated here for reference.

$$\left(\boldsymbol{K}+\lambda_j\boldsymbol{K}_\sigma\right)\boldsymbol{\phi}_j=\boldsymbol{0};\qquad j=1,2,...,n_{DOF} \tag{5.14}$$

Differentiation with respect to a design variable, a_i, yields

$$\frac{d}{da_i}\left[\left(\boldsymbol{K}+\lambda_j\boldsymbol{K}_\sigma\right)\boldsymbol{\phi}_j\right]=\boldsymbol{0}\quad\Leftrightarrow \tag{5.15}$$

$$\left(\frac{\partial\boldsymbol{K}}{\partial a_i}+\left(\frac{d\lambda_j}{da_i}\boldsymbol{K}_\sigma+\lambda_j\frac{d\boldsymbol{K}_\sigma}{da_i}\right)\right)\boldsymbol{\phi}_j+\left(\boldsymbol{K}+\lambda_j\boldsymbol{K}_\sigma\right)\frac{d\boldsymbol{\phi}_j}{da_i}=\boldsymbol{0}\quad\Leftrightarrow \tag{5.16}$$

$$\frac{d\lambda_j}{da_i}\boldsymbol{K}_\sigma\boldsymbol{\phi}_j=-\left(\frac{\partial\boldsymbol{K}}{\partial a_i}+\lambda_j\frac{d\boldsymbol{K}_\sigma}{da_i}\right)\boldsymbol{\phi}_j-\left(\boldsymbol{K}+\lambda_j\boldsymbol{K}_\sigma\right)\frac{d\boldsymbol{\phi}_j}{da_i} \tag{5.17}$$

If the eigenvectors $\boldsymbol{\phi}_j$ are $\boldsymbol{K}_\sigma$-orthonormalized (i.e. $\boldsymbol{\phi}_j^T\boldsymbol{K}_\sigma\boldsymbol{\phi}_j=1$) pre-multiplication by $\boldsymbol{\phi}_j^T$ yields

$$\frac{d\lambda_j}{da_i}=-\boldsymbol{\phi}_j^T\left(\frac{\partial\boldsymbol{K}}{\partial a_i}+\lambda_j\frac{d\boldsymbol{K}_\sigma}{da_i}\right)\boldsymbol{\phi}_j-\boldsymbol{\phi}_j^T\left(\boldsymbol{K}+\lambda_j\boldsymbol{K}_\sigma\right)\frac{d\boldsymbol{\phi}_j}{da_i} \tag{5.18}$$

If we utilize that $\left(\boldsymbol{K}+\lambda_j\boldsymbol{K}_\sigma\right)$ is symmetric, $\boldsymbol{\phi}_j^T$ and $\frac{d\boldsymbol{\phi}_j}{da_i}$ can be interchanged in the last term of equation (5.18) which together with equation (5.14) results in the following expression for the sensitivity of the buckling load factor.

$$\frac{d\lambda_j}{da_i}=-\boldsymbol{\phi}_j^T\left(\frac{\partial\boldsymbol{K}}{\partial a_i}+\lambda_j\frac{d\boldsymbol{K}_\sigma}{da_i}\right)\boldsymbol{\phi}_j \tag{5.19}$$

This expression for the sensitivity of the buckling load factor contains the derivatives of the stiffness and the stress stiffness matrix with respect to a design variable. The derivative of the stiffness matrix with respect to a design variable, $\frac{d\boldsymbol{K}}{da_i}$, is readily obtained on the element level either by finite differences or by analytical derivatives obtained by symbolic differentiation of element matrices. In case of lamination parameters acting as design variables it is shown in Appendix B. The sensitivity of the stress stiffness matrix, $\frac{d\boldsymbol{K}_\sigma}{da_i}$, requires a bit more consideration. Recall that the initial stress stiffness matrix is obtained on basis of the stresses determined by a static analysis, i.e. it depends on the displacements. Thus the initial stress stiffness matrix is an implicit function of the displacements, i.e. $\boldsymbol{K}_\sigma=\boldsymbol{K}_\sigma\left(\boldsymbol{d}\left(\boldsymbol{a}\right),\boldsymbol{a}\right)$. Formally, this means that the sensitivity of the initial stress stiffness matrix attains the following form

$$\frac{d\boldsymbol{K}_\sigma}{da_i}=\frac{\partial\boldsymbol{K}_\sigma}{\partial a_i}+\frac{\partial\boldsymbol{K}_\sigma}{\partial\boldsymbol{d}}\frac{d\boldsymbol{d}}{da_i} \tag{5.20}$$

However, to evaluate this expression we need the partial derivatives of the stress stiffness matrix with respect to the displacements, $\frac{\partial\boldsymbol{K}_\sigma}{\partial\boldsymbol{d}}$, which is not trivial. So, instead of evaluating each term on the right hand side of equation (5.20), the stress stiffness

matrix sensitivity is obtained from a central finite difference approximation at the element level.

$$\frac{d\boldsymbol{K}_\sigma}{da_i} \approx \frac{\boldsymbol{K}_\sigma\left(a_i + \Delta a_i, \boldsymbol{d} + \Delta \boldsymbol{d}\right) - \boldsymbol{K}_\sigma\left(a_i - \Delta a_i, \boldsymbol{d} - \Delta \boldsymbol{d}\right)}{2\Delta a_i} \tag{5.21}$$

with $\Delta \boldsymbol{d} \approx \frac{d\boldsymbol{d}}{da_i}\Delta a_i$ where the displacement sensitivity $\frac{d\boldsymbol{d}}{da_i}$ is obtained by solving equation (5.12) for the design variable, a_i. For fibre angle design variables, a perturbation of $\Delta a_i = 10^{-3}$ turns out to be adequate.

5.6 Laminate optimization

So far, we have presented the optimization problems in terms of generalized design variables. In this section we address the issue of laminate optimization with orthotropic materials for which the design variables may be, for instance, layer orientation, thickness or lamination parameters.

5.6.1 Non-convexity in fibre angle optimization

The major problem of a fibre angle parametrization is that the objective, e.g. the compliance, is non-convex. That is, there may exist multiple local minima and we cannot ensure that a gradient-based optimization algorithm leads to a global optimum solution. In fact, as we will show below, we may even obtain solution 'close' to an absolutely non-optimal solution if a local minimum and the initial guess is in the vicinity of the global maximum.

Two-layer example

To illustrate problems concerning non-convexity of a fibre angle parametrization, we study the design space of a simple problem with two design variables. We want to minimize the compliance of a cantilevered plate loaded in shear or tension in the plane of the plate, see Figure 5.1. The plate consists of two fixed thickness orthotropic layers whose fibre orientations, θ_1 and θ_2, may be varied independently. In Figure 5.1 both

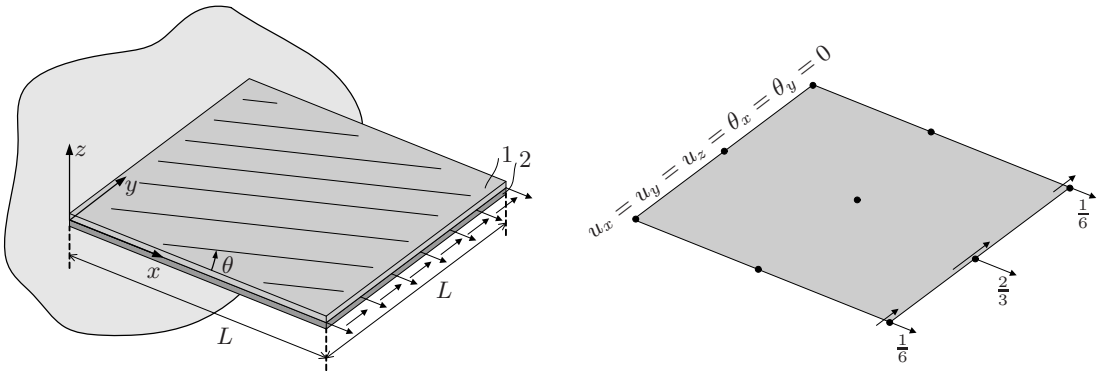

Figure 5.1: Left: Sketch of cantilevered two-layer plate example with tensile and shear load imposed. Dimensions: $L = 1$, layer thicknesses, $h = 0.025$. Right: one-element discretization with boundary conditions and equivalent nodal loads.

load cases, tension and shear, are shown simultaneously. In the optimization, however,

the two load cases are treated individually. In the following we investigate the design space of each load case when both fibre angles are independent design variables. The small size of the problem enables us to search the entire design space and thus visualize the objective. Of course, this luxury is not an option in real life problems but for this demonstration example it serves to gain insight into the problem.

From Figure 5.2 we see that the in-plane shear problem has two equally good global optima. These are found for $\theta_1 = -24.8725$, $\theta_2 = 24.8725$ or $\theta_1 = 24.8725$, $\theta_2 = -24.8725$. These optimum solutions are only found if the initial guess is close enough to one of the optimum solutions. Otherwise, gradient-based algorithms will return local minima as the solution.

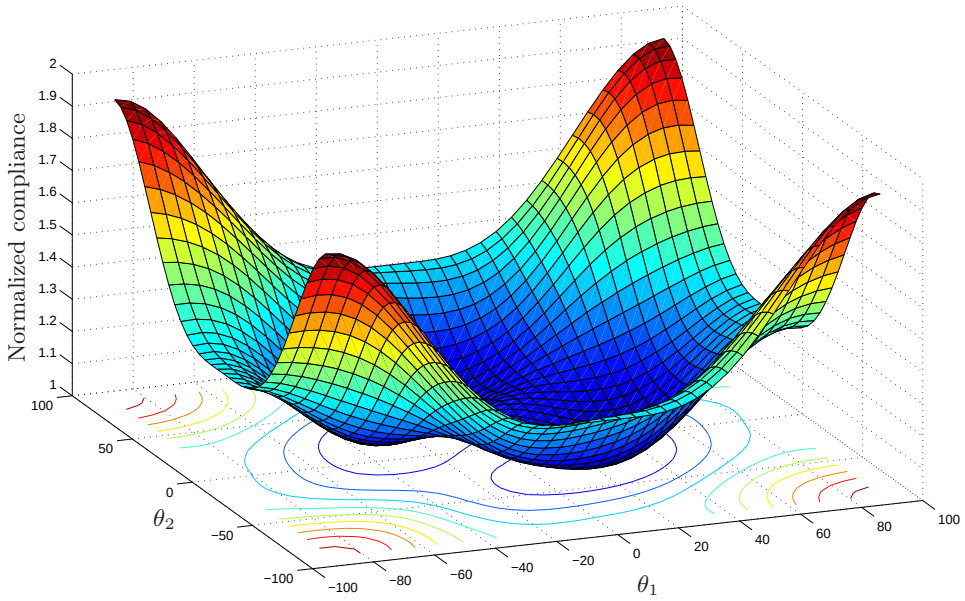

Figure 5.2: In-plane shear example: normalized compliance against fibre angles, θ_1 and θ_2. Normalized against optimal compliance: $3.9075 \cdot 10^{-9}$.

For the tensile load case the optimal fibre directions are, not surprisingly, $\theta_1 = \theta_2 = 0$. This is readily recovered in Figure 5.3. From the figure we observe several local minima including the minima at $\theta_{1,2} = \pm 90$ that are close to the worst possible compliance about four times as big as the optimum compliance! This result is somewhat discouraging and calls for an alternative parametrization. The previous examples in a simple manner illustrate some of the problems encountered in non-convex optimization problems. Optimization results depend on the quality of the initial guess and the global optimum may only be reached from initial guesses within some safe region. In the next section we will show an extension of an existing laminate optimization scheme.

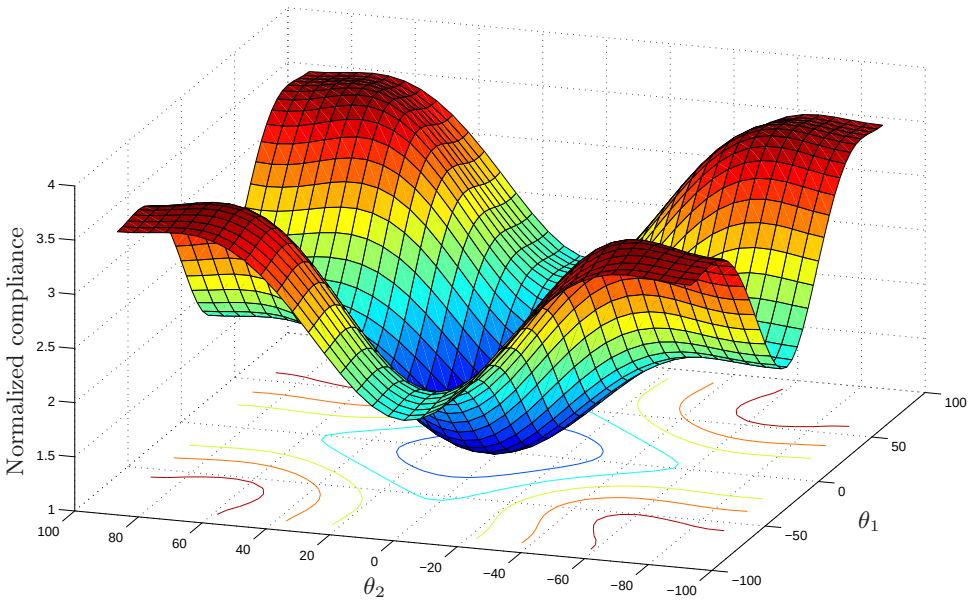

Figure 5.3: In-plane tensile example: normalized compliance against fibre angles, θ_1 and θ_2. Normalized against optimal compliance: $4.3747 \cdot 10^{-9}$.

5.6.2 Optimization with lamination parameters

To circumvent the non-convexity of a continuous fibre angle parametrization several approaches involving lamination parameters have been proposed as seen in Section 1.1.2 where an overview was given. In this section it is outlined how the laminate optimization method proposed by Foldager et al. (1998) may be extended to general shell geometries by use of the element formulations shown in this project. This step entails that the number of lamination parameters is extended from the previous 12 to 28 as shown in equation (4.67).

In Section 1.1.2 it was found that for combined in-plane and bending loads the feasible regions of the lamination parameters have not been determined. Foldager et al. (1998) approached the general laminate design problem from a different angle. Their idea is to use fibre angles and laminae thicknesses as design variables while using lamination parameters to provide convexity. This approach calls for a procedure that can identify physical lay-ups in terms of orientations and thicknesses from an optimized set of lamination parameters.

The procedure shown in Figure 5.4 is formulated as an optimization problem in the layer angles, $\boldsymbol{\theta}$ and thicknesses, $\boldsymbol{h}$. The procedure consists of the following steps

1. A conventional fibre angle optimization returns a set of (sub-)optimal angles and thicknesses, $\left({}^{OPT}\boldsymbol{\theta}^k, {}^{OPT}\boldsymbol{h}^k\right)$.

2. Ply angles and thicknesses $\left({}^{OPT}\boldsymbol{\theta}^k, {}^{OPT}\boldsymbol{h}^k\right)$ are converted to lamination parameters, ${}^{OPT}\boldsymbol{\xi}$, by use of equation (4.68). At the current design point, sensitivities of the objective with respect to lamination parameters are evaluated, $\frac{\partial f}{\partial \boldsymbol{\xi}}$. For compliance this amounts to evaluating equation (5.13) and for buckling (5.19).

3. Identification of a new starting point: This step is performed by an identification procedure whose objective is to find a new set of angles and thicknesses $\left({}^{OPT}\boldsymbol{\theta}^{k+1}, {}^{OPT}\boldsymbol{h}^{k+1}\right)$ that minimize the difference between the current set of lamination parameters, $\boldsymbol{\xi}^*$ and those obtained on basis of the new angles and thicknesses, $\boldsymbol{\xi}\left({}^{OPT}\boldsymbol{\theta}^{k+1}, {}^{OPT}\boldsymbol{t}^{k+1}\right)$, subject to the constraint that the new set of angles and thicknesses must have a lower objective f than the previous set. If a new starting point is found, the optimization loop is continued from step 1 else the current design must be the global optimum and consequently the optimization is terminated.

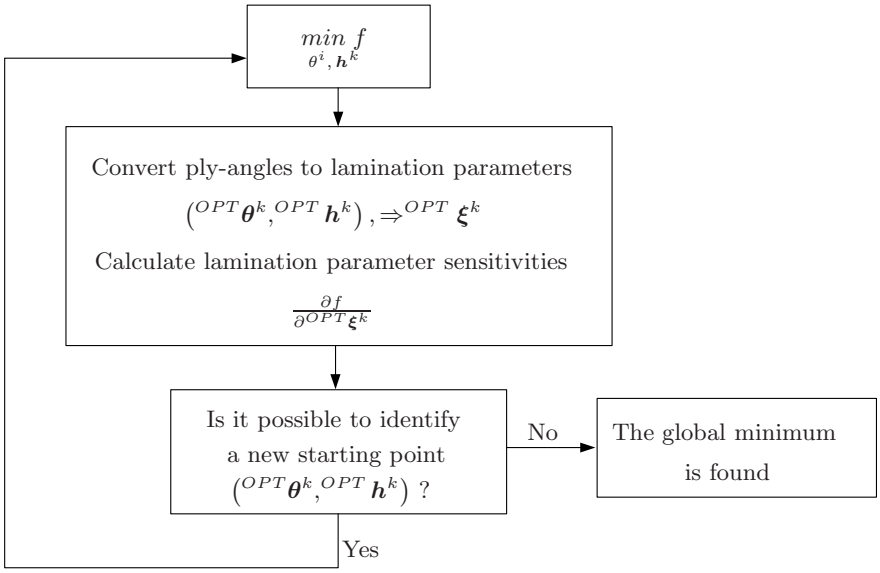

Figure 5.4: Schematic flow diagram of the optimization procedure proposed by Foldager et al. (1998).

These steps should lead to a physically realisable lay-up that is global optimum. In the following we briefly describe some details of the identification procedure.

Identification

The identification procedure described in the last step of the optimization loop above is based on an optimization itself. The aim is to find a new lay-up that minimizes the difference between the lamination parameters corresponding to the previous design and those obtained by the new lay-up subject to the constraint that it must improve the objective function f. This ensures that the design sequentially is driven towards a

global optimum solution. The identification objective is given by

$$I = 4f_1\left(\xi^*, \xi\left(\theta_i, t_i\right)\right) + f_2\left(\xi^*, \xi\left(\theta_i, t_i\right), \frac{\partial f}{\partial \xi^*}\right) \tag{5.22}$$

Contrary to the original development it is our opinion that f_1 should be the squared difference between the current and the new design, i.e. we optimize in a least squares sense.

$$f_1\left(\xi^*, \xi\left(\theta_i, t_i\right)\right) = \sum_{i=1}^{N_{LP}} \left(\xi_i^* - \xi_i\left(\theta_i, t_i\right)\right)^2 \tag{5.23}$$

The f_2 function depends on derivatives with respect to lamination parameters, $\frac{\partial f}{\partial \xi^*}$ and is included to favour lay-ups with a lower objective f, for details about this function see Foldager et al. (1998).

5.7 Summary

In this chapter structural design optimization was presented as a tool to rationally design optimal structures for a given objective. The objective could be e.g. to design for maximum stiffness or maximum stability and for these objectives it was shown how to obtain sensitivities with respect to generalized design variables. For a layer angle parametrization in laminate optimization, non-convexity of the stiffness was illustrated by two simple examples. Eventually, a procedure is shown that provides convexity in stiffness design based on lamination parameters.

6

Numerical examples

KNOWING THE LIMITATIONS, SHORTCOMINGS AND ADVANTAGES of a given element formulation is essential when modelling by finite elements. The finite element method approximates the originally continuous problem by discretizing the governing equations and subsequently interpolates the solution obtained at discrete points within elements. It is obvious that a finer discretization improves accuracy, however, this accuracy comes at a price in terms of larger systems of equations to be solved. Therefore, in a finite element context, a discussion of element accuracy is necessarily accompanied by an assessment of computational efficiency. In addition, it is important to verify that the implementations of the element routines are correct. This is naturally done prior to and during the coding phase by thorough planning of the routines and subsequent de-bugging. The tests are primarily focused on verification of the 9-node element. The implementation is of general nature and also caters for the 16-node version of the element, but this element is not tested as extensively as the 9-node element.

6.1 Test strategy

In order to verify the implementation of the new elements a number of standard tests with known solutions are performed. The set of tests covers a variety of loading situations and geometrical configurations which ensures that the elements are tested comprehensively.

First, we perform so-called patch tests in order to demonstrate that the elements are able to represent constant stresses throughout a distorted mesh which is important for convergence. Next, accuracy and convergence is assessed in a number of standard test examples for shell elements from MacNeal and Harder (1985). These tests should reveal possible shortcomings and limitations of the elements.

To asses the influence of the approximations made to enable explicit thickness integration, the results obtained with the new element formulations are compared to those obtained with the existing 9-node isoparametric shell element. The isoparametric 9-node shell element formulations are denoted as follows:

- SHELL9: existing formulation with layer-wise numerical thickness integration, see Section 4.2.1.
- SHELL9Expl: explicit integration through the thickness based on assumption of

the inverse Jacobian matrix through the thickness, see Section 4.2.2.

- SHELL9ExplApp: same integration scheme as SHELL9Expl with further approximations ($\boldsymbol{G}_3 = \boldsymbol{B}_3 = \boldsymbol{0}$).

Also, the performances of the elements are compared. Tests with increasing numbers of layers are carried out to asses the performance gain and to identify the break-even number of layers with respect to element formulation time. Finally, a number of small-scale optimization examples are shown in order to verify the efficiency gain in a multi-layer setting.

6.2 Patch tests

Patch tests serve to demonstrate whether given elements are able to exhibit states of constant strain and stress in distorted meshes, respectively. This property is important in order to ensure well-behaved convergence characteristics since elements should exhibit constant strain in the limiting case of infinitely small elements.

We want to investigate the ability to exhibit constant stresses in membrane loading and the ability to show constant bending stresses in pure bending. The tests are performed on a 'patch' of elements proposed by MacNeal and Harder (1985), shown in Figure 6.1.

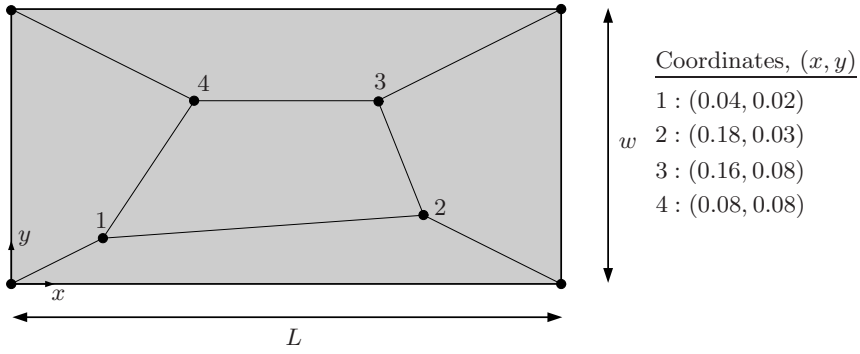

Figure 6.1: Patch test geometry and coordinates of inner nodes. $L = 0.24$, $w = 0.12$ and thickness, $h = 0.001$. Isotropic material properties: Young's modulus, $E = 10^6$ and Poisson's ratio, $\nu = 0.25$.

6.2.1 In-plane membrane patch test

In order to test the ability to demonstrate states of constant membrane stress throughout a distorted mesh, the in-plane membrane patch test is applied. The test prescribes a pure membrane displacement field that should result in constant in-plane stresses throughout the distorted mesh.

$$u = 10^{-3}\left(x + \tfrac{y}{2}\right) \tag{6.1}$$

$$v = 10^{-3}\left(y + \tfrac{x}{2}\right) \tag{6.2}$$

$$w = 0 \tag{6.3}$$

This should theoretically result in the following stresses

$$\sigma_{xx} = \sigma_y = 1333 \qquad \sigma_{xy} = 400 \tag{6.4}$$

Results of the membrane patch tests are shown for SHELL9Expl in Figure 6.2 and for SHELL9ExplApp in Figure C.1 in the Appendix.

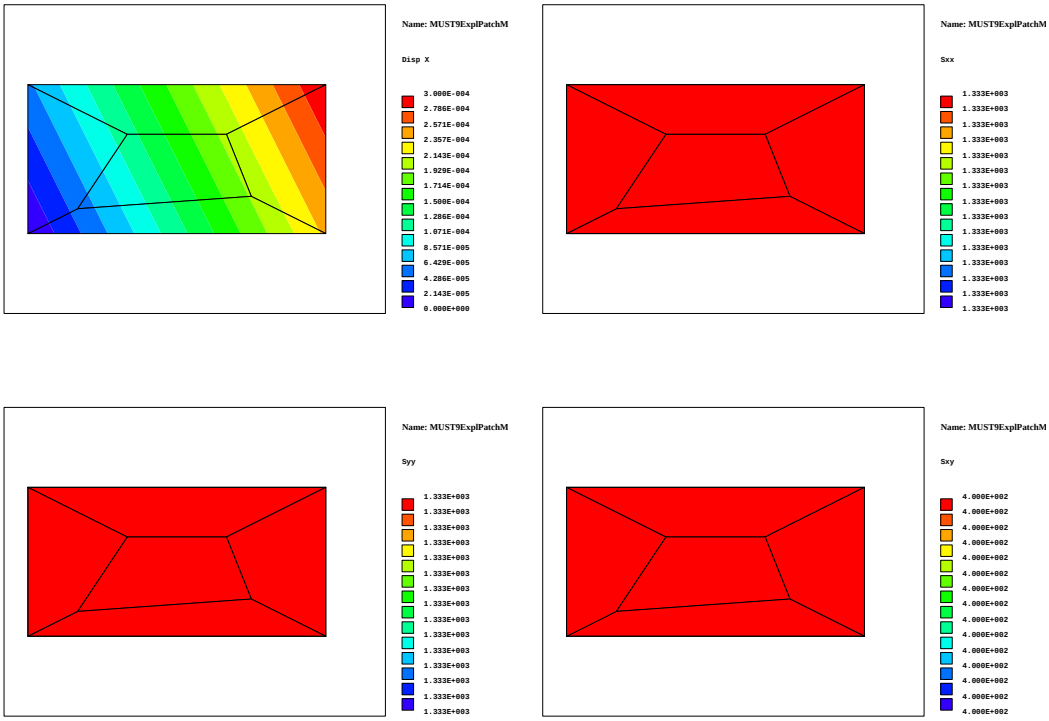

Figure 6.2: Membrane patch test results for the explicitly integrated 9-node formulation, SHELL9Expl. From top left to bottom right: u_x, σ_{xx}, σ_{yy} and σ_{xy}, respectively.

Both formulations pass the in-plane membrane patch test by exhibiting continuous linear displacement contours and constant values of the stress components throughout the mesh.

6.2.2 Out-of-plane bending patch test

To demonstrate the ability to represent constant bending stresses throughout the mesh, we impose a pure bending displacement field:

$$w = 10^{-3}\left(x^2 + xy + y^2\right)/2 \tag{6.5}$$
$$\theta_x = 10^{-3}\left(y + \tfrac{x}{2}\right) \tag{6.6}$$
$$\theta_y = -10^{-3}\left(x + \tfrac{x}{2}\right) \tag{6.7}$$

This should theoretically result in the following constant stresses

$$\sigma_{xx} = \sigma_y = \pm 0.667 \qquad \sigma_{xy} = \pm 0.200 \tag{6.8}$$

Results of the membrane patch tests are shown in Figure 6.3 and C.2.

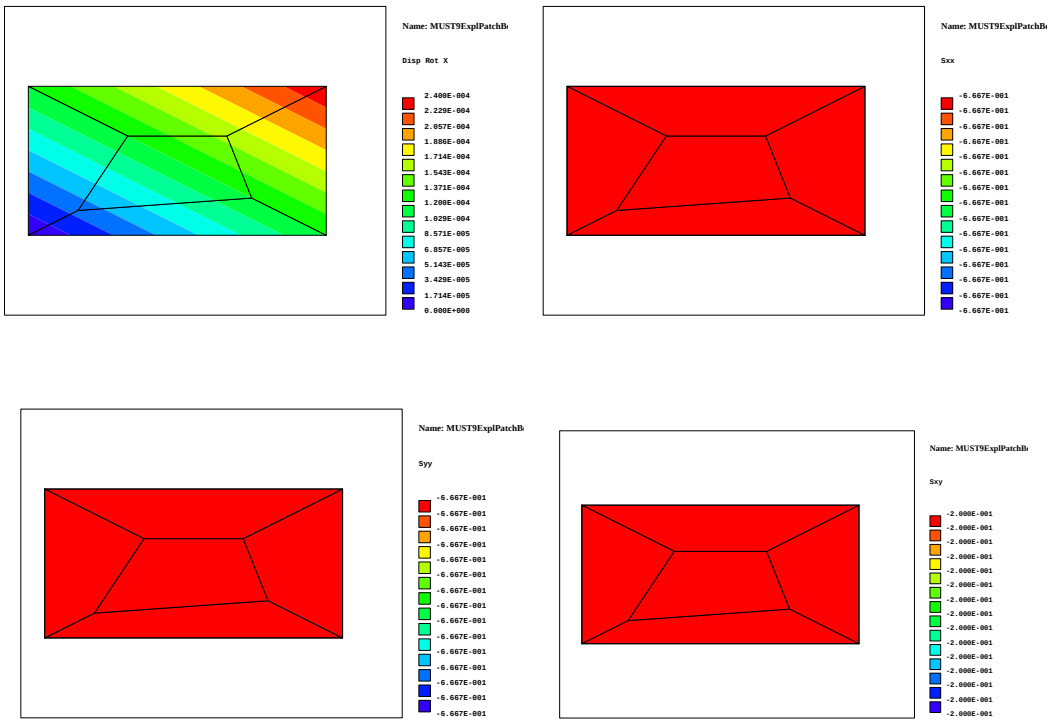

Figure 6.3: Bending patch test results for the explicitly integrated 9-node formulation, SHELL9Expl. From top left to bottom right: θ_x, σ_{xx}, σ_{yy} and σ_{xy}, respectively.

Again, both formulations pass the out-of-plane bending patch test by exhibiting continuous linear rotation contours and constant values of the stress components throughout the mesh.

6.2.3 Layered patch tests

To verify the implementation of the explicit and the approximate explicit thickness integration schemes, a bending and a membrane patch test is performed on a mesh of layered elements. Material properties and total stack thickness is the same as for single layer patch tests. The difference being that the stack is now made up of three layers with thicknesses $(0.00025, 0.0005, 0.00025)$. The results (given in Appendix C) show that both formulations pass the patch tests and thus it is concluded that the two explicit thickness integration schemes are implemented correct for evaluation of the stiffness matrix. The stress recovery routines are also verified by the above. For integration of the remaining element matrices we must resort to standard test problems with known solutions which is shown below.

6.3 Numerical accuracy

In this section the previously mentioned standard tests are carried out. The tests serve to verify whether the solutions obtained with the elements converge towards known solutions. Also, the approximation introduced in obtaining an explicit expression of the inverse Jacobian is assessed for varying radius of curvature-to-thickness ratios. Furthermore it is tested whether the approximation makes the element more sensitive to twist.

6.3.1 Pinched hemisphere

To test the shell elements' convergence behaviour in mixed membrane and bending situations, the doubly curved pinched hemisphere problem is employed. The pinched hemisphere is loaded by two sets of pinching point loads at equator. The 18° opening in the top is introduced in order to avoid triangular elements near the pole. The problem is illustrated in Figure 6.4. Due to symmetry only one quarter is modelled.

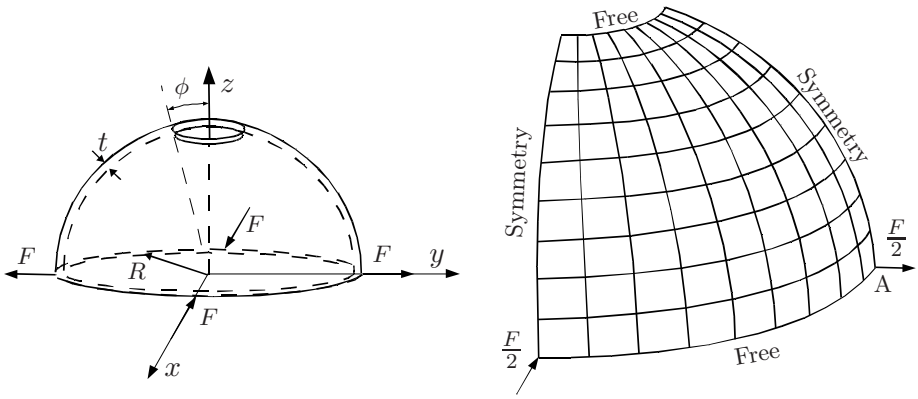

Figure 6.4: Geometry and boundary conditions for topless pinched hemisphere. Load: $F = 2$. Dimensions: $R = 10.0$, $t = 0.04$, $\phi = 18.0°$. Isotropic material properties: $E = 6.825 \cdot 10^7$, $\nu = 0.3$.

For comparison purposes we monitor the radial deflection of point A. A theoretical

lower bound of 0.0924 is known from an exact solution for a closed pinched hemisphere. A more realistic result for the open hemisphere is 0.0940, MacNeal and Harder (1985), which is used for normalization in the following.

Convergence is studied by refining an $N \times N$ mesh applied to one quarter of the hemisphere. The normalized radial displacement of point A is shown graphically in Figure 6.5. Results are shown for all three element formulations and from the graph no difference is seen. Convergence seems to be reached equally for all three formulations at a mesh size of 32×32. Thus the approximations introduced do not alter the convergence compared to the SHELL9 element.

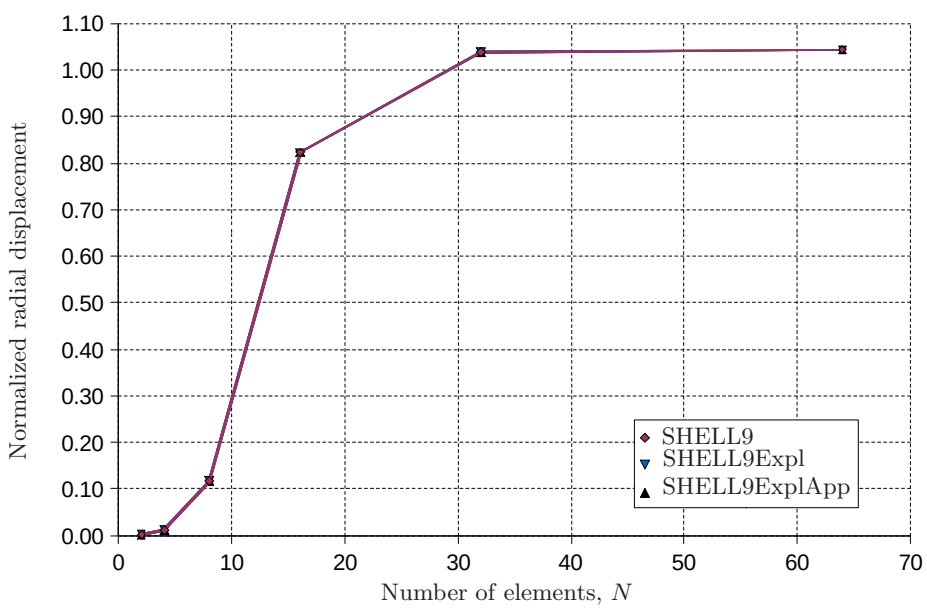

Figure 6.5: Pinched hemisphere: normalized radial displacement of point A vs. number of elements in $N \times N$ mesh. Normalized by: 0.0940.

Next, we study the influence of the curvature to thickness ratio.

6.3.2 Influence of R/h-ratio

To enable explicit thickness integration we assumed the radius of curvature to be significantly larger than the shell thickness, Section 4.1.4. Now we use the pinched hemisphere example to study the precision of this approximation for varying radius of curvature-to-thickness ratios. The deflection of point A, obtained by the explicitly integrated element formulations, is compared to the same displacement obtained by the completely numerically integrated formulation, SHELL9. The relative difference is defined as

$$D = \left(\frac{v_A^{Expl}}{v_A^{SHELL9}} - 1 \right) \cdot 100\% \tag{6.9}$$

In Figure 6.6 the relative difference of the displacement of point A compared to the SHELL9 solution is plotted against the radius of curvature-to-thickness ratio of the

pinched hemisphere. For plates (i.e. $\frac{R}{h} = \infty$) the relative difference caused by the approximation is zero. This is reflected in that the relative difference is less than 4% for shells with a $\frac{R}{h}$-ratio larger than 5 and beyond, the error asymptotically approaches zero. For shells in the thin shell range, that is, $\frac{R}{h} > 25$ virtually no difference is observed, as expected.

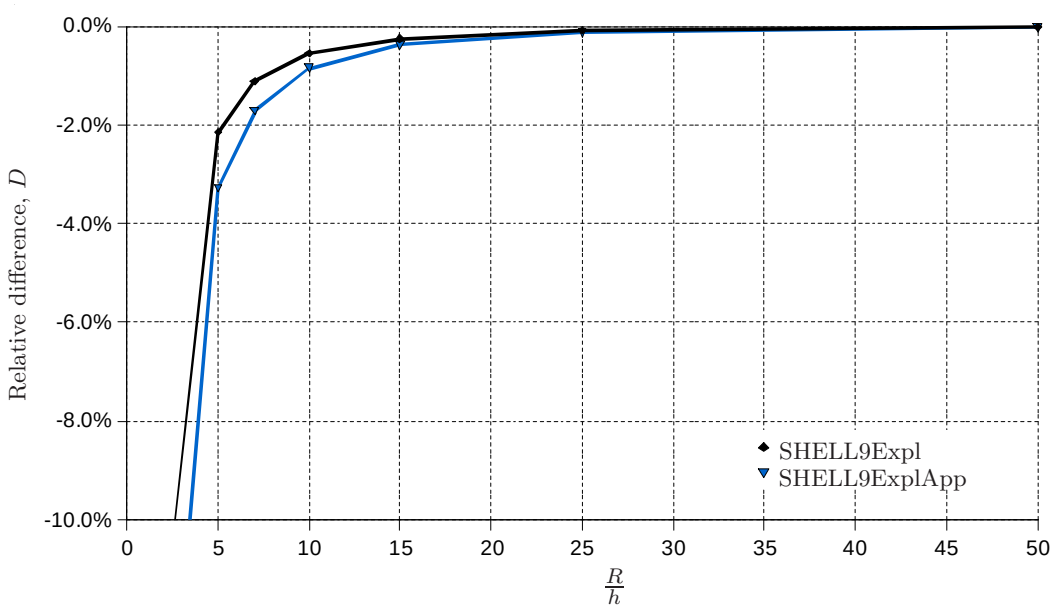

Figure 6.6: Relative difference of point A displacements of SHELL9Expl and SHELL9ExplApp compared to complete numerically integrated 9-node shell element, SHELL9.

The plot shows that the approximation introduced to enable explicit thickness integration is reasonable for radius-to-thickness ratios that are typically modelled as shell structures. It is seen that SHELL9ExplApp is slightly more un-precise than the SHELL9Expl formulation in the moderately thick shell range but still very close to the SHELL9 formulation in the thin shell range. Though the plot displays $\frac{R}{h}$ values below 10, it is questionable whether such structures are adequately modelled as shells.

6.3.3 Scordelis-Lo roof

The Scordelis-Lo roof example is a standard test to asses convergence in a combined bending-membrane problem with the membrane action being dominant. The roof is modelled as a cylindrical shell loaded by self-weight and supported by rigid diaphragms at each end, see Figure 6.7. The roof is relatively shallow with a radius of curvature-to-thickness ratio of $\frac{R}{h} = 100$. According to MacNeal and Harder (1985) the original reference solution is a roof edge deflection at midspan of $v = 0.3086$, but $v = 0.3024$ seems to have become the reference solution for this problem and we will use the latter value for normalization of our results. Convergence is assessed through consecutive refinement of an $N \times N$ mesh, from $N = 2$ to 64.

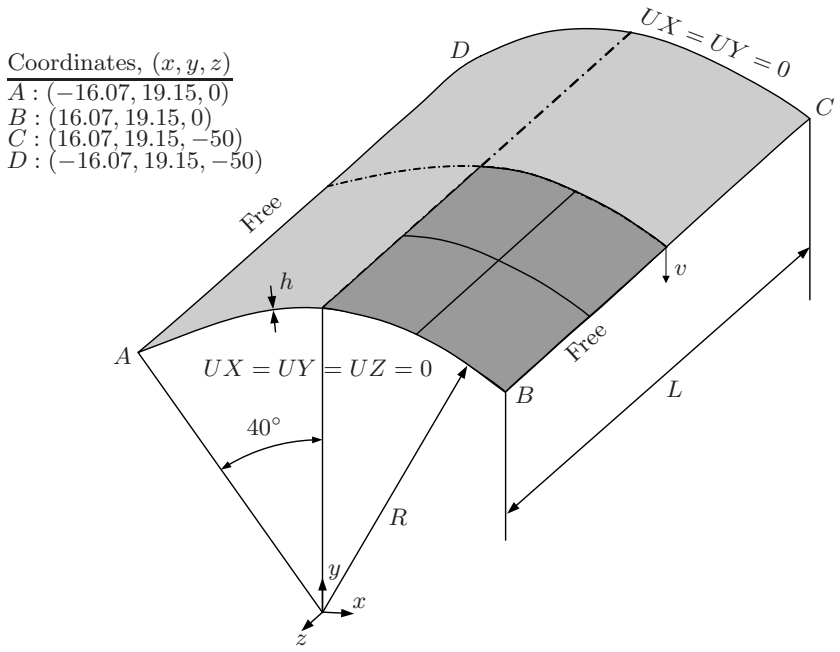

Figure 6.7: Scordelis-Lo roof with end diaphragms loaded by self weight. Dimensions: $R = 25$, $L = 50$ and $h = 0.25$. Isotropic material properties: Young's modulus, $E = 4.32 \cdot 10^8$, and Poisson's ratio, $\nu = 0$.

The loading pr. unit area is 90. With a gravity of 9.82 and a thickness, $h = 0.25$ this yields a mass density of 36.66.

The results obtained with the three implementations of the 9-node element are shown in Figure 6.8. The three formulations yield virtually identical results and may not be distinguished from each other from the plot. All formulations exhibit monotonic convergence towards the reference solution. Thus for equivalent meshes the approximation introduced in the SHELL9Expl and SHELL9ExplApp do not influence the results obtained. This supports the conclusions drawn in Section 6.3.2, namely that the approximation only introduces notable deviations for shells with a radius of curvature-to-thickness ratio below 25.

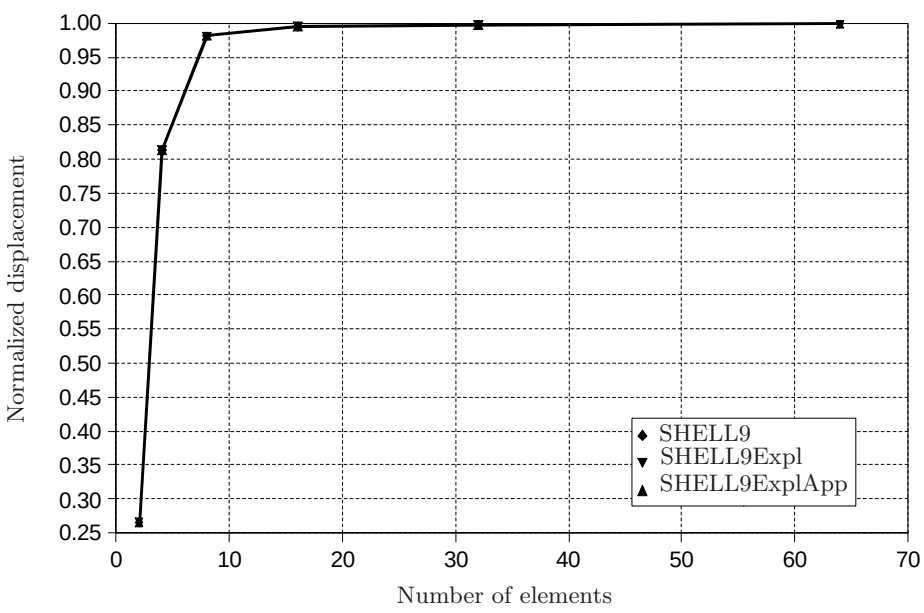

Figure 6.8: Scordelis-Lo roof: normalized displacement vs. number of elements in $N \times N$ mesh. Reference solution: $v = 0.3024$.

6.3.4 Pinched cylinder

Analysis of the singly curved pinched cylinder with end diaphragms is carried out in order to evaluate the convergence behaviour in a singly curved structure subjected to combined bending and membrane stresses. Geometry and boundary conditions of the cylinder are shown in Figure 6.9.

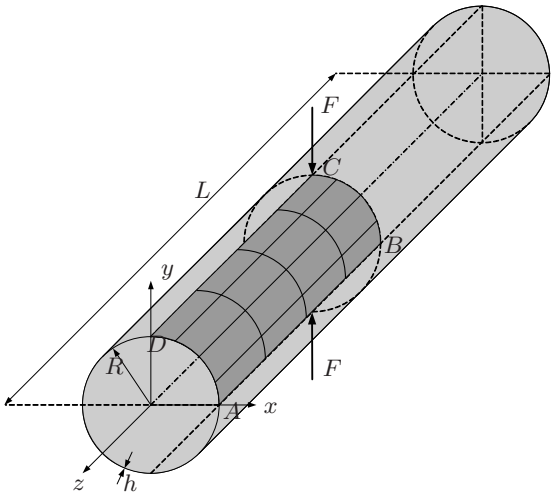

Figure 6.9: Pinched cylinder with end diaphragms with an applied load of, $F = 1$ at $\frac{L}{2}$. Geometrical properties of the cylinder: $L = 600$, $R = 300$ and $h = 3$, i.e. $\frac{R}{h} = 100$. Isotropic material properties: Youngs modulus, $E = 3 \cdot 10^6$ and Poissons ratio, $\nu = 0.3$.

To asses the convergence of the elements one octant of the geometry is meshed by an $N \times N$ mesh as shown at Figure 6.9, where N attains the values 2, 4, 8, 16, 25, 32 and 40. Values of normalized displacements based on these meshes are shown in Table 6.1. The displacements are normalized by values given in Heppler and Hansen (1986), i.e. $u_B = -\frac{164.24F}{Eh} = -5.2222 \cdot 10^{-8}$, $v_C = -\frac{0.47F}{Eh} = -1.8248 \cdot 10^{-5}$ and $w_D = -\frac{4.114F}{Eh} = -4.5711 \cdot 10^{-7}$.

Table 6.1: Pinched cylinder: normalized displacement at points B, C and D in the x, y and z-direction respectively. N denotes the number of elements in an $N \times N$ mesh.

	Normalized u_B			**Normalized v_C**			**Normalized w_D**		
N	**9**	**9Expl**	**9ExplApp**	**9**	**9Expl**	**9ExplApp**	**9**	**9Expl**	**9ExplApp**
2	−5.95	−5.95	−5.95	0.05	0.05	0.05	0.12	0.12	0.12
4	10.80	10.80	10.80	0.16	0.16	0.16	0.30	0.30	0.30
8	17.15	17.15	17.15	0.56	0.56	0.56	0.76	0.76	0.76
16	−2.74	−2.74	−2.74	0.91	0.91	0.91	0.97	0.97	0.97
25	1.39	1.39	1.39	0.98	0.98	0.98	0.99	0.99	0.99
32	1.15	1.15	1.15	1.00	1.00	1.00	1.00	1.00	1.00
40	1.05	1.05	1.05	1.00	1.00	1.00	1.00	1.00	1.00

Convergence of the three element schemes seems to be identical. The normalized displacements presented in Table 6.1 are plotted in Figure 6.10 to asses the convergence at each point of interest. Due to coinciding values of normalized displacement only one graph is shown for each of the points B, C and D.

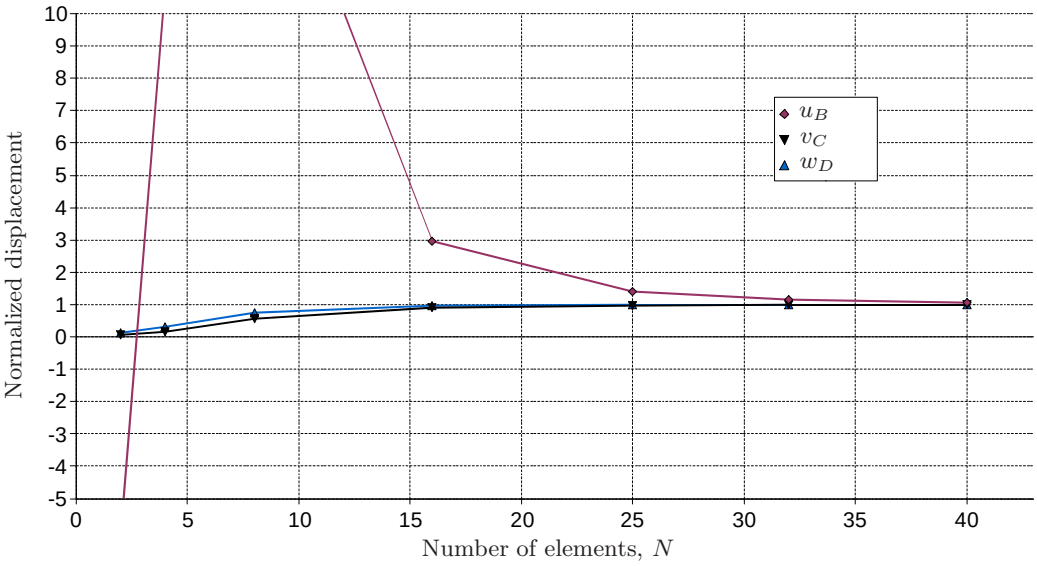

Figure 6.10: Pinched cylinder: Normalized displacement vs. number of elements in $N \times N$ mesh. The graph is based on values for the SHELL9ExplApp element.

Displacements at points C and D converge nicely towards the values used for

normalization and with a 40×40 mesh the displacements have converged. The convergence history of the displacement at point B is oscillating, but it seems that the displacement has converged at a 40×40 mesh. The apparent difficulties with u_B displacements may be due to the reference value being significantly smaller than the remaining displacements and thus a minor absolute deviation will show as a large relative deviation.

6.3.5 Twisted beam

The twisted beam test example is used to evaluate how elements perform in a twisted situation. For explicitly integrated elements Vlachoutsis (1990) reports an increased sensitivity to twist, compared to the completely numerically integrated equivalents. As shown below, this tendency has not been recovered in our numerical tests of the present implementation.

The beam is loaded by a unit in-plane and a transverse tip load applied as equivalent nodal forces in each test case, and a sketch of the problem is shown in Figure 6.11. MacNeal and Harder (1985) report theoretical solutions to the problem, however, no reference is given to how the theoretical result is obtained and it was not possible in the present work to recover the results. For this reason we take as a reference solution a result obtained by Ansys with the use of their SHELL91[1] element on a 12×2-mesh. This yields transverse tip deflections of the center node of $2.39 \cdot 10^{-3}$ and $6.7 \cdot 10^{-3}$ for the out-of-plane and in-plane transverse load case, respectively.

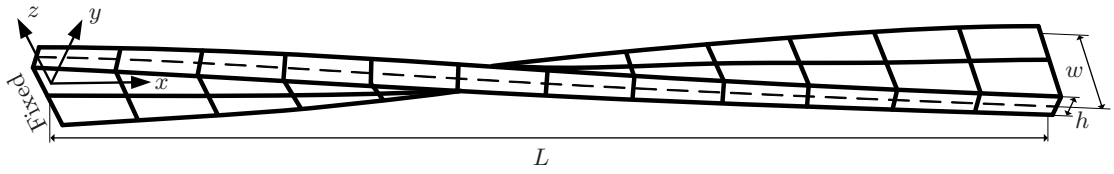

Figure 6.11: Twisted beam with fixed end. Dimensions: $L = 12.0$, $w = 1.1$, $h = 0.32$ and twist $= 90°$. Isotropic material properties; $E = 29.0 \cdot 10^6$, $\nu = 0.22$.

In Table 6.2 the normalized tip displacement in case of an out-of-plane shear load is shown. It is seen that mesh refinement and thus less twisted elements yields more precise results. The explicit and approximate explicit integration schemes, however, only seem to have a minor influence on the results and virtually no difference exists among the models. The 16-node version is seen to be less sensitive against twist and again the explicit integration schemes do not seem to alter the results.

[1] SHELL91 is a quadratic degenerated shell element. It has layered capabilities and employs layer-wise integration through the thickness.

Table 6.2: Twisted beam: normalized tip displacement for out-of-plane shear load. Normalized by: $2.39 \cdot 10^{-3}$.

		SHELL9			SHELL16		
N	**Twist pr. element, (°)**	**9**	**Expl**	**ExplApp**	**16**	**Expl**	**ExplApp**
2	45.0	0.74	0.74	0.74	N/A	N/A	N/A
3	30.0	0.89	0.89	0.89	0.99	0.99	0.99
4	22.5	0.95	0.94	0.94	1.00	0.99	0.99
6	15.0	0.98	0.98	0.98	1.00	1.00	1.00
12	7.5	1.00	1.00	1.00	1.00	1.00	1.00

For the in-plane transverse shear loaded beam we observe the same tendencies as for the out-of-plane shear loaded twisted beam, see Table 6.3.

Table 6.3: Twisted beam: normalized tip displacement for in-plane shear load. Normalized by: $6.70 \cdot 10^{-3}$.

		SHELL9			SHELL16		
N	**Twist pr. element, (°)**	**9**	**Expl**	**ExplApp**	**16**	**Expl**	**ExplApp**
2	45.0	0.78	0.78	0.78	N/A	N/A	N/A
3	30.0	0.90	0.90	0.90	0.99	0.99	0.99
4	22.5	0.95	0.95	0.95	1.00	0.99	0.99
6	15.0	0.99	0.98	0.98	1.00	1.00	1.00
12	7.5	1.00	1.00	1.00	1.00	1.00	1.00

In result, it seems that an element twist angle less than 15° yields acceptable results, within 5% of the reference solution for the 9-node elements. The 16-node element is less sensitive to twist. The influence of the integration scheme is regarded as being insignificant since only minor differences are observed amongst the different schemes.

6.3.6 Buckling of axially compressed cylinder

To verify the implementation of the stress stiffness matrix (and thus also the stress recovery calculation), we compare the critical stress obtained from finite element solutions to an analytically obtained solution. For short (but not too short) simply supported axially compressed circular cylinders Brush and Almroth (1975) report an analytical solution for the critical stress of

$$\sigma_{cr} = \frac{Et/r}{\sqrt{3\left(1-\nu^2\right)}} \text{ for } Z = \frac{L^2}{rt}\left(1-\nu^2\right)^{1/2} > 2.85 \tag{6.10}$$

For the example shown in Figure 6.12 the analytical critical stress is $\sigma_{cr} = 788 N/mm^2$.

To obtain reasonable results with the nine-node element formulation a relatively fine discretization is required. The buckling problem is solved with a 96×24 mesh of nine-

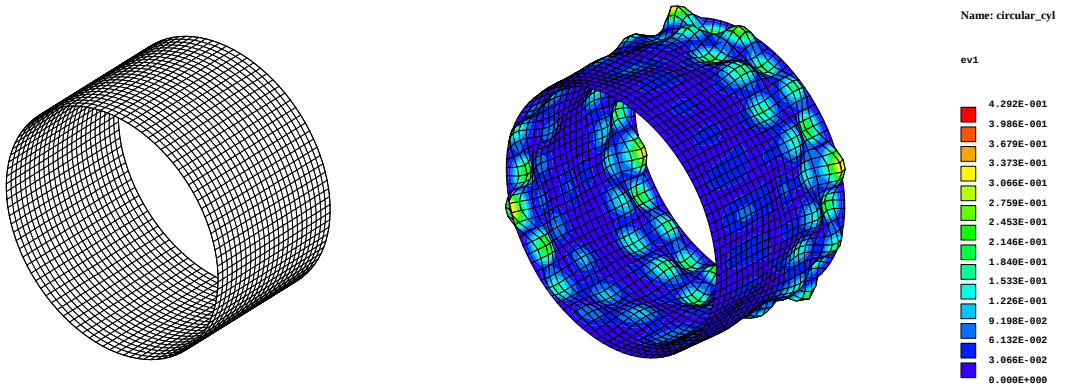

Figure 6.12: Left: Axially compressed cylinder, 96×24 mesh. Geometry: length, $L = 20.0$, radius, $r = 15.9$, thickness, $h = 0.1$. Isotropic material properties: Young's modulus, $E = 207GPa$, Poisson's ratio, $\nu = 0.3$. Boundary conditions: both ends simply supported. One end subjected to uniformly distributed axial compressive load. Right: 1st buckling mode shape.

node and 16-node elements, respectively. The critical stress from the solution with the different element formulations are shown in Table 6.4.

Table 6.4: Critical stress for axially loaded circular cylinder as obtained from different element formulations.

Element formulation	$\sigma_{\mathbf{cr}}$ $[N/mm^2]$
SHELL9	803.381723472207
SHELL9Expl	803.385218818312
SHELL9ExplApp	803.381057212717
SHELL16	790.015734798536
SHELL16Expl	790.021289723162
SHELL16ExplApp	790.016870315811

The critical stresses obtained from the nine-node finite element solutions are within 2% of the analytical solution, which is regarded as being satisfactory. The 16-node solutions are seen to have converged almost to the exact result.

The virtually identical results indicate that the stress stiffness matrix and the stress recovery calculations are implemented correctly.

6.4 Performance

Having assessed the accuracy, the next step is to investigate the performance, that is, the computational efficiency of the implemented elements. In industry, laminated shell structures with a few hundred layers are not uncommon. Such structures are expensive to analyse both in terms of pre-processing and solution time and therefore it is of interest to reduce element integration time.

To asses the computational efficiency we perform a numerical example that illustrates differences in formulation time of element matrices for the three formulations. These performance assessments are carried out in a so-called release compiled version of MUST in order to show the real potential and performance of the implementation.

The accuracy investigations shown above revealed that the SHELL9ExplApp element is more or less as accurate as the SHELL9 and the SHELL9Expl formulations which may favour use of the SHELL9ExplApp formulation, but for completeness we compare the performance of all three formulations.

The performance assessment is carried out by investigating element matrix formulation time as a function of layers for 100 rectangular plate elements including the time for assembly, since this is performed within the same element loop. The use of plate elements means that $\alpha = \frac{2\Delta_V}{h\Delta_A}$ vanishes since the variation Δ_V of the Jacobian determinant through the thickness is zero for plate elements. This means that many of the terms that make up the $\boldsymbol{E}$-matrices in theory disappear. In practice, however, since the matrices are still present (but with all entries zero) this has no influence on computation time, because the matrix products are still evaluated.

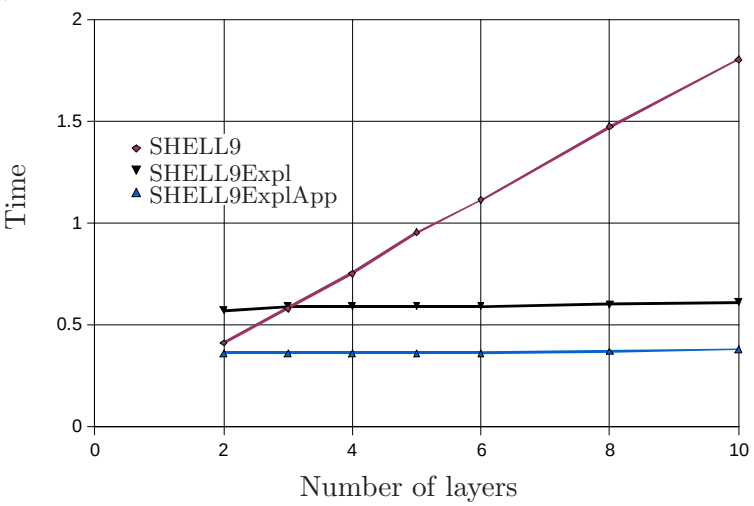

Figure 6.13: Time of formulation and assembly of stiffness matrix for 100 elements by the three formulations.

The first assessment concerns the time used to set up the element stiffness matrix. This is shown in Figure 6.13 from which we for all formulations observe a linear relation between the number of layers and the computation time for the stiffness matrix. For elements with more than two-three layers the new SHELL9Expl and the SHELL9ExplApp formulations are seen to be faster than the existing SHELL9 element formulation. The comparatively flat curves of the two new element formulations mean that substantial savings in formulation times are attained for high layer numbers. For the stress stiffness matrix the same tendency is retrieved, except for the break-even point which is encountered at four layers instead of two-three.

In general it may be concluded that both new formulations result in substantial savings, especially for models with a large number of layers, say, more than 10, which is not uncommon in industry relevant problems.

6.5 Optimization examples

The purpose of this section is to compare the efficiency of 9-node shell elements in MUST when performing optimization. For this purpose two different models are applied. The first is concerned with optimization of structural stiffness and the second with structural stability. Results of the two tests are reported in the following.

6.5.1 Maximum stiffness design

To enable a comparison of computationally efficiency when performing structural stiffness optimization, the geometry and boundary conditions shown in Figure 6.14 are used. The quadratic plate with side lengths, $L = 1m$ consists of 10 plies each with a thickness of $0.001m$ and fibres aligned with the x-axis. Material properties of the plies are: $E_1 = 3.4 \cdot 10^{10}$, $E_2 = E_3 = 8.2 \cdot 10^9$, $\nu_{12} = 0.29$ and $G_{12} = G_{23} = G_{13} = 4.5 \cdot 10^9$. The plate is meshed by a 10×10 mesh and clamped at one end while two out of plane forces, $P = 1N$ with opposite directions, are applied at each corner at the other end. The choice of mesh is based on a convergence test, which revealed that the deflection in the z-direction at the nodes of the applied forces deviates by less than 1% from a 10×10 mesh to a 40×40 mesh and thus the 10×10 mesh is chosen.

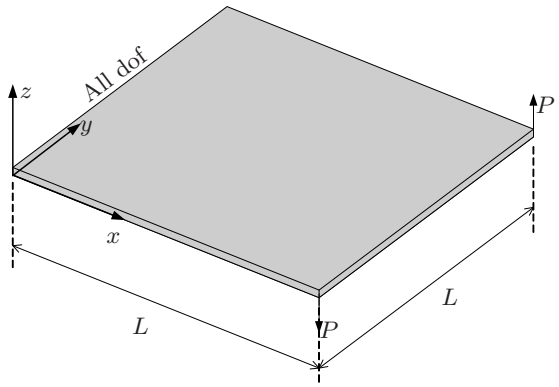

Figure 6.14: Geometry and boundary conditions of the compliance optimization example.

The MMA optimizer is allowed to change the fibre angle within each element whereby the number of design variables is 1000. The maximum number of iterations is set to 200. Results from the optimization are showed in Table 6.5.

All three element formulations converge to a compliance of $0.257592 \cdot 10^{-3}$ in 116 iterations. Comparing the computational time of the two 'new' formulations to the SHELL9 element reveals an efficiency improvement of approximately 17.3% for the SHELL9Expl element and 30.1% for the SHELL9Expl element with no loss in accuracy.

Table 6.5: Results from stiffness optimization with SHELL9, SHELL9Expl and SHELL9ExplApp. Objective function denotes the compliance at the final iteration.

Formulation	Iterations	Total runtime $[s]$	Objective function
9	116	329.3	$0.257592 \cdot 10^{-3}$
9Expl	116	272.5	$0.257592 \cdot 10^{-3}$
9ExplApp	116	230.2	$0.257592 \cdot 10^{-3}$

6.5.2 Maximum stability design

The stability optimization example is in many ways similar to the stiffness optimization. Material properties, lay up and mesh are unchanged. A convergence test revealed a deviation of less than 2% between the first eigenvalue of a 10×10 and a 40×40 mesh. Boundary conditions of the buckling optimization problem can be seen from Figure 6.15. The right edge of the plate is subjected to a distributed load of, $w = 1\frac{N}{m}$. Since the plate width is, $L = 1m$ and the total thickness is, $0.01m$ the applied load equals a stress of $\sigma_x = 100Pa$

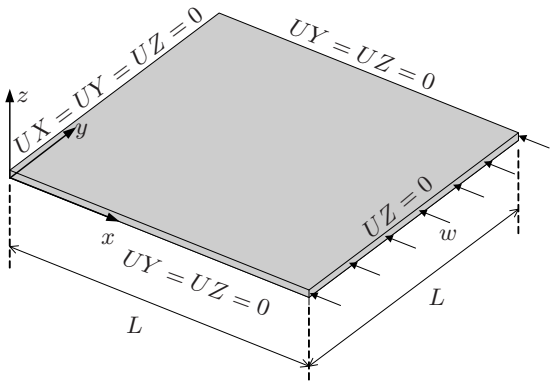

Figure 6.15: Geometry and boundary conditions of the buckling optimization example.

Again, the optimizer is allowed to change the fibre angles within each element, resulting in 1000 design variables to be changed within 200 iterations. The result of the optimization is from Table 6.6

Table 6.6: Results from stability optimization with SHELL9, SHELL9Expl and SHELL9ExplApp. Objective function denotes the first eigenvalue, i.e. the lowest buckling load.

Formulation	Iterations	Total runtime $[s]$	Objective function
9	200	14120	75914.8
9Expl	200	6541	75974.4
9ExplApp	200	4277	75974.4

A small deviation of the optimized lowest buckling load is observed. This might be due to small deviations in the critical stress as seen from Table 6.4. A comparison of the

total runtime reveals a computational saving of approximately 53.7% or a factor 2.2 for the SHELL9Expl element and 69.7% or a factor 3.3 for the SHELL9ExplApp element.

6.6 Summary

The patch tests showed that both new element formulations pass the patch tests. This was shown for a non-layered and a layered configuration. The latter proves that the explicit thickness integration scheme is implemented correct. In addition, the patch tests verify that the stress calculation in itself is correct.

To the precision shown in the print, the results obtained regarding numerical accuracy to a large extent seem identical. The raw data, however, yields minor differences below the 6-7'th significant digit. The convergence studies show that the explicitly integrated elements display convergence behaviour similar to the usual 9-nine node isoparametric shell element.

Investigations of whether the approximations made to enable explicit integration through the thickness show that the approximation is very accurate for shells in the thin shell range $\left(\frac{R}{h} \geq 25.0\right)$. For thicker shells $\left(5.0 \leq \frac{R}{h} \leq 25.0\right)$ the approximation is reasonable but a deviation of up to 4% is seen on the displacements. For even thicker shells the approximation is rude and the error increases rapidly for increasing shell thickness. This result is perfectly viable and should not cause any problems in practice, since structures in this radius of curvature-to-thickness range should probably not be regarded or modelled as shells anyway. Another test of the approximation showed that the new elements are not more sensitive to twist of the elements than the previous formulation.

The accuracy and performance assessments in combination demonstrate substantial savings in computation time without virtually any sacrifice in accuracy. This combination of properties is attractive and thus we see no reason for not using one of the new formulations in multi-layered settings with more than 4 layers if the alternative otherwise is a conventional 9-node isoparametric degenerated shell element. In fact, the accuracy of the SHELL9ExplApp formulation appears to be as good as the two other formulations which is good news seen in the light of the intended use for optimization with lamination parameters as shown in Section 5.6.2.

7

Conclusion

The primary objective of the present work was to develop and implement an efficient degenerated shell element formulation for analysis and optimization of multi-layered composite structures. Secondly, it was the intention to generalize the applicability of lamination parameters to general curved degenerated shell elements.

The first goal was achieved through the development of an efficient explicitly thickness integrated degenerated shell element formulation. The elements have been implemented in a biquadratic 9-node and a bicubic 16-node version in MUST. The implementations have been validated through a number of standard numerical test examples. Accuracy and convergence behaviour is almost identical to that of the existing degenerated isoparametric shell element formulation. The advantage of the new formulation is it's performance in connection with multi-layered shells consisting of many layers. Specifically, it is found that for shells consisting of more than two layers in linear static stress analysis and more than four layers in linearized buckling problems the new formulation is superior in terms of computational efficiency. The geometric approximations enabling explicit thickness integration render the formulation inappropriate for modelling structures with a radius of curvature-to-thickness ratio, $\frac{R}{h} \leq 5$ for which the deviation from the existing formulation exceeds 4%. A number of small optimization examples confirm the potential savings obtainable with the new formulation.

The second objective of generalizing lamination parameters to be applicable for generally curved shell geometries was accomplished by a few additional manipulations of the expressions developed for explicitly integrating through the thickness to evaluate element matrices. Furthermore it was outlined how these developments may be used in laminate optimization with an existing procedure using lamination parameters to enforce convexity.

As such, the objectives of the project have been reached and on basis of the promising results it is interesting to pursue further developments into laminate optimization to fully exploit the potential of the new element formulation.

Further work

Based on the developments with lamination parameters it is interesting to endeavour laminate optimization with lamination parameters to obtain global optimum solutions for generally curved shell structures.

The substantial savings demonstrated for the new formulation, make it interesting for geometrically non-linear analysis of laminated shell structures with a large number of layers. This extension should be straightforward in view of the existing facilities for geometrically non-linear analysis in MUST.

Another interesting direction of research could be to investigate the possibility of stabilising explicitly thickness integrated elements. This could lead to highly efficient stabilized lower-order explicitly thickness integrated elements for analysis of multi-layered structures.

Bibliography

Abrate, S. (1994), 'Optimal design of laminated plates and shells', *Compos. Struct.(USA)* **29**(3), 269–286. 1.1.2

Ahmad, S., B.M. Irons and O.C. Zienkiewicz (1970), 'Analysis of thick and thin shell structures by curved finite elements', *International Journal for Numerical Methods in Engineering* **2**, 419–451. 1.1.1, 4

Brush, D.O. and B.O. Almroth (1975), *Buckling of Bars, Plates, and Shells*, McGraw-Hill. 6.3.6

Cook, R.D., D.S. Malkus, M.E. Plesha and R.J. Witt (2002), *Concepts and applications of finite element analysis*, fourth edn, John Wiley & Sons, Inc., John Wiley & Sons, Inc., 111 River Street, Hoboken, NJ 07030. ISBN 0-471-35605-0. 2.4.1, 3.3.1, 3.5

Foldager, J., J.S. Hansen and N. Olhoff (1998), 'A general approach forcing convexity of ply angle optimization in composite laminates', *Structural and Multidisciplinary Optimization* **16**(2), 201–211. 1.1.2, 5.6.2, 5.4, 5.6.2

Gürdal, Z., R.T. Haftka and P. Hajela (1999), *Design and Optimization of Laminated Composite Materials*, Wiley-Interscience. 2.4

Grenestedt, J.L. (1994), 'Lamination parameters for Reissner-Mindlin plates', *AIAA Journal* **32**(11), 2328–2331. 1.1.2

Heppler, G.R. and J.S. Hansen (1986), 'A Mindlin element for thick and deep shells', *Computer Methods in Applied Mechanics and Engineering* **54**(1), 21–47. 6.3.4

Hughes, T.J.R. (2000), *The Finite Element Method: linear static and dynamic finite element analysis*, Dover Publications. ISBN 0-486-41181-8. 2.3.2, 3.3.2

Jensen, L.R., J.C. Rauhe and J. Stegmann (2002), Finite elements for geometric non-linear analysis of composite laminates and sandwich structures, Master's thesis, Aalborg University, Pontoppidanstræde 101, 9220 Aalborg Øst. Revised edition. 1, 2.3.1, 4.1.2, 4.2.3

Jones, R.M. (1999), *Mechanics of Composite Materials*, second edn, Taylor & Francis, Inc., 325 Chestnut Street, Philadelphia, PA 19106. ISBN 1-56032-712-X. 1.1.1, 4.2.3

Lund, E. (2007), 'Buckling topology optimization of laminated multi-material composite shell structures', *Journal of Composite Structures* . Accepted. 5.5.2

MacNeal, R.H. and R.L. Harder (1985), 'A proposed standard set of problems to test finite element accuracy', *Finite Elements in Analysis and Design* **1**, 3–20. 6.1, 6.2, 6.3.1, 6.3.3, 6.3.5

Miki, M. (1982), 'Material Design of Composite Laminates with Required In-Plane Elastic Properties', *Progress in Science and Engineering of Composites* **2**, 1725–1731. 1.1.2

Miki, M. and Y. Sugiyama (1993), 'Optimum design of laminated composite plates using lamination parameters', *AIAA Journal* **31**(5), 921–922. 1.1.2

Milford, R.V. and W.C. Schnobrich (1986), 'Degenerated isoparametric finite elements using explicit integration', *International Journal for Numerical Methods in Engineering* **23**, 133–154. 1.1.1

Panda, S. and R. Natarajan (1981), 'Analysis of laminated composite shell structures by finite element method', *Computers & Structures* **14**, 225–230. 1.1.1, 1.1.1, 4.2

Prema Kumar, W.P. and R. Palaninathan (1997), 'Finite element analysis of laminated shells with exact through-thickness integration', *Computers and structures* **60**, 173–184. 1.1.1, 4.1.4, 4.2

Prema Kumar, W.P. and R. Palaninathan (1999), 'Explicit through-thickness integration schemes for geometric nonlinear analysis of laminated composite shells', *Finite Elements in Analysis and Design* **32**, 235–256. 1.1.1, 4.2, 4.2.2

Przemieniecki, J.S. (1968), *Theory of Matrix Structural Analysis*, Dover Publications. 3.2

Sokolnikoff, I.S. (1946), *Mathematical theory of elasticity*, second edn, McGraw-Hill Book Company, Inc. 3.1

Stegmann, J. (2005), Analysis and Optimization of Laminated Composite Shell Structures, PhD thesis, Aalborg University, Pontoppidanstræde 101, 9220 Aalborg Øst. 1

Tsai, S.W. and N.J. Pagano (1968), *Invariant Properties of Composite Materials*, Technomic Publishing Co. 1.1.2

Venkataraman, S. and R.T. Haftka (1999), 'Optimization of composite panels–a review', *Proceedings of the 14th annual technical conference of the American society of composites, Dayton OH* pp. 479–88. 1.1.2

Vlachoutsis, S. (1990), 'Explicit integration for three-dimensional degenerated shell finite elements', *International Journal for Numerical Methods in Engineering* **29**, 861–880. 1.1.1, 4.1.4, 6.3.5

Yunus, S.M., P.C. Kohnke and S. Saigal (1989), 'An efficient through-thickness integration scheme in an unlimited layer doubly curved isoparametric composite shell element', *International Journal for Numerical Methods in Engineering* **28**, 2777–2793. 1.1.1, 4.2

Zienkiewicz, O.C. (1977), *The Finite Element Method*, third edn, McGraw-Hill. 3.2, 3.3.1, 3.4, 3.5

Zienkiewicz, O.C., R.L. Taylor and J.M. Too (1971), 'Reduced integration technique in general analysis of plates and shells', *International Journal for Numerical Methods in Engineering* **3**, 275–290. 1.1.1, 1.1.1

A

Shape functions

In this appendix the shape functions of the plane 9- and 16-node isoparametric Lagrangian elements are presented. The shape functions are described in terms of two natural coordinates r and s.

9-node element

Shape functions of the 9-node element with node numbering as shown in Figure A.1 are given by

$$
\begin{aligned}
N_1(r,s) &= \tfrac{1}{4}(1-r)(1-s) - \tfrac{1}{2}(N_5+N_8) - \tfrac{1}{4}N_9 \\
N_2(r,s) &= \tfrac{1}{4}(1+r)(1-s) - \tfrac{1}{2}(N_5+N_6) - \tfrac{1}{4}N_9 \\
N_3(r,s) &= \tfrac{1}{4}(1+r)(1+s) - \tfrac{1}{2}(N_6+N_7) - \tfrac{1}{4}N_9 \\
N_4(r,s) &= \tfrac{1}{4}(1-r)(1+s) - \tfrac{1}{2}(N_7+N_8) - \tfrac{1}{4}N_9 \\
N_5(r,s) &= \tfrac{1}{2}(1-r^2)(1-s) - \tfrac{1}{2}N_9 \\
N_6(r,s) &= \tfrac{1}{2}(1+r)(1-s^2) - \tfrac{1}{2}N_9 \\
N_7(r,s) &= \tfrac{1}{2}(1-r^2)(1+s) - \tfrac{1}{2}N_9 \\
N_8(r,s) &= \tfrac{1}{2}(1-r)(1-s^2) - \tfrac{1}{2}N_9 \\
N_9(r,s) &= (1-r^2)(1-s^2)
\end{aligned}
\tag{A.1}
$$

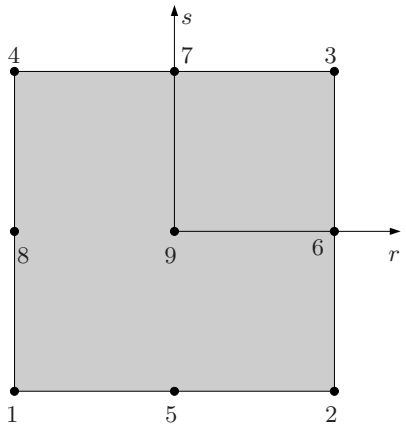

Figure A.1: 9-node isoparametric Lagrange element with natural coordinates.

16-node element

Shape functions of the 16-node element with node numbering as shown in Figure A.2 are given by the Lagrange polynomials

$$\begin{aligned} L_0(x) &= \tfrac{9}{16}\,(1-x)\,\left(x+\tfrac{1}{3}\right)\,\left(x-\tfrac{1}{3}\right) \\ L_1(x) &= \tfrac{27}{16}\,(1+x)\,(x-1)\,\left(x-\tfrac{1}{3}\right) \\ L_2(x) &= \tfrac{27}{16}\,(1-x)\,(x+1)\,\left(x+\tfrac{1}{3}\right) \\ L_0(x) &= \tfrac{9}{16}\,(1+x)\,\left(x+\tfrac{1}{3}\right)\,\left(x-\tfrac{1}{3}\right) \end{aligned} \tag{A.2}$$

$$\begin{array}{llll} N_1 = L_0(r)L_0(s) & N_2 = L_3(r)L_0(s) & N_3 = L_3(r)L_3(s) & N_4 = L_0(r)L_3(s) \\ N_5 = L_1(r)L_0(s) & N_6 = L_2(r)L_0(s) & N_7 = L_3(r)L_1(s) & N_8 = L_3(r)L_2(s) \\ N_9 = L_2(r)L_3(s) & N_{10} = L_1(r)L_3(s) & N_{11} = L_0(r)L_2(s) & N_{12} = L_0(r)L_1(s) \\ N_{13} = L_1(r)L_1(s) & N_{14} = L_2(r)L_1(s) & N_{15} = L_2(r)L_2(s) & N_{16} = L_1(r)L_2(s) \end{array} \tag{A.3}$$

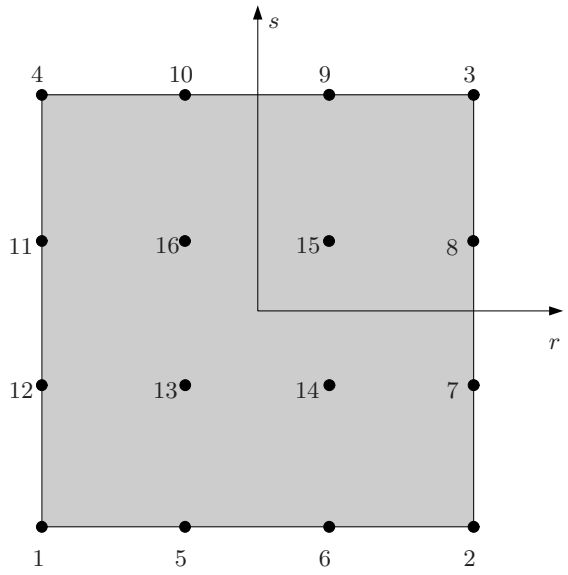

Figure A.2: 16-node isoparametric Lagrange element with natural coordinates.

B

DSA

The purpose of this appendix is to show how analytical design sensitivities of the stiffness matrix (equation (4.45)) with respect to lamination parameters are obtained.

B.1 Stiffness matrix sensitivities

In Section 4.2.2 the expression of the element stiffness were developed in terms of integrated constitutive properties. The integrated constitutive properties may be expressed in terms of lamination parameters as shown in equation (4.72) and (4.73) whereby sensitivities are easily obtained by symbolic differentiation. The sensitivity of the element stiffness matrix with respect to each of the lamination parameters is written as

$$\begin{aligned}\frac{\partial \boldsymbol{K}^e}{\partial \xi_i^j} = \int_{-1}^{1}\int_{-1}^{1} \Bigg(& \boldsymbol{B_1}^T \frac{\partial \boldsymbol{E_1}}{\partial \xi_i^j}\boldsymbol{B_1} + \boldsymbol{B_1}^T \frac{\partial \boldsymbol{E_2}}{\partial \xi_i^j}\boldsymbol{B_2} + \boldsymbol{B_1}^T \frac{\partial \boldsymbol{E_3}}{\partial \xi_i^j}\boldsymbol{B_3} + \\ & \boldsymbol{B_2}^T \frac{\partial \boldsymbol{E_2}}{\partial \xi_i^j}\boldsymbol{B_1} + \boldsymbol{B_2}^T \frac{\partial \boldsymbol{E_3}}{\partial \xi_i^j}\boldsymbol{B_2} + \boldsymbol{B_2}^T \frac{\partial \boldsymbol{E_4}}{\partial \xi_i^j}\boldsymbol{B_3} + \\ & \boldsymbol{B_3}^T \frac{\partial \boldsymbol{E_3}}{\partial \xi_i^j}\boldsymbol{B_1} + \boldsymbol{B_3}^T \frac{\partial \boldsymbol{E_4}}{\partial \xi_i^j}\boldsymbol{B_2} + \boldsymbol{B_3}^T \frac{\partial \boldsymbol{E_5}}{\partial \xi_i^j}\boldsymbol{B_3} \Bigg) \frac{2}{h}\Delta_a^2 \, dr \, ds \end{aligned} \tag{B.1}$$

where $i = 1, 2, 3, 4$ and $j = A, B, D, E, F, G, H$

In the following the sensitivity with respect to each of the lamination parameters are developed. It should be remarked that the integrated constitutive properties $E1$ to $E5$ depend on the lamination parameters as follows

$$\begin{aligned} E_1 &= E_1(\xi_i^A, \xi_i^B, \xi_i^D) \\ E_2 &= E_2(\xi_i^B, \xi_i^D, \xi_i^E) \\ E_3 &= E_3(\xi_i^D, \xi_i^E, \xi_i^F) \\ E_4 &= E_4(\xi_i^E, \xi_i^F, \xi_i^G) \\ E_5 &= E_5(\xi_i^F, \xi_i^G, \xi_i^H) \end{aligned} \tag{B.2}$$

B.1.1 Sensitivity wrt. lamination parameters A

$$\frac{\partial \boldsymbol{K}^e}{\partial \xi_i^A} = \int_{-1}^{1}\int_{-1}^{1} \left({\boldsymbol{B}_1}^T \frac{\partial \boldsymbol{E}_1}{\partial \xi_i^A} \boldsymbol{B}_1 \right) \tfrac{2}{h}\Delta_a^2 \, dr \, ds \tag{B.3}$$

where

$$\frac{\partial E_1}{\partial \xi_1^A} = \boldsymbol{T}^T \boldsymbol{U} h \begin{bmatrix} 0 & 1 & 0 & 0 & 0 \end{bmatrix}^T \boldsymbol{T} \tag{B.4a}$$

$$\frac{\partial E_1}{\partial \xi_2^A} = \boldsymbol{T}^T \boldsymbol{U} h \begin{bmatrix} 0 & 0 & 1 & 0 & 0 \end{bmatrix}^T \boldsymbol{T} \tag{B.4b}$$

$$\frac{\partial E_1}{\partial \xi_3^A} = \boldsymbol{T}^T \boldsymbol{U} h \begin{bmatrix} 0 & 0 & 0 & 1 & 0 \end{bmatrix}^T \boldsymbol{T} \tag{B.4c}$$

$$\frac{\partial E_1}{\partial \xi_4^A} = \boldsymbol{T}^T \boldsymbol{U} h \begin{bmatrix} 0 & 0 & 0 & 0 & 1 \end{bmatrix}^T \boldsymbol{T} \tag{B.4d}$$

B.1.2 Sensitivity wrt. lamination parameters B

$$\frac{\partial \boldsymbol{K}^e}{\partial \xi_i^B} = \int_{-1}^{1}\int_{-1}^{1} \left({\boldsymbol{B}_1}^T \frac{\partial \boldsymbol{E}_1}{\partial \xi_i^B} \boldsymbol{B}_1 + {\boldsymbol{B}_1}^T \frac{\partial \boldsymbol{E}_2}{\partial \xi_i^B} \boldsymbol{B}_2 + {\boldsymbol{B}_2}^T \frac{\partial \boldsymbol{E}_2}{\partial \xi_i^B} \boldsymbol{B}_1 \right) \tfrac{2}{h}\Delta_a^2 \, dr \, ds \tag{B.5}$$

where

$$\frac{\partial E_1}{\partial \xi_1^B} = \boldsymbol{T}^T \boldsymbol{U} 2\gamma \tfrac{h^2}{4} \begin{bmatrix} 0 & 1 & 0 & 0 & 0 \end{bmatrix}^T \boldsymbol{T} \tag{B.6a}$$

$$\frac{\partial E_1}{\partial \xi_2^B} = \boldsymbol{T}^T \boldsymbol{U} 2\gamma \tfrac{h^2}{4} \begin{bmatrix} 0 & 0 & 1 & 0 & 0 \end{bmatrix}^T \boldsymbol{T} \tag{B.6b}$$

$$\frac{\partial E_1}{\partial \xi_3^B} = \boldsymbol{T}^T \boldsymbol{U} 2\gamma \tfrac{h^2}{4} \begin{bmatrix} 0 & 0 & 0 & 1 & 0 \end{bmatrix}^T \boldsymbol{T} \tag{B.6c}$$

$$\frac{\partial E_1}{\partial \xi_4^B} = \boldsymbol{T}^T \boldsymbol{U} 2\gamma \tfrac{h^2}{4} \begin{bmatrix} 0 & 0 & 0 & 0 & 1 \end{bmatrix}^T \boldsymbol{T} \tag{B.6d}$$

$$\frac{\partial E_2}{\partial \xi_1^B} = \boldsymbol{T}^T \boldsymbol{U} \tfrac{h^2}{4} \begin{bmatrix} 0 & 1 & 0 & 0 & 0 \end{bmatrix}^T \boldsymbol{T} \tag{B.6e}$$

$$\frac{\partial E_2}{\partial \xi_2^B} = \boldsymbol{T}^T \boldsymbol{U} \tfrac{h^2}{4} \begin{bmatrix} 0 & 0 & 1 & 0 & 0 \end{bmatrix}^T \boldsymbol{T} \tag{B.6f}$$

$$\frac{\partial E_2}{\partial \xi_3^B} = \boldsymbol{T}^T \boldsymbol{U} \tfrac{h^2}{4} \begin{bmatrix} 0 & 0 & 0 & 1 & 0 \end{bmatrix}^T \boldsymbol{T} \tag{B.6g}$$

$$\frac{\partial E_2}{\partial \xi_4^B} = \boldsymbol{T}^T \boldsymbol{U} \tfrac{h^2}{4} \begin{bmatrix} 0 & 0 & 0 & 0 & 1 \end{bmatrix}^T \boldsymbol{T} \tag{B.6h}$$

B.1.3 Sensitivity wrt. lamination parameters D

$$\frac{\partial \boldsymbol{K}^e}{\partial \xi_i^D} = \int_{-1}^{1}\int_{-1}^{1} \Bigg({\boldsymbol{B}_1}^T \frac{\partial \boldsymbol{E}_1}{\partial \xi_i^D} \boldsymbol{B}_1 + {\boldsymbol{B}_1}^T \frac{\partial \boldsymbol{E}_2}{\partial \xi_i^D} \boldsymbol{B}_2 + {\boldsymbol{B}_1}^T \frac{\partial \boldsymbol{E}_3}{\partial \xi_i^D} \boldsymbol{B}_3 + {\boldsymbol{B}_2}^T \frac{\partial \boldsymbol{E}_2}{\partial \xi_i^D} \boldsymbol{B}_1 + {\boldsymbol{B}_2}^T \frac{\partial \boldsymbol{E}_3}{\partial \xi_i^D} \boldsymbol{B}_2 + {\boldsymbol{B}_3}^T \frac{\partial \boldsymbol{E}_3}{\partial \xi_i^D} \boldsymbol{B}_1 \Bigg) \tfrac{2}{h} \Delta_a^2 \, dr \, ds \tag{B.7}$$

$$\frac{\partial E_1}{\partial \xi_1^D} = \boldsymbol{T}^T \boldsymbol{U} \gamma^2 \tfrac{h^3}{12} \begin{bmatrix} 0 & 1 & 0 & 0 & 0 \end{bmatrix}^T \boldsymbol{T} \tag{B.8a}$$

$$\frac{\partial E_1}{\partial \xi_2^D} = \boldsymbol{T}^T \boldsymbol{U} \gamma^2 \tfrac{h^3}{12} \begin{bmatrix} 0 & 0 & 1 & 0 & 0 \end{bmatrix}^T \boldsymbol{T} \tag{B.8b}$$

$$\frac{\partial E_1}{\partial \xi_3^D} = \boldsymbol{T}^T \boldsymbol{U} \gamma^2 \tfrac{h^3}{12} \begin{bmatrix} 0 & 0 & 0 & 1 & 0 \end{bmatrix}^T \boldsymbol{T} \tag{B.8c}$$

$$\frac{\partial E_1}{\partial \xi_4^D} = \boldsymbol{T}^T \boldsymbol{U} \gamma^2 \tfrac{h^3}{12} \begin{bmatrix} 0 & 0 & 0 & 0 & 1 \end{bmatrix}^T \boldsymbol{T} \tag{B.8d}$$

$$\frac{\partial E_2}{\partial \xi_1^D} = \boldsymbol{T}^T \boldsymbol{U} 2\gamma \tfrac{h^3}{12} \begin{bmatrix} 0 & 1 & 0 & 0 & 0 \end{bmatrix}^T \boldsymbol{T} \tag{B.8e}$$

$$\frac{\partial E_2}{\partial \xi_2^D} = \boldsymbol{T}^T \boldsymbol{U} 2\gamma \tfrac{h^3}{12} \begin{bmatrix} 0 & 0 & 1 & 0 & 0 \end{bmatrix}^T \boldsymbol{T} \tag{B.8f}$$

$$\frac{\partial E_2}{\partial \xi_3^D} = \boldsymbol{T}^T \boldsymbol{U} 2\gamma \tfrac{h^3}{12} \begin{bmatrix} 0 & 0 & 0 & 1 & 0 \end{bmatrix}^T \boldsymbol{T} \tag{B.8g}$$

$$\frac{\partial E_2}{\partial \xi_4^D} = \boldsymbol{T}^T \boldsymbol{U} 2\gamma \tfrac{h^3}{12} \begin{bmatrix} 0 & 0 & 0 & 0 & 1 \end{bmatrix}^T \boldsymbol{T} \tag{B.8h}$$

$$\frac{\partial E_3}{\partial \xi_1^D} = \boldsymbol{T}^T \boldsymbol{U} \tfrac{h^3}{12} \begin{bmatrix} 0 & 1 & 0 & 0 & 0 \end{bmatrix}^T \boldsymbol{T} \tag{B.8i}$$

$$\frac{\partial E_3}{\partial \xi_2^D} = \boldsymbol{T}^T \boldsymbol{U} \tfrac{h^3}{12} \begin{bmatrix} 0 & 0 & 1 & 0 & 0 \end{bmatrix}^T \boldsymbol{T} \tag{B.8j}$$

$$\frac{\partial E_3}{\partial \xi_3^D} = \boldsymbol{T}^T \boldsymbol{U} \tfrac{h^3}{12} \begin{bmatrix} 0 & 0 & 0 & 1 & 0 \end{bmatrix}^T \boldsymbol{T} \tag{B.8k}$$

$$\frac{\partial E_3}{\partial \xi_4^D} = \boldsymbol{T}^T \boldsymbol{U} \tfrac{h^3}{12} \begin{bmatrix} 0 & 0 & 0 & 0 & 1 \end{bmatrix}^T \boldsymbol{T} \tag{B.8l}$$

B.1.4 Sensitivity wrt. lamination parameters E

$$\frac{\partial \boldsymbol{K}^e}{\partial \xi_i^E} = \int_{-1}^{1}\int_{-1}^{1} \Bigg({\boldsymbol{B}_1}^T \frac{\partial \boldsymbol{E}_2}{\partial \xi_i^E} \boldsymbol{B}_2 + {\boldsymbol{B}_1}^T \frac{\partial \boldsymbol{E}_3}{\partial \xi_i^E} \boldsymbol{B}_3 + {\boldsymbol{B}_2}^T \frac{\partial \boldsymbol{E}_2}{\partial \xi_i^E} \boldsymbol{B}_1 + {\boldsymbol{B}_2}^T \frac{\partial \boldsymbol{E}_3}{\partial \xi_i^E} \boldsymbol{B}_2 + {\boldsymbol{B}_2}^T \frac{\partial \boldsymbol{E}_4}{\partial \xi_i^E} \boldsymbol{B}_3 + {\boldsymbol{B}_3}^T \frac{\partial \boldsymbol{E}_3}{\partial \xi_i^E} \boldsymbol{B}_1 + {\boldsymbol{B}_3}^T \frac{\partial \boldsymbol{E}_4}{\partial \xi_i^E} \boldsymbol{B}_2 \Bigg) \tfrac{2}{h} \Delta_a^2 \, dr \, ds \tag{B.9}$$

$$\frac{\partial E_2}{\partial \xi_1^E} = \boldsymbol{T}^T \boldsymbol{U} \gamma^2 \tfrac{h^4}{32} \begin{bmatrix} 0 & 1 & 0 & 0 & 0 \end{bmatrix}^T \boldsymbol{T} \tag{B.10a}$$

$$\frac{\partial E_2}{\partial \xi_2^E} = \boldsymbol{T}^T \boldsymbol{U} \gamma^2 \tfrac{h^4}{32} \begin{bmatrix} 0 & 0 & 1 & 0 & 0 \end{bmatrix}^T \boldsymbol{T} \tag{B.10b}$$

$$\frac{\partial E_2}{\partial \xi_3^E} = \boldsymbol{T}^T \boldsymbol{U} \gamma^2 \tfrac{h^4}{32} \begin{bmatrix} 0 & 0 & 0 & 1 & 0 \end{bmatrix}^T \boldsymbol{T} \tag{B.10c}$$

$$\frac{\partial E_2}{\partial \xi_4^E} = \boldsymbol{T}^T \boldsymbol{U} \gamma^2 \tfrac{h^4}{32} \begin{bmatrix} 0 & 0 & 0 & 0 & 1 \end{bmatrix}^T \boldsymbol{T} \tag{B.10d}$$

$$\frac{\partial E_3}{\partial \xi_1^E} = \boldsymbol{T}^T \boldsymbol{U} 2\gamma \tfrac{h^4}{32} \begin{bmatrix} 0 & 1 & 0 & 0 & 0 \end{bmatrix}^T \boldsymbol{T} \tag{B.10e}$$

$$\frac{\partial E_3}{\partial \xi_2^E} = \boldsymbol{T}^T \boldsymbol{U} 2\gamma \tfrac{h^4}{32} \begin{bmatrix} 0 & 0 & 1 & 0 & 0 \end{bmatrix}^T \boldsymbol{T} \tag{B.10f}$$

$$\frac{\partial E_3}{\partial \xi_3^E} = \boldsymbol{T}^T \boldsymbol{U} 2\gamma \tfrac{h^4}{32} \begin{bmatrix} 0 & 0 & 0 & 1 & 0 \end{bmatrix}^T \boldsymbol{T} \tag{B.10g}$$

$$\frac{\partial E_3}{\partial \xi_4^E} = \boldsymbol{T}^T \boldsymbol{U} 2\gamma \tfrac{h^4}{32} \begin{bmatrix} 0 & 0 & 0 & 0 & 1 \end{bmatrix}^T \boldsymbol{T} \tag{B.10h}$$

$$\frac{\partial E_4}{\partial \xi_1^E} = \boldsymbol{T}^T \boldsymbol{U} \tfrac{h^4}{32} \begin{bmatrix} 0 & 1 & 0 & 0 & 0 \end{bmatrix}^T \boldsymbol{T} \tag{B.10i}$$

$$\frac{\partial E_4}{\partial \xi_2^E} = \boldsymbol{T}^T \boldsymbol{U} \tfrac{h^4}{32} \begin{bmatrix} 0 & 0 & 1 & 0 & 0 \end{bmatrix}^T \boldsymbol{T} \tag{B.10j}$$

$$\frac{\partial E_4}{\partial \xi_3^E} = \boldsymbol{T}^T \boldsymbol{U} \tfrac{h^4}{32} \begin{bmatrix} 0 & 0 & 0 & 1 & 0 \end{bmatrix}^T \boldsymbol{T} \tag{B.10k}$$

$$\frac{\partial E_4}{\partial \xi_4^E} = \boldsymbol{T}^T \boldsymbol{U} \tfrac{h^4}{32} \begin{bmatrix} 0 & 0 & 0 & 0 & 1 \end{bmatrix}^T \boldsymbol{T} \tag{B.10l}$$

B.1.5 Sensitivity wrt. lamination parameters F

$$\frac{\partial \boldsymbol{K}^e}{\partial \xi_i^F} = \int_{-1}^{1}\int_{-1}^{1} \Big({\boldsymbol{B}_1}^T \frac{\partial \boldsymbol{E}_3}{\partial \xi_i^F} \boldsymbol{B}_3 + {\boldsymbol{B}_2}^T \frac{\partial \boldsymbol{E}_3}{\partial \xi_i^F} \boldsymbol{B}_2 + {\boldsymbol{B}_2}^T \frac{\partial \boldsymbol{E}_4}{\partial \xi_i^F} \boldsymbol{B}_3 \\ {\boldsymbol{B}_3}^T \frac{\partial \boldsymbol{E}_3}{\partial \xi_i^F} \boldsymbol{B}_1 + {\boldsymbol{B}_3}^T \frac{\partial \boldsymbol{E}_4}{\partial \xi_i^F} \boldsymbol{B}_2 + {\boldsymbol{B}_3}^T \frac{\partial \boldsymbol{E}_5}{\partial \xi_i^F} \boldsymbol{B}_3 \Big) \tfrac{2}{h} \Delta_a^2 \, dr \, ds \tag{B.11}$$

$$\frac{\partial E_3}{\partial \xi_1^F} = \boldsymbol{T}^T \boldsymbol{U} \gamma^2 \tfrac{h^5}{80} \begin{bmatrix} 0 & 1 & 0 & 0 & 0 \end{bmatrix}^T \boldsymbol{T} \tag{B.12a}$$
$$\frac{\partial E_3}{\partial \xi_2^F} = \boldsymbol{T}^T \boldsymbol{U} \gamma^2 \tfrac{h^5}{80} \begin{bmatrix} 0 & 0 & 1 & 0 & 0 \end{bmatrix}^T \boldsymbol{T} \tag{B.12b}$$
$$\frac{\partial E_3}{\partial \xi_3^F} = \boldsymbol{T}^T \boldsymbol{U} \gamma^2 \tfrac{h^5}{80} \begin{bmatrix} 0 & 0 & 0 & 1 & 0 \end{bmatrix}^T \boldsymbol{T} \tag{B.12c}$$
$$\frac{\partial E_3}{\partial \xi_4^F} = \boldsymbol{T}^T \boldsymbol{U} \gamma^2 \tfrac{h^5}{80} \begin{bmatrix} 0 & 0 & 0 & 0 & 1 \end{bmatrix}^T \boldsymbol{T} \tag{B.12d}$$
$$\frac{\partial E_4}{\partial \xi_1^F} = \boldsymbol{T}^T \boldsymbol{U} 2\gamma \tfrac{h^5}{80} \begin{bmatrix} 0 & 1 & 0 & 0 & 0 \end{bmatrix}^T \boldsymbol{T} \tag{B.12e}$$
$$\frac{\partial E_4}{\partial \xi_2^F} = \boldsymbol{T}^T \boldsymbol{U} 2\gamma \tfrac{h^5}{80} \begin{bmatrix} 0 & 0 & 1 & 0 & 0 \end{bmatrix}^T \boldsymbol{T} \tag{B.12f}$$
$$\frac{\partial E_4}{\partial \xi_3^F} = \boldsymbol{T}^T \boldsymbol{U} 2\gamma \tfrac{h^5}{80} \begin{bmatrix} 0 & 0 & 0 & 1 & 0 \end{bmatrix}^T \boldsymbol{T} \tag{B.12g}$$
$$\frac{\partial E_4}{\partial \xi_4^F} = \boldsymbol{T}^T \boldsymbol{U} 2\gamma \tfrac{h^5}{80} \begin{bmatrix} 0 & 0 & 0 & 0 & 1 \end{bmatrix}^T \boldsymbol{T} \tag{B.12h}$$
$$\frac{\partial E_5}{\partial \xi_1^F} = \boldsymbol{T}^T \boldsymbol{U} \tfrac{h^5}{80} \begin{bmatrix} 0 & 1 & 0 & 0 & 0 \end{bmatrix}^T \boldsymbol{T} \tag{B.12i}$$
$$\frac{\partial E_5}{\partial \xi_2^F} = \boldsymbol{T}^T \boldsymbol{U} \tfrac{h^5}{80} \begin{bmatrix} 0 & 0 & 1 & 0 & 0 \end{bmatrix}^T \boldsymbol{T} \tag{B.12j}$$
$$\frac{\partial E_5}{\partial \xi_3^F} = \boldsymbol{T}^T \boldsymbol{U} \tfrac{h^5}{80} \begin{bmatrix} 0 & 0 & 0 & 1 & 0 \end{bmatrix}^T \boldsymbol{T} \tag{B.12k}$$
$$\frac{\partial E_5}{\partial \xi_4^F} = \boldsymbol{T}^T \boldsymbol{U} \tfrac{h^5}{80} \begin{bmatrix} 0 & 0 & 0 & 0 & 1 \end{bmatrix}^T \boldsymbol{T} \tag{B.12l}$$

B.1.6 Sensitivity wrt. lamination parameters G

$$\frac{\partial \boldsymbol{K}^e}{\partial \xi_i^G} = \int_{-1}^{1}\int_{-1}^{1} \left({\boldsymbol{B}_2}^T \frac{\partial \boldsymbol{E}_4}{\partial \xi_i^G} \boldsymbol{B}_3 + {\boldsymbol{B}_3}^T \frac{\partial \boldsymbol{E}_4}{\partial \xi_i^G} \boldsymbol{B}_2 + {\boldsymbol{B}_3}^T \frac{\partial \boldsymbol{E}_5}{\partial \xi_i^G} \boldsymbol{B}_3 \right) \tfrac{2}{h} \Delta_a^2 \, dr \, ds \tag{B.13}$$

$$\frac{\partial E_4}{\partial \xi_1^G} = \boldsymbol{T}^T \boldsymbol{U} \gamma^2 \tfrac{h^6}{192} \begin{bmatrix} 0 & 1 & 0 & 0 & 0 \end{bmatrix}^T \boldsymbol{T} \tag{B.14a}$$
$$\frac{\partial E_4}{\partial \xi_2^G} = \boldsymbol{T}^T \boldsymbol{U} \gamma^2 \tfrac{h^6}{192} \begin{bmatrix} 0 & 0 & 1 & 0 & 0 \end{bmatrix}^T \boldsymbol{T} \tag{B.14b}$$
$$\frac{\partial E_4}{\partial \xi_3^G} = \boldsymbol{T}^T \boldsymbol{U} \gamma^2 \tfrac{h^6}{192} \begin{bmatrix} 0 & 0 & 0 & 1 & 0 \end{bmatrix}^T \boldsymbol{T} \tag{B.14c}$$
$$\frac{\partial E_4}{\partial \xi_4^G} = \boldsymbol{T}^T \boldsymbol{U} \gamma^2 \tfrac{h^6}{192} \begin{bmatrix} 0 & 0 & 0 & 0 & 1 \end{bmatrix}^T \boldsymbol{T} \tag{B.14d}$$
$$\frac{\partial E_5}{\partial \xi_1^G} = \boldsymbol{T}^T \boldsymbol{U} 2\gamma \tfrac{h^6}{192} \begin{bmatrix} 0 & 1 & 0 & 0 & 0 \end{bmatrix}^T \boldsymbol{T} \tag{B.14e}$$
$$\frac{\partial E_5}{\partial \xi_2^G} = \boldsymbol{T}^T \boldsymbol{U} 2\gamma \tfrac{h^6}{192} \begin{bmatrix} 0 & 0 & 1 & 0 & 0 \end{bmatrix}^T \boldsymbol{T} \tag{B.14f}$$
$$\frac{\partial E_5}{\partial \xi_3^G} = \boldsymbol{T}^T \boldsymbol{U} 2\gamma \tfrac{h^6}{192} \begin{bmatrix} 0 & 0 & 0 & 1 & 0 \end{bmatrix}^T \boldsymbol{T} \tag{B.14g}$$
$$\frac{\partial E_5}{\partial \xi_4^G} = \boldsymbol{T}^T \boldsymbol{U} 2\gamma \tfrac{h^6}{192} \begin{bmatrix} 0 & 0 & 0 & 0 & 1 \end{bmatrix}^T \boldsymbol{T} \tag{B.14h}$$

B.1.7 Sensitivity wrt. lamination parameters H

$$\frac{\partial \boldsymbol{K}^e}{\partial \xi_i^H} = \int_{-1}^{1}\int_{-1}^{1} \left({\boldsymbol{B}_3}^T \frac{\partial \boldsymbol{E}_5}{\partial \xi_i^H} \boldsymbol{B}_3 \right) \tfrac{2}{h} \Delta_a^2 \, dr \, ds \tag{B.15}$$

$$\frac{\partial E_5}{\partial \xi_1^H} = \boldsymbol{T}^T \boldsymbol{U} \gamma^2 \tfrac{h^7}{448} \begin{bmatrix} 0 & 1 & 0 & 0 & 0 \end{bmatrix}^T \boldsymbol{T} \tag{B.16a}$$
$$\frac{\partial E_5}{\partial \xi_2^H} = \boldsymbol{T}^T \boldsymbol{U} \gamma^2 \tfrac{h^7}{448} \begin{bmatrix} 0 & 0 & 1 & 0 & 0 \end{bmatrix}^T \boldsymbol{T} \tag{B.16b}$$
$$\frac{\partial E_5}{\partial \xi_3^H} = \boldsymbol{T}^T \boldsymbol{U} \gamma^2 \tfrac{h^7}{448} \begin{bmatrix} 0 & 0 & 0 & 1 & 0 \end{bmatrix}^T \boldsymbol{T} \tag{B.16c}$$
$$\frac{\partial E_5}{\partial \xi_4^H} = \boldsymbol{T}^T \boldsymbol{U} \gamma^2 \tfrac{h^7}{448} \begin{bmatrix} 0 & 0 & 0 & 0 & 1 \end{bmatrix}^T \boldsymbol{T} \tag{B.16d}$$

C

Patch test results

Results from the patch tests for the 9-node isoparametric elements not contained in the report are contained within this appendix.

C.1 Membrane patch test

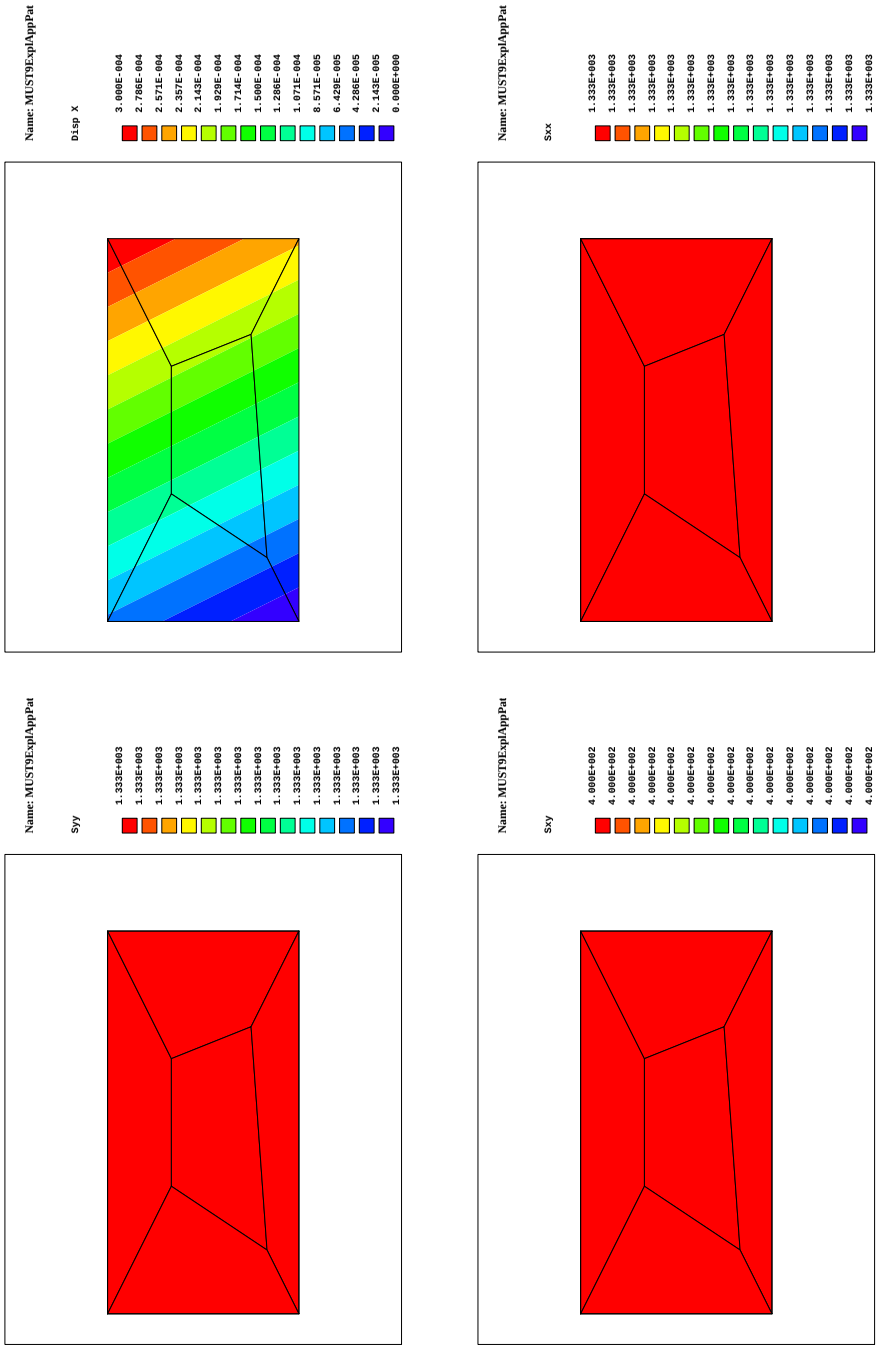

Figure C.1: Membrane patch test results for the explicitly integrated formulation with further approximations, SHELL9ExplApp. From top left to bottom right: u_x, σ_{xx}, σ_{yy} and σ_{xy}, respectively.

C.2 Bending patch test

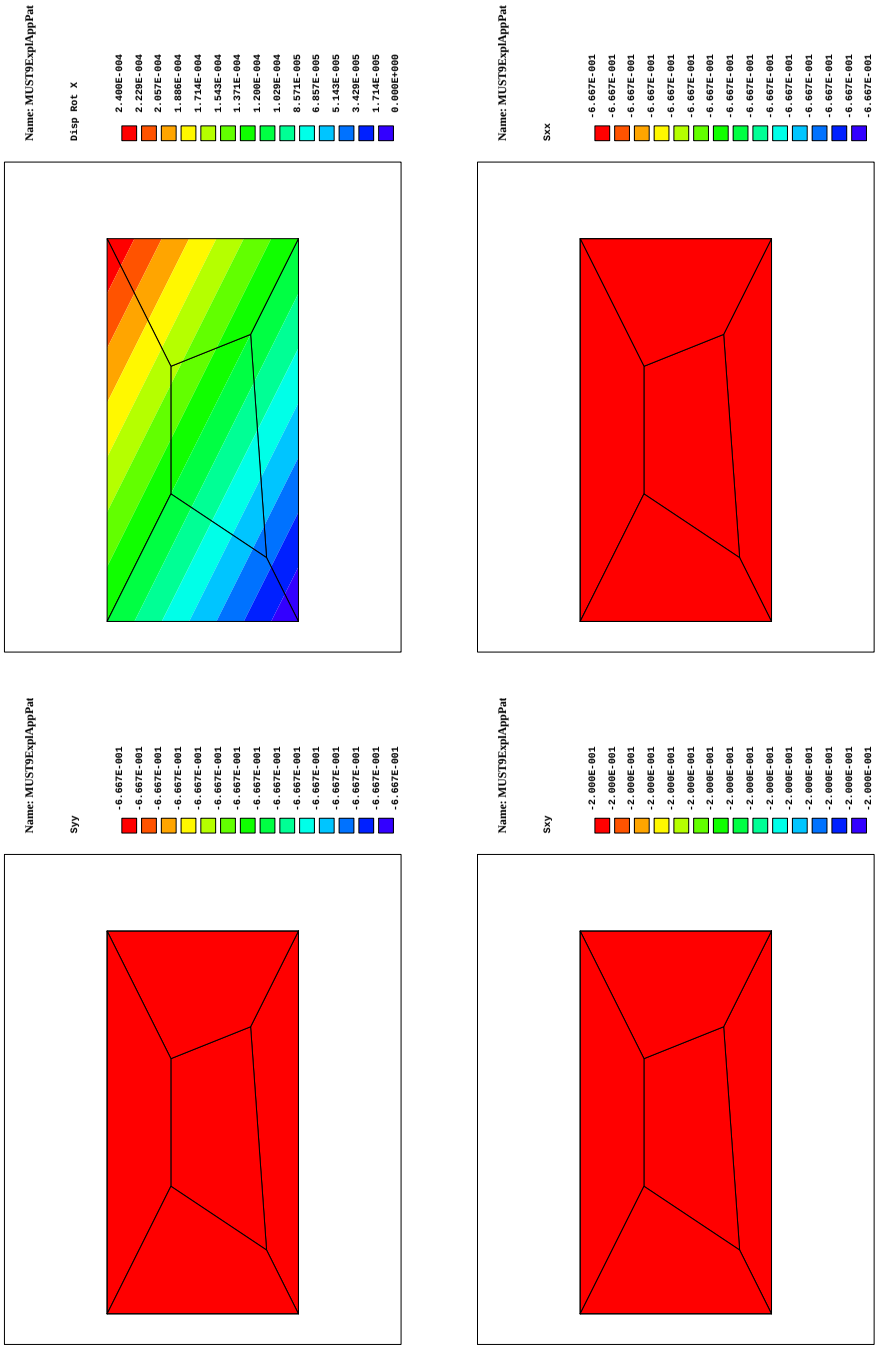

Figure C.2: Bending patch test results for the explicitly integrated formulation with further approximations, SHELL9ExplApp. From top left to bottom right: θ_x, σ_{xx}, σ_{yy} and σ_{xy}, respectively.

C.3 Layered membrane patch test

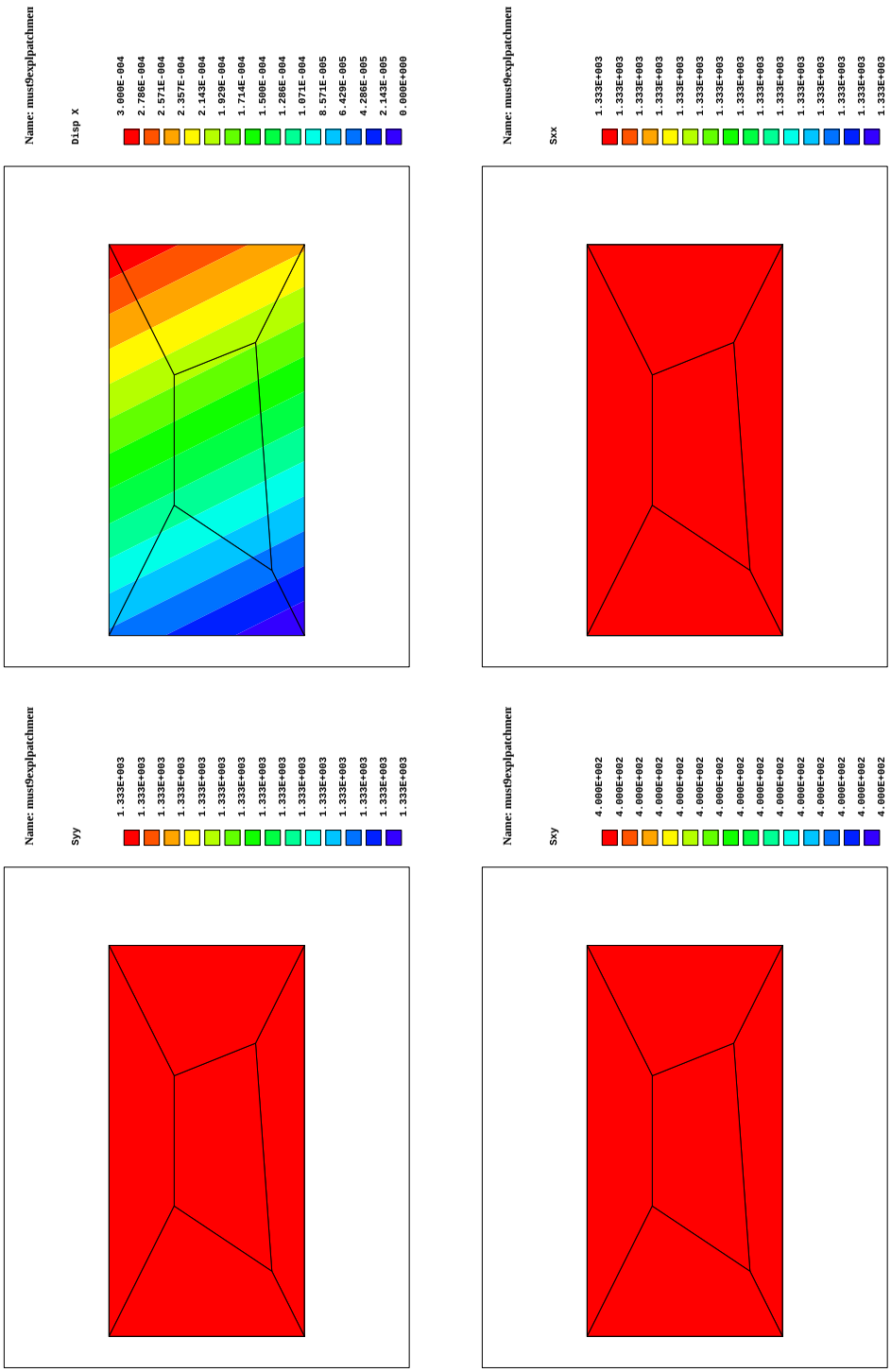

Figure C.3: Layered membrane patch test results for the SHELL9Expl formulation. From top left to bottom right: u_x, σ_{xx}, σ_{yy} and σ_{xy}, respectively.

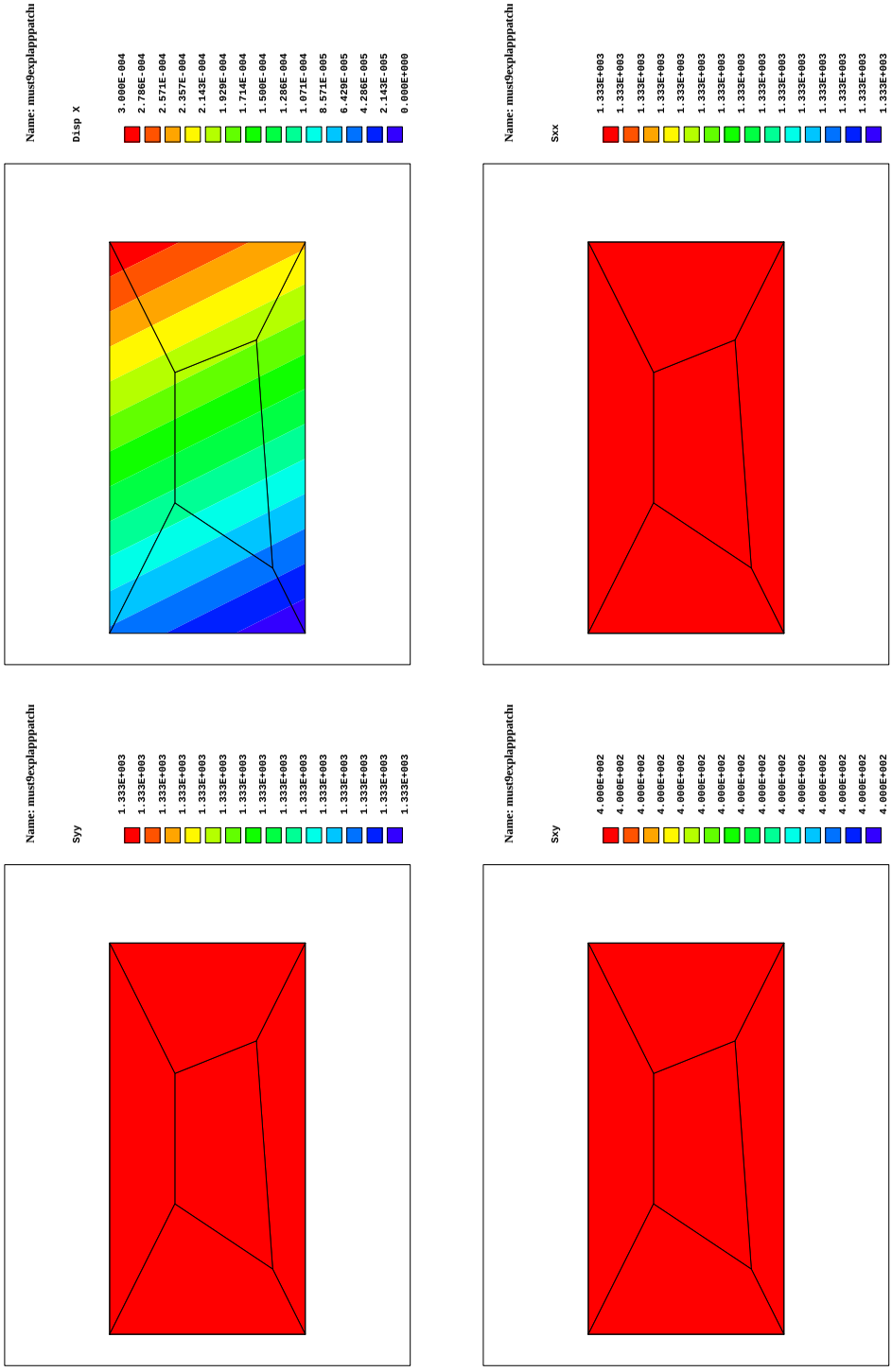

Figure C.4: Layered membrane patch test results for the SHELL9ExplApp formulation. From top left to bottom right: u_x, σ_{xx}, σ_{yy} and σ_{xy}, respectively.

C.4 Layered bending patch test

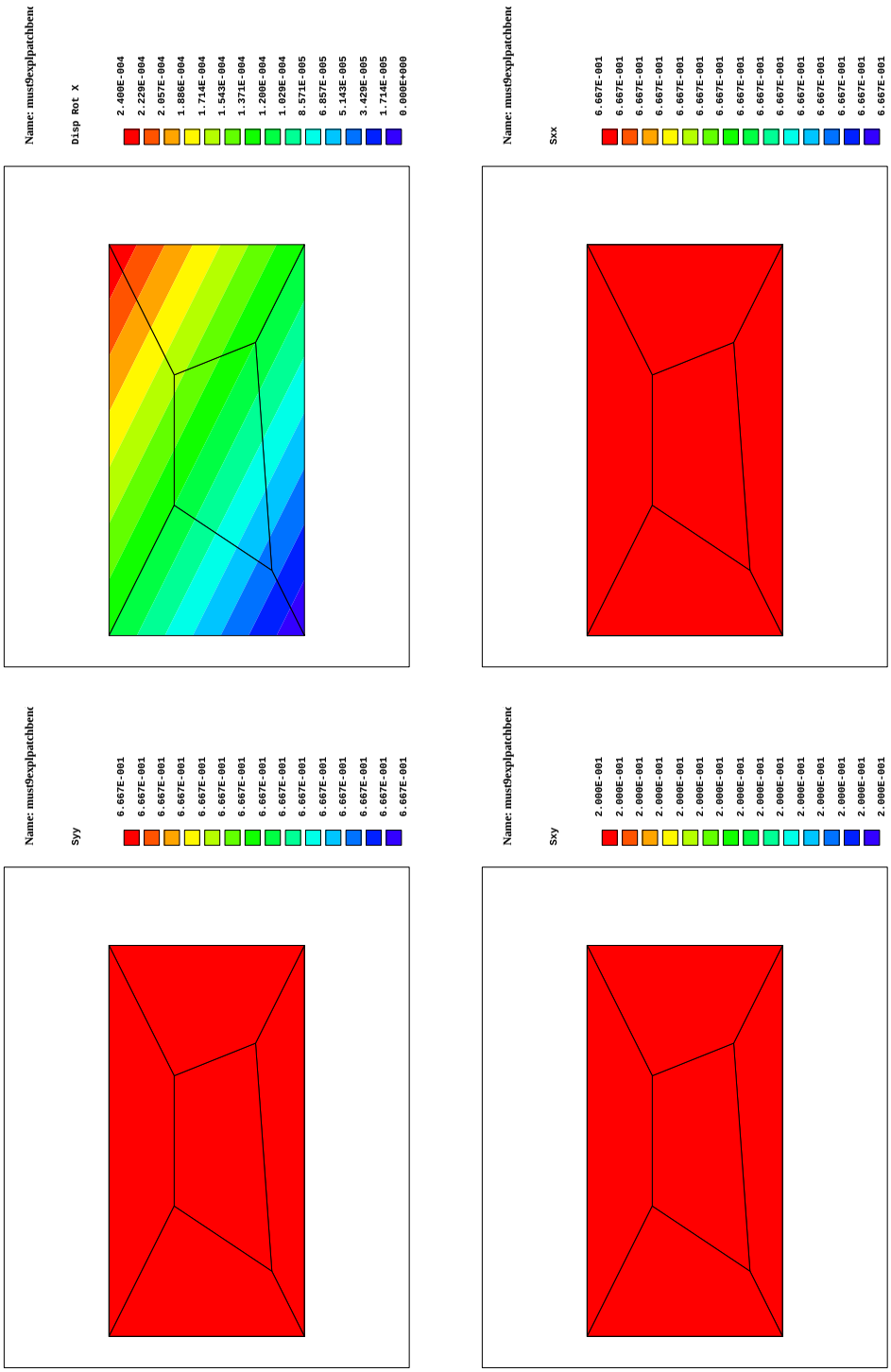

Figure C.5: Layered bending patch test results for the SHELL9Expl formulation. From top left to bottom right: θ_x, σ_{xx}, σ_{yy} and σ_{xy}, respectively.

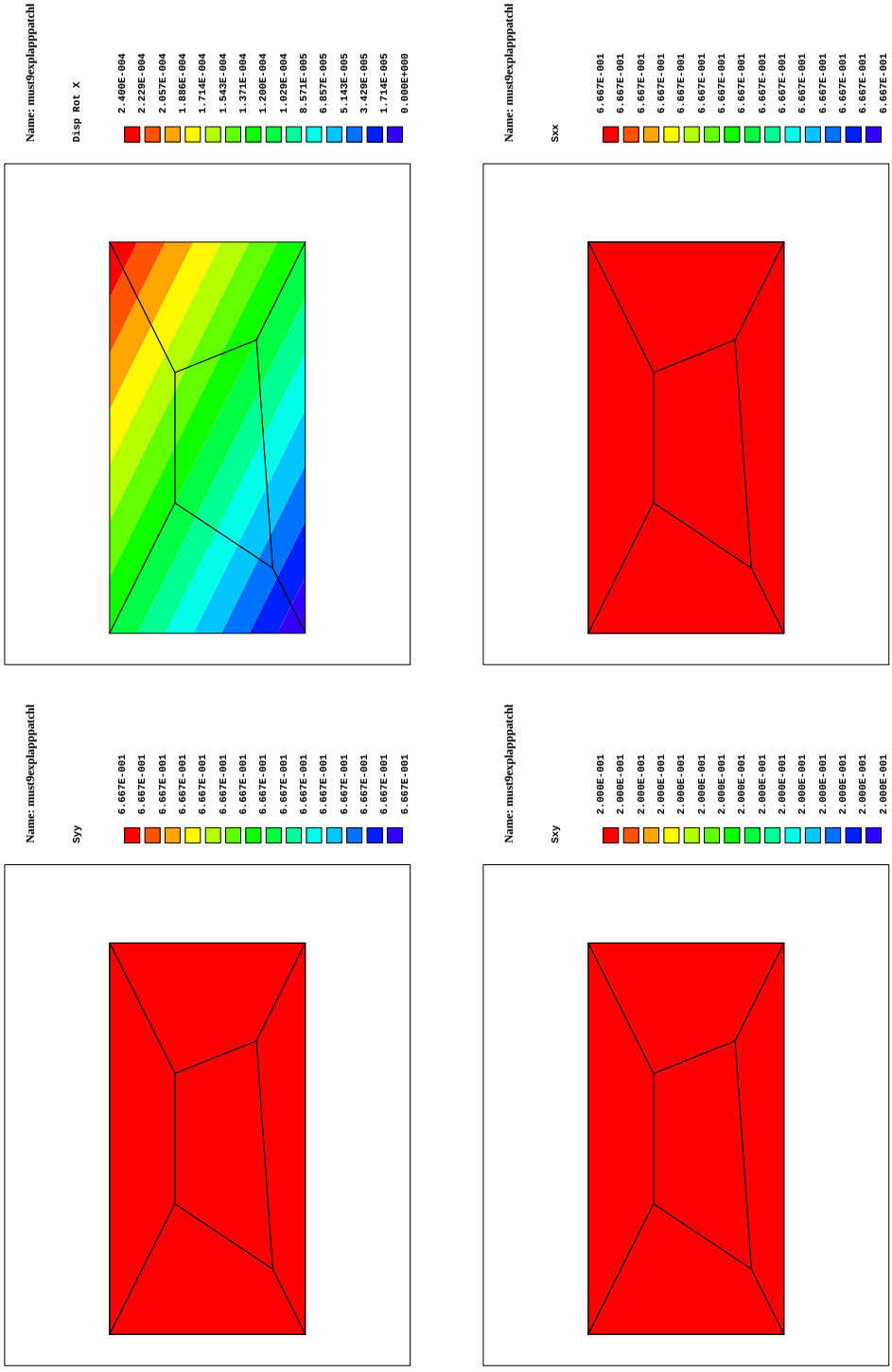

Figure C.6: Layered bending patch test results for the SHELL9ExplApp formulation. From top left to bottom right: θ_x, σ_{xx}, σ_{yy} and σ_{xy}, respectively.